DYNAMIC RESPONSE OF A MOBILE OFFSHORE BASE HYDROELASTIC TEST MODEL

Master's Thesis
by

Venkataraman, Vijay
Graduate Research Assistant

Vincent Caccese, Ph.D., P.E.
Associate Professor of Mechanical Engineering
Thesis Advisor

Sponsored by

Office of Naval Research
Mobile Offshore Base Program

THE UNIVERSITY OF
MAINE

Department of Mechanical Engineering
University of Maine
Orono, ME 04469
(207) 581-2131

Final Report No. C-9920-01

December, 2001

20011231 114

DYNAMIC RESPONSE OF A MOBILE OFFSHORE BASE

HYDROELASTIC TEST MODEL

By

Vijay Venkataraman

B.S. University of Maine, 1998

A THESIS

Submitted in Partial Fulfillment of the

Requirements for the Degree of

Master of Science

(in Mechanical Engineering)

The Graduate School

The University of Maine

August, 2001

Advisory Committee:

Vincent Caccese, Associate Professor of Mechanical Engineering, Advisor

Donald Grant, Chair and R.C. Hill Professor of Mechanical Engineering

Richard Sayles, Associate Professor of Mechanical Engineering

DYNAMIC RESPONSE OF A MOBILE OFFSHORE BASE

HYDROELASTIC TEST MODEL

By Vijay Venkataraman

Thesis Advisor: Dr. Vincent Caccese

An Abstract of the Thesis Presented
in Partial Fulfillment of the Requirements for the
Degree of Master of Science
(in Mechanical Engineering)
August, 2001

The objective of the work presented in this thesis deals with the study of dynamic response of a Mobile Offshore Base (MOB) hydroelastic test model. The MOB is a very large floating structure consisting of multiple self-propelled, semi-submersible modules. Physical scale model testing of a notional MOB concept has been conducted and the experimental results have been provided for one, two and four module configurations. This thesis focuses on utilizing the experimental data to understand the dynamic response of the MOB hydroelastic scale module. The analysis of the data is conducted using popular linear and nonlinear data processing techniques. The objectives are to obtain the modal shapes of the dynamic response, investigate the effect of connector dynamics in multi-module scale models and determine the nonlinear characteristics of the response.

The results of this study suggest that the MOB module acts as an elastic structure. Single module configurations show good heave, pitch and surge response under head seas and include a good roll response under quartering seas. Torsion of the module is also observed under quartering seas for the single module. The single module configurations also show the development of a nonlinear damping force. The two and four module configurations show both in-phase and out-of-phase response characteristics between the interconnected modules constrained rigidly by the connectors.

ACKNOWLEDGEMENTS

TABLE OF CONTENTS

LIST OF TABLES

LIST OF FIGURES

Chapter 1

Introduction

A Mobile Offshore Base (MOB) is a self-propelled, floating platform classified as a very large floating structure. The present vision for the MOB consists of several self-propelled semi-submersible modules that can be dispatched to a geographic region of interest and assembled to primarily function as a logistics platform capable of conducting flight, maintenance, supply, and other military support operations (Remmers, 1997). Several MOB conceptions have been put forward with the MOB modules connected serially (Figure 1.1). Length is the most critical factor driving cost and technical risk for a MOB (Zueck, 2001). A conventional takeoff and landing (CTOL) aircraft require runways as long as 6,500 feet for safe operation. A CTOL capable MOB raises concerns about unproven experience with high-strength connectors, long-crested waves and simulation tools to predict multi-module structural response.
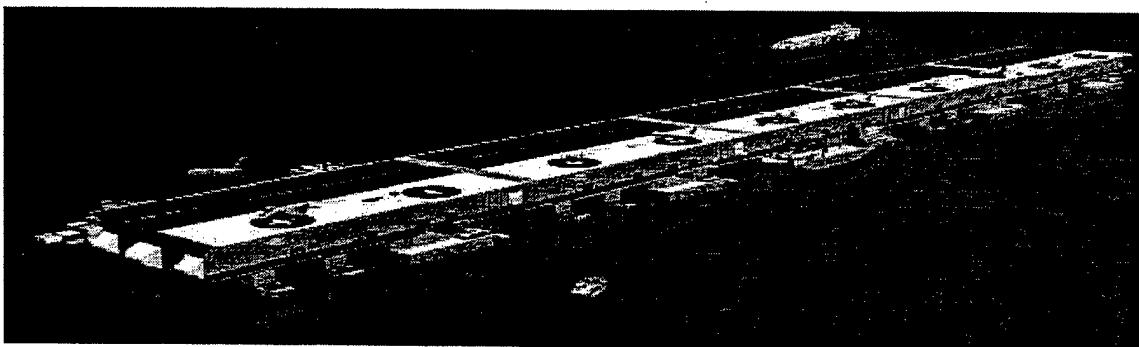
Figure 1.1: McDermott Shipping, Inc. MOB Concept

Each MOB module is designed so that it can function independently (Figure 1.2). Two parallel pontoons having multiple columns support the MOB module's box-type deck. The pontoons are ballastically submerged below the surface wave zone to reduce wave-induced dynamics and its influence on deck motions. The decks are designed to be above wave crests, largely eliminating problems like below-sea-level voids and damage due to flooding. This semi-submersible hull is designed to be rolling much less than 1 degree under wave conditions. One of the popular MOB concepts proposed by McDermott shipping, Inc. consists of five semi-submersible modules that are 1000 by 400 feet in dimension. These modules are larger than those of other MOB concepts. Another unique feature of this MOB concept is that the modules are hinge-connected at the deck level only.
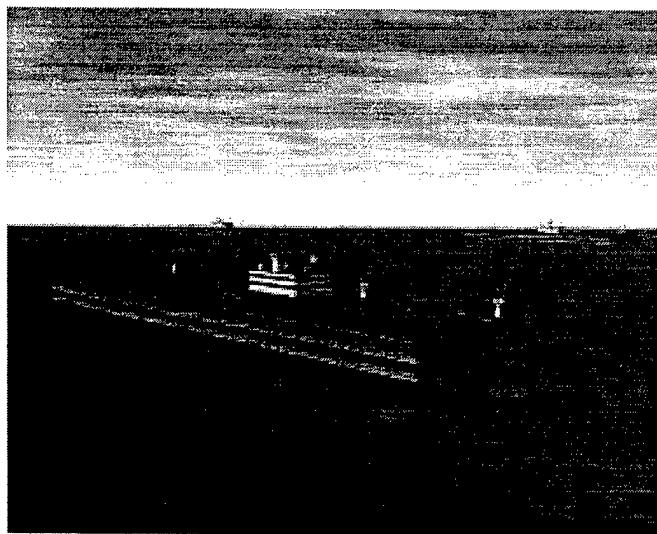
Figure 1.2: Nominal MOB Semi-Submersibles

The Office of Naval Research (ONR) has undertaken a Science & Technology (S&T) program to advance critical MOB design technologies to investigate the areas of cargo transfer, hydrodynamics, structural dynamics, material science and control systems. The thrust of the S&T program are: (1) *Requirements derivation* procedure to

define the mission needs, (2) a set of *performance tools* to measure the cost and performance of a MOB concept, (3) *wave characterization* on a large scale, (4) *MOB classification guide* to document performance and reliability, (5) *hydrodynamic and hydroelastic computer models* for the analysis of critical MOB aspects like connector loads, air gap limits between ocean and bottom of deck, transit behavior, stability and extreme response, (6) *control software* to coordinate up to eight thrusters located on each of the MOB modules, and (7) four unique, innovative *MOB concept designs* distinguished by their method of connection. The technology developed through this program can be extended to a host of commercial applications like Ocean Thermal Conversion (OTEC), offshore industrial bases, and offshore aquaculture.

This thesis work aims at providing necessary validation data to satisfy the objective of developing hydrodynamic and hydroelastic computer models for the analysis of critical MOB aspects. It utilizes physical scale model testing data that is provided and attempts to describe the response of the MOB in terms of frequency mode shapes and investigates the nonlinear characteristics of the response.

1.1 Physical Scale Model Tests

The ONR has sponsored a physical scale model testing on a 1:60 scale model of a notional Mobile Offshore Base (MOB) for conducting seakeeping and structural loads tests. The objective of the test program is to provide data for the validation of analytical hydro computer programs using the physical model as the prototype. The models will be Froude scaled (Sikora, 1998), including the scaling of the space frames for structural frequency for dynamic responses.

The tests have been conducted in the Maneuvering and Seakeeping (MASK) at the Naval Surface Warfare Center, Carderock Division (NSWCCD) for the following cases: (1) single module, (2) a pair of connected modules (two module), and (4) four connected modules. Wave related headings include head seas, bow quartering seas and beam seas. All tests are conducted at zero speed.

The current test program represents a study of a hydroelastically scaled model. Prior data from the NSWCCD tests of a 1/59th scale model of McDermott MOB concept (Smith, 1998) are models that were not structurally scaled. Furthermore, one data set from a particular design does not built sufficient confidence for universal use of those models extrapolated to any MOB platform concept. The unusual size and mission requirements also demand thorough validation of the tools that will be used for design.

The primary objectives of this series of tests are: (1) to provide "generic" validation data for the analytical hydro models/codes, (2) provide an accurate, traceable database of module and module-to-module connector wave induced loads in the linear and nonlinear response regimes for the validation of analytical codes, (3) wave induced loads are defined as longitudinal, vertical and lateral bending moments, vertical and lateral shear forces, and torsion caused by weight minus buoyancy loads, (4) focus on the global response and loads of the hull girder and connectors rather than local plate or shell loads and response, and (5) collect data in both the linear and nonlinear regimes to provide a full validation of the hydro codes.

1.2 Objective

The objectives of this thesis are to study, analyze, and interpret the experimental data available from the hydroelastic test model conducted at MASK as discussed in section 1.1. The goals of this effort can be summarized as follows:

- Develop data reduction and analysis procedures to interpret the hydroelastic test data.

- Perform dynamic parameter estimation to obtain the modal frequency of the MOB models.

- Investigate nonlinear dynamic characteristics using MISO direct and reverse modeling.

The above procedure is achieved through the following steps: (1) Reduce and process the experimental data, and (2) perform linear and nonlinear analysis of data using the wave motion response as the primary input and the module motion response (heave, pitch, roll, etc.) as the primary output response to generate a frequency response function (FRF) and their statistical parameters, and (3) animate the response of the MOB scale model and determine the mode shapes.

For data reduction and processing, a program *Dynamic Data* has been developed based on Delphi to read the experiment data files and perform a data reduction. The same program is also used to average the Z acceleration data channels to obtain the heave acceleration response in the absence of a heave sensor. The Dynamic Data program is also used to perform a linear Single-Input/Single-Output

(SI/SO) analysis of the data and generate corresponding FRF, coherence and phase plots.

To perform a nonlinear analysis, the reduced data is processed using the *ITAP 2000* data processing package on MATLAB™, to perform a Multiple-Input/Single-Output (MI/SO) analysis to generate the FRF, coherence and phase plots. This involves developing differentiation and integration schemes to obtain the motion or velocity from the accelerations or the displacements.

To visualize the response of the MOB scale model, a program MOB_Animate has been developed based on Delphi to read the frequency domain X, Y and Z acceleration data and their phases and perform an animation of the response at different frequency values. This program can depict a combination of modes that occur at any particular frequency.

1.3 Scope of Work

The theoretical background of fluid-structure, wave theory, and wave spectrums is discussed in Chapter Two of this thesis. Chapter Three discusses the physical scale model and the data reduction, differentiation and integration techniques. Chapter Four discusses the analysis techniques including FRFs, coherence and phase, SI/SO and MI/SO. Chapter Five summarizes the analysis results for a single scale module for two different waves spectrums. Chapter Six summarizes the analysis results for a two and four module scale model. Discussion of summary, conclusions and future work is carried out in Chapter Seven.

Chapter 2

Fluid-Structure Interaction and Wave Theory

An elementary understanding of fluid-structure interaction theory is an essential component of understanding the dynamics of the MOB scale model. The theory is introduced with fundamentals and the non-dimensional parameters analyzed herein specifically associated with fluid-structure interaction theory. It is then developed by discussing vortex-induced vibration, both in laminar and turbulent situations and a brief examination of a ship motion in a seaway. The concept of "added mass" effect is briefly examined. The discussion is concluded with a brief overview of waves and wave spectrum. The latter is due to our interest in analyzing large oceanic floating platforms.

2.1 Fundamentals

Fluid structure interaction is dynamic in nature and depends on several factors. The most important of those factors are summarized below:

- Position of structure relative to the fluid flow.

- Velocity of the motion of the structure relative to the fluid flow.

- Turbulence generators (time dependent) in the upstream fluid flow.

- Characteristics of the fluid flow.

Structures can be optimized for efficiency in fluid conditions or be "bluff structures" – structures in which the flow separates from a large section of the

structural surface. These structures are not optimized for hydrodynamic efficiency. All are expected to withstand fluid forces. Most fluid flow equations contain nonlinearities (e.g. nonlinear deformation of structure with increasing load) and nonlinear extrapolations of the measurements of lift, drag or surface pressure are used in solving equations. However, a few general solutions do exist utilizing sets of non-dimensional parameters that can be useful in obtaining solutions for a wide variety of problems. For more complex models, however, the use of a research-quality numerical analysis program becomes quite indispensable. Non-dimensional parameters of a two-dimensional, spring-supported, damped structural model exposed to a steady flow are given in appendix A.

2.2 Fluid-Structure Interaction – Basic Vortex Theory

The shear layers bounding the structure create vortices in the fluid flow past the structure. This vortex creates a structural vibration called vortex-induced vibration. These vibrations of can be of large amplitude. The nature of the vibrations depends largely upon the Reynolds numbers of the fluid flow. Much of the vortex theory is developed for circular cylinders and hence most of the theory discussed pertains specifically to circular cylinders. Approximations for other shapes can however be made by finding their circular equivalent.

For a smooth, circular cylinder in subsonic flow, the period of the oscillation is a function of Reynolds number. Based on the Reynolds number, the vortex can be described as follows:

(a)   Re < 5:   Un-separated flow.

(b)   5-15 ≤ Re < 40:   A fixed pair of vortices are present.

(c)   40 ≤ Re < 150:   Vortex street is laminar (range of Staggered Vortices).

(d)   150 ≤ Re < 300:   Transition range to turbulence in vortex (Sub critical

                                 range).

(e)   300 ≤ Re < 3E5:   Vortex street is fully turbulent.

(f)   3E5 ≤ Re < 3.5E6:   Wake is narrower and disorganized.

(g)   3.5E6 ≤ Re: Re-establishment of turbulent vortex street (Supercritical

                                 range).

2.2.1 Effect of Cylinder Motion on Wake of Vortex Induced Vibration

Cylinder vibration, *at or near the shedding frequency* can have the following effects:

- Increase the vortex strength.

- Increase span wise correlation of the wake.

- Increase drag force.

- If frequency is in a sufficiently close range, then it can cause the shedding frequency to vibrate at the structure's natural frequency. This effect is known as "lock-in" effect. The lock-in effect can also occur if the frequency is multiple or sub-multiple of the shedding frequency. This lock-in effect causes resonance resulting in large amplitudes that can damage the structure.

- An integrated analysis of the vortex-induced vibration (using the Navier-Stokes equations) is not available for a vast majority of practical cases. Limited models are therefore available which describe the cylinder fluid interaction that do not use the Navier-Stokes equations but do include the experimentally observed dynamic effects).

9

2.2.2 Vortex Induced Oscillations – Models

Two important models have been developed to describe the vortex induced oscillations. These are:

- Wake Oscillator Model (cylindrical structures only).

- Correlation model (right circular cylinder).

2.2.2.1 Wake Oscillator Model (Cylindrical Structures Only)

This model is valid in the Reynolds number range $10^3 - 10^5$ of a 2-D flow. It makes the assumptions that the flow field outside the near wake is inviscid and that well-formed vortex sheet and shedding frequency is present. The vortex is formed only in the boundary layer (BL) and grows uniformly to a maximum strength and moves downstream. Fluid force on cylinder is dependent on average fluid velocity and acceleration.

The natural frequency of the shedding frequency is given by the equation (Blevins, 1977)

$$\omega = K' \frac{u_t}{U} \frac{U}{D} \qquad \text{Eq(2.1)}$$

As $\dfrac{u_t}{U}$ (u_t – translational velocity of the vortex street, U- free stream velocity, D – cylinder diameter, K' – proportionality constant)is a constant for a large range of Re numbers, ω is proportional to the ratio of the free stream velocity to the cylinder diameter. This model predicts that the elastically mounted cylinder will exhibit large amplitudes of oscillation as the vortex shedding frequency approaches the natural

cylinder frequency. The frequency of the vortex shedding is entrained by the natural frequency of the structural oscillation and this effect is called "entrainment effect". The peak resonant cylinder amplitude can be expressed in terms of reduced damping, δ_r (Blevins, 1977)

$$\delta_r = \frac{2m(2\pi\zeta)}{\rho D^2}$$ Eq(2.2)

where

m = mass of structure
ζ = damping factor
ρ = density of structure material
D = diameter of cylinder

As damping reduces, the peak resonant amplitude increases until maximum limiting amplitude is reached. The amplitude ratio for 2E2 < Re < 2E5 is given by (Blevins, 1977)

$$\frac{A_Y}{D} = \frac{0.07\gamma}{(\delta_r + 1.9)S^2}\left[0.30 + \frac{0.72}{(\delta_r + 1.9)S}\right]^{\frac{1}{2}}$$

Eq(2.3)

where A_y is the vibration amplitude, δ_r is reduced damping, S is the Strouhal

number, $\gamma = \psi_{Max}\left(z/L\right)\left\{\dfrac{\displaystyle\int_0^L \psi^2(z)dz}{\displaystyle\int_0^L \psi^4(z)dz}\right\}^{\frac{1}{2}}$ is the geometric factor[1] as a function of the mode

---

[1] A list of mode shapes, natural frequencies and geometric factors for different types of cylindrical objects are provided in Table 3-2, pg. 32 of "flow-induced vibration" by Robert D.Blevins. See bibliography.

11

shape ψ and equivalent mass term $\dfrac{\int_0^L \psi^2(z)dz}{\int_0^L \psi^4(z)dz}$. The motion of the cylinder can be

given by $y = A_Y \psi(z)\cos\omega_S t$.

2.2.2.2 Correlation Model (Right Circular Cylinder)

The correlation model is based on span wise correlation and the cylinder amplitude dependence on the vortex forces, which are absent in the wake oscillator model. This model is valid in the Re range of 2E2 < Re < 2E5 and is limited to the resonance of a single mode of vortex shedding. At resonance, the amplitude of the correlated life force on the cylinder can be represented as a continuous function of cylinder amplitude and a characteristic correlation length can represent spanwise correlation of the fluid force.

The amplitude ratio obtained by this model is given by (Blevins, 1977)

$$\frac{A_Y}{D} = \frac{\pi}{(2\pi S)^2} \frac{C_{LE}}{\delta_r} \frac{\int_0^L \psi \ (z)dz}{\int_0^L \psi^2(z)dz} \qquad \text{Eq(2.4)}$$

where, $C_{LE} = \dfrac{\int_0^L C_L(z)\psi(z)dz}{\int_0^L \psi(z)dz}$, is the uniform lift coefficient per unit length and $C_L(z)$

is the lift coefficient. The motion of the cylinder can be given by

$Y(z,t) = A_Y \psi(z)\cos\omega_S t$. The amplitude ratio $\dfrac{A_Y}{D}$ is a function of the damping

$\dfrac{2m(2\pi\zeta)}{\rho D^2}(2\pi S)^2$ and fineness ratio $\dfrac{L}{D}$. At resonant vibration amplitudes of 0.1 diameter or smaller, the spanwise correlation has a strong effect on cylinder response as follows:

- The equivalent force per unit length decreases as aspect ratio increases.

- The correlated vortex forces increase with amplitude.

- At resonant vibration amplitudes of 1 or smaller, the vortex forces tend to decrease to zero with increasing amplitude.

- This model is better than the wake oscillator model for prediction of vortex-induced vibrations at low amplitudes.

2.2.3 Reduction of Vortex-Induced Vibration

Vortex induced vibrations need to be reduced to minimize possible damage to the oscillating structure. This can be achieved in the following ways:

- Using composite materials such as fiber reinforced plastic (FRP) instead of welded steel.

- Using materials of high internal damping.

- Using external dampers.

- Using devices to dissipate energy.

- Avoiding resonance by keeping the reduced velocity below 1. This is achieved in small structures by increasing the natural frequency through the modification of the structure.

13

- Change cross section - vortex shedding is eliminated or minimized in a streamlined profile, which reduce side forces.

2.3 Basic Structural Vibration

For this report, only topics related to the following criteria will be discussed:

- Free vibration.

- Linear vibration.

- Single or two degree of freedom (DOF) vibration.

- Viscous damping.

2.3.1 Basic Vibration Definitions

2.3.1.1 Spring Stiffness

The spring stiffness is determined by the amount displacement that occurs in a spring when subjected to a certain force according to the linear relation

$$K = F/\Delta \qquad \text{Eq(2.5)}$$

Where
K – spring stiffness
F – the force the spring is subjected to.
Δ – the displacement the spring undergoes when subjected to the force F

2.3.1.2 Natural Frequency of Vibration

The natural frequency of vibration of a single degree of freedom structure is given by the following formula

$$\omega^2 = K/M; \quad f = \omega/(2\pi) \qquad \text{Eq(2.6)}$$

Where ω – natural frequency
                                K – spring stiffness
                                M – the effective mass of the structure including any added mass
                                f – the natural frequency in Hz

In a complex structure, there can be several natural frequencies with corresponding mode shapes. The primary frequency is referred to as the 1st or fundamental mode, the secondary as 2nd mode and so on. One of the techniques of FEA model validation is to match the actual mode shapes of the physical structure (obtained through experimentation) and compare it with those obtained through numerical analysis.

2.3.2 Vibrational Damping

In the physical realm, all free vibration comes to a stop over a period of time. One reason for this is because the fluid (air, water, etc.) surrounding the vibrating structure dampens the vibration until the vibration stops. Damping is higher, typically, with denser surrounding fluid. Structures vibrating in water therefore are subjected to greater damping when compared to that in air. There are 3 major types of damping:

- Viscous damping - Damping due to surrounding fluid or "viscous like".

- Coulomb damping - Damping due to dry or Coulomb friction.

- Hysteretic damping - Damping caused by friction between internal layers, which slip or slide when the structure deforms.

For practical purposes the damping offered by air is considered negligible. In such cases where the surrounding fluid offers negligible damping, the structures damp

out due to material damping (internal) which is viscous like in nature. Only viscous damping is discussed in this report, which is the case with most fluid-structure interaction scenarios.

Viscous damping occurs when the surrounding fluid or material (internal) offers damping. The basic equation of motion for the free vibration of the structure subjected to viscous damping is (Rao, 1995)

$$m\ddot{x} + c\dot{x} + kx = 0 \qquad\qquad Eq(2.7)$$

where m   – mass of vibrating structure
         x   – displacement
         c   – damping constant
         k   – spring constant

The resultant frequency of the vibrating structure due to viscous damping is different from the natural frequency of the vibrating structure and is given by (Rao, 1995)

$$\omega_D = \omega_N \sqrt{1 - \zeta^2} \qquad\qquad Eq(2.8)$$

where ω_D – damped frequency (rad/sec)
        ω_N – natural frequency (rad/sec)
        $\zeta = c/c_c$ – damping factor
        c_c – critical damping constant

The value of ζ determines the type of damped case

$0 \le \zeta < 1$ - Under-damped case

$\zeta = 1$ - Critically damped case

$\zeta > 1$ - Over-damped case

The under-damped and critically damped cases are more frequently encountered. The solution of Eq(2.7) for the under-damped case is given by (Rao, 1995)

16

$$x(t) = e^{-\zeta \omega_N t} \left\{ x_0 \cos \sqrt{1-\zeta^2}\ \omega_N t + \frac{x_o + \zeta \omega_N x_0}{\sqrt{1-\zeta^2}\ \omega_N} \sin \sqrt{1-\zeta^2}\ \omega_N t \right\} \qquad Eq(2.9)$$

The equation of motion for the critically damped case is given by (Rao, 1995)

$$x(t) = (C_1 + C_2 * t)e^{-\omega_N t} \qquad Eq(2.10)$$

$$\text{where } C_1 \quad - x_0$$
$$C_2 \quad - x_0 + \omega_N x_0$$

2.4 Added Mass Effect

The added mass effect is the phenomenon in which an oscillating mass immersed in fluid experiences effects of an increased mass, mass moment of inertia and damping. This 'virtual' increase in mass, mass moment of inertia or damping due to the effects of the surrounding fluid is called the added mass, added mass moment of inertia or added damping. This effect is pronounced when the surrounding fluid density is comparable to that of the structure. Added mass effect is of three types:

- Added mass.

- Added mass moment of inertia.

- Added damping.

2.4.1 Added Mass or the Inertial Mass of the Entrained Fluid

Added mass is the inertial mass of the fluid entrained by the structure and increases the effective mass of the structure for consideration in determining the frequency of vibration. For certain symmetries[2], increasing the mass of the structure can incorporate

---

[2] Added-mass tables are available in "Structural Vibrations in a fluid", Chapter 14, see bibliography item no. 4

the added mass. Added mass effect tends to decrease the natural frequency of the structure compared to that in dry vacuum. The added mass of an oscillating structure strongly depends on:

- The geometry of the surface of the structure.

- The amplitude and direction of vibration relative to the free stream velocity.

- A Reynolds number like parameter $fD2/v$ where f is the frequency of vibration, D is a characteristic diameter and v is the kinematic viscosity.

The added mass effect for a still fluid and oscillating fluid can be given by the following relationships (Blevins, 1979)

$$A_{StillFluid} = \rho F_e (geometry, \frac{X_o}{D}, \frac{fD^2}{\upsilon}) \text{ and}$$
<div align="right">Eq(2.11)</div>

$$A_{VibFluid} = \rho F_e (geometry, \frac{U_o}{fD}, \frac{U_o D}{\upsilon})$$

where X_o is the amplitude of vibration and U_o is the amplitude of the fluid velocity which oscillates with frequency f in a given plane.

The resultant natural frequency due to the added mass is given by (Blevins, 1979)

$$\frac{f_{fluid}}{f_{vaccum}} = \frac{1}{(1+\frac{A}{m})^{\frac{1}{2}}}$$
<div align="right">Eq(2.12)</div>

where A is the added mass per unit length obtained from tables and m is the mass of the structural material per unit length. f_{fluid} gives the resultant natural frequency.

2.4.2 Added Mass Moment of Inertia

Added mass moment of inertia of the fluid entrained by the structure as it rotates about a fixed point. Similar to the added mass, the added mass moment of inertia increases the effective mass moment of inertia of the vibrating structure. If the structure has certain symmetries, the added mass moment of inertia can be incorporated directly in the analysis to obtain the final response. In FEA models, the added mass moment of inertia can be ignored if a sufficient number of elements are present. If the elements are small, the mass moments of inertia of individual elements are negligible. The added mass moment of inertia will be accounted for in a distributed manner. Added mass moment of inertia tables are available (*see footnote 2*).

2.4.3 Added Damping

Added damping is contributed by a damping forces that occurs due to water viscosity. The damping force is assumed to be directly proportional to the relative speed between the structure and the fluid for a linear response. The damping force can be expressed by

$$Q = b\,(\dot{x} - \dot{y}\,e^{-kD})$$

Eq(2.13)

where $\dot{x}$ is the speed of the structure, $\dot{y}\,e^{-kD}$ is the vertical component of the fluid particle speed and b is the linear coefficient of friction. For a continuous structure oscillating at its natural frequency in one mode in the y-direction, the equivalent viscous damping coefficient for vibration in that direction is

19

$$\zeta = \frac{\int\limits_0^L \int\limits_0^T F_D \, \overset{o}{y}(t)\psi(z) \, dt \, dz}{2\pi \int\limits_0^L m(z)[\overset{0}{y}(t)]_{max}^2 \, \psi^2(z) \, dz} \qquad \text{Eq(2.14)}$$

where the numerator term is the energy expended in damping. The lower integral is proportional to the maximum kinetic energy of the structure. $[\overset{0}{y}(t)]_{max}^2$ is the maximum squared velocity achieved during one period (T) of vibration. F_d is the damping force per unit length in Y direction, $Y(z,t) = \psi(z)y(t)$ is the total displacement of the structure in the y direction, m(z) is the mass per unit length of the structure including the mass of entrained fluid, and z is the spanwise coordinate extending from z = 0 to z = L.

2.5 Vibrations Induced by an Oscillating Flow

The in-line forces associated with the oscillating flow are the inertial force acting in phase with the acceleration of the flow, and a drag force, which acts in phase with the velocity of the flow. The solution of linearized equations of motion for in-line motion is given by (Blevins, 1977)

$$\frac{\omega_N}{\omega_0} = \frac{\zeta_N}{\zeta_0} = \frac{1}{(1 + \frac{\rho A C_I}{m_o})^{1/2}} \qquad \text{Eq(2.15)}$$

where $\omega_o = (k_x/m_o)^{1/2}$ – circular natural frequency in vacuum
$\omega_N = (k_x/m)^{1/2}$ – circular natural frequency in fluid
ζ_0 – damping factor in vacuum
ζ_N – damping factor in fluid
k_x – effective spring constant
C_I – added mass coefficient
A – cross-sectional area

ρ – density of fluid
m_0 – mass per unit length of structure
m – total mass per unit length (inc. added mass)

The total damping in the structure for an oscillatory flow with zero mean flow is obtained using the following equation (Blevins, 1979)

$$\zeta_N = \frac{\zeta_0}{(1+\frac{\rho A C_1}{m_o})^{1/2}} + \frac{1}{\pi}(\frac{\rho D^2}{m})(\frac{U_m}{\omega_N D})C_D \qquad \text{Eq(2.16)}$$

where U_m – mean fluid velocity
       C_D – coefficient of discharge of fluid

To incorporate the effects of cross-sectional geometry, influence factors are added, which are available in Table 6.1 in Chapter 6 of *"Flow-induced vibration"* (*See bibliography*).

2.6 Ship Motion in a Seaway

2.6.1 Introduction

It is essential to predict the nature of sea waves and the response of a floating structure to the sea waves to meet the following criteria:

- The floating structure must not experience structural failure and should be capable of working under damaged conditions.

- The floating structure must not develop excessive motions to prevent the use of critical machinery in heavy seas.

21

- The floating structure must have acceptable levels of passenger and crew comfort.

The primary difference between the analysis of a ship motion in a seaway to that of flow-induced vibrations discussed above is in the treating of ship motions as rigid body motions (ship deformations are negligible). The sea motion being non-deterministic, is replaced within the limits of linearity and the response of the ship to a complex sea can be found by summing the responses of a ship to a series of regular waves. This analysis can be extended to other large floating platforms. Connected platforms must consider the elasticity of the connector.

There are 3 translatory motions and 3 rotational motions associated with this analysis:

3 Translatory motions:

η_1 = surge (in the direction of the headway)

η_2 = sway (horizontally perpendicular to the direction of the headway)

η_3 = heave (translatory oscillation in the vertical direction)

3 Rotational motions:

η_4 = roll (about the longitudinal axis)

η_5 = pitch (about the transverse axis)

η_6 = yaw (about the vertical axis)

2.6.2 Stability

The forces acting on a ship in sea motion can be summarized as follows:

- The gravitational force acting downwards at the center of gravity (CG) of the structure. This point is fixed unless the mass of the ship is shifted about.

- The net buoyancy force acting upward with its center at the center of mass of the fluid displaced by the ship. This point unlike the CG depends on the oscillation of the ship with respect to the sea.

- In the case where the center of gravity is above the center of buoyancy, the ship is stable when the center of buoyancy is directly above the center of gravity. When the ship rolls slightly a righting moment tends to restore the ship to equilibrium if the center of buoyancy moves towards the center of gravity. However, if the center of buoyancy moves further away from the CG, the ship becomes unstable. Therefore the ship's stability increases as the width or beam increases.

- For structures where the beam is not wide or cannot be made wide, stability is achieved by having the center of gravity below the center of buoyancy, and the structure has pendulum stability. Buoyancy tanks can be used for achieving this stability, as is the case with submarines.

- The metacentric height GM is the difference between the heights in CG and the center of buoyancy. The value is positive for stable ships (Figure 2.1).

| (a) ship at equilibrium | (b) stable ship (moment tends to return ship to equilibrium) | (c) unstable ship (moment tends to increase roll) |

G – Center of gravity; B – Center of buoyancy
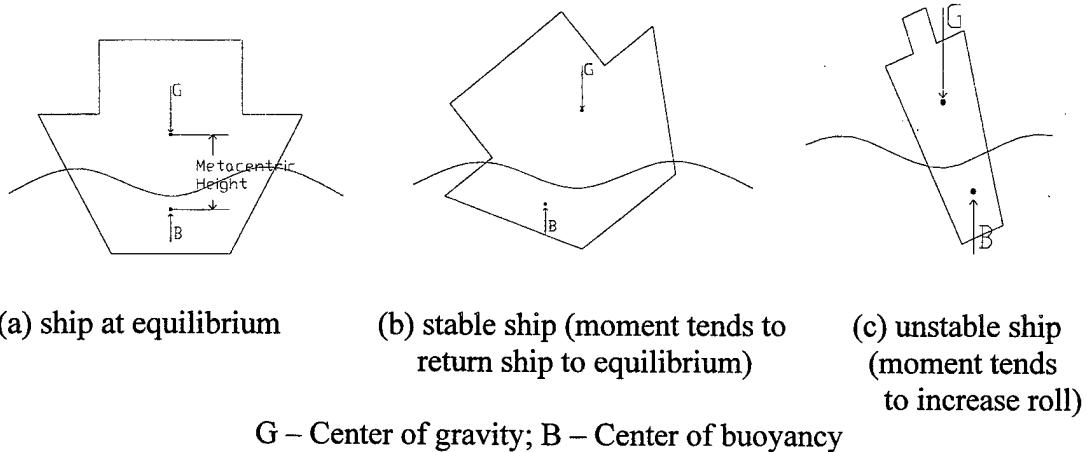
Figure 2.1: Stability of Ship in Roll

2.6.3 Natural Frequencies

The natural frequency of roll, pitch and heave are given by the following equations:

2.6.3.1 Natural Frequency of Roll

The natural roll of a ship in motion will have a frequency of ω_R (rad/s) given by the following relationship (Blevins, 1977)

$$\frac{\omega_R}{2\pi} = f_R = \frac{1}{2\pi}(\frac{\rho V_d gGM}{I_{44} + A_{44}})^{1/2} \qquad \text{Eq(2.17)}$$

where

	f_R	-	Roll frequency (Hz)
	ρ	-	Water density
	V_d	-	Volume of water displaced by hull
	I_{44}	-	Polar mass moment of inertia for rotation about longitudinal axis
	A_{44}	-	Polar mass moment of inertia of the added mass of water entrained by the hull.
	g	-	Acc. due to gravity
	GM	-	Metacentric height

The formula is simplified by noting that I_{44} is proportional to mass of ship multiplied by the square of the beam.

$$f_R = \frac{c_4(g*GM)^{1/2}}{b}$$

c_4 -   Prop. Constant (0.35 – 0.4)
GM -   Metacentric height
b   -   Beam of the ship

The average natural frequency of most ships is generally between 0.033Hz to 0.25Hz. The larger the ship, the lower the natural frequency of roll.

2.6.3.2 Natural Frequency of Pitch

The natural pitch of a ship in motion will have a frequency ω_P (rad/s) given by the following relation (Blevins, 1977)

$$\frac{\omega_P}{2\pi} = f_P = \frac{1}{2\pi}\left(\frac{\rho g \int_L x^2 b(x)dx}{I_{55} + A_{55}}\right)^{1/2}$$

Eq(2.19)

where f_P -   Pitch frequency (Hz)
ρ -   Water density
I_{55} -   Polar mass moment of inertia for pitch of the ship
A_{55} -   Polar mass moment of inertia of the added mass of water entrained by the hull as the hull pitches.
g   -   Acc. due to gravity
b(x)   -   Beam of the ship as a function of x.
L   -   Length of the ship

The formula is simplified by noting that $I_{55} + A_{55}$ is proportional to ML^2, and $\rho g \int_L x^2 b(x)dx$ is proportional to MgL^2/d we get

$$f_P = c_5(g/d)^{1/2} \qquad \text{Eq(2.20)}$$

where f_P - pitch frequency (Hz)

              c_5 - prop. Constant (0.13)

              g - acc. due to gravity

              d - depth of hull

An asymmetry about the transverse (y) axis in the ship results in a net vertical force on the ship as the ship pitches, which causes the ship to heave. As a result the pitch and heave motions of the ships are generally intercoupled.

2.6.3.3 Natural Frequency of Heave

The natural pitch of a ship in motion will have a frequency ω_H (rad/s) given by the following relation (Blevins, 1977)

$$\frac{\omega_H}{2\pi} = f_H = \frac{1}{2\pi}\left(\frac{\rho g S}{M + A_{33}}\right)^{1/2} \qquad \text{Eq(2.21)}$$

where f_H - Heave frequency (Hz)

              ρ - Water density

              A_{33} - Added mass of water

              g - Acc. due to gravity

              S - Plane area enclosed by the waterline

              M - Mass of the ship

The formula is simplified by noting that $M + A_{33} \propto \rho S d$, we get

$$f_H = c_3(g/d)^{1/2} \qquad \text{Eq(2.22)}$$

where f_H - pitch frequency (Hz)

              c_3 - prop. Constant (0.13)

              g - acc. due to gravity

              d - depth of hull

The pitch and heave are approximately the same for ships that are not symmetric about the transverse axis (heaving also induces pitch).

2.7 Sea Waves and Wave Spectrums

Given the random nature of waves, it is difficult to describe ocean waves and wave forces as realistically as possible. For the purposes of theoretical investigation, a random sea state is simulated using the linear wave theory. The discussion on sea waves is introduced with a description of sea state representation and an introduction to linear wave theory and concludes with a brief introduction to wave spectrums, namely the Bretschneider and Ochi wave spectrum formulas.

2.7.1 Sea State Representation

Wind driven waves are classified into sea states based on observation on the oceans of the world (Berteaux, 1976).

- Sea State 0 – No measurable wind speed and glassy smooth seas (significant wave heights from 0-0.08 feet).

- Sea State 5 – Normal sea state (significant wave heights from 8-10 feet).

- Sea State 7 – Air operations are no longer possible and MOB modules may need to be disconnected (significant wave heights from 22-50 feet).

- Sea State 9 – Severe hurricane force winds where wave heights can reach 200 feet (significant wave heights greater than 90 feet).

The MOB is expected to function at a sea state of 5.

2.7.2 Linear Wave Theory

The linear wave theory assumes that the fluid is incompressible, frictionless, irrotational, and that the wave height is small in comparison to the wavelength and ocean depth, d (Figure 2.2). The significant wave height is the average of the 1/3 highest waves and the significant wave period represents the period of maximum energy content. At a sea state of 5, the significant wave height is 10 feet and significant wave period is 6.9 sec.
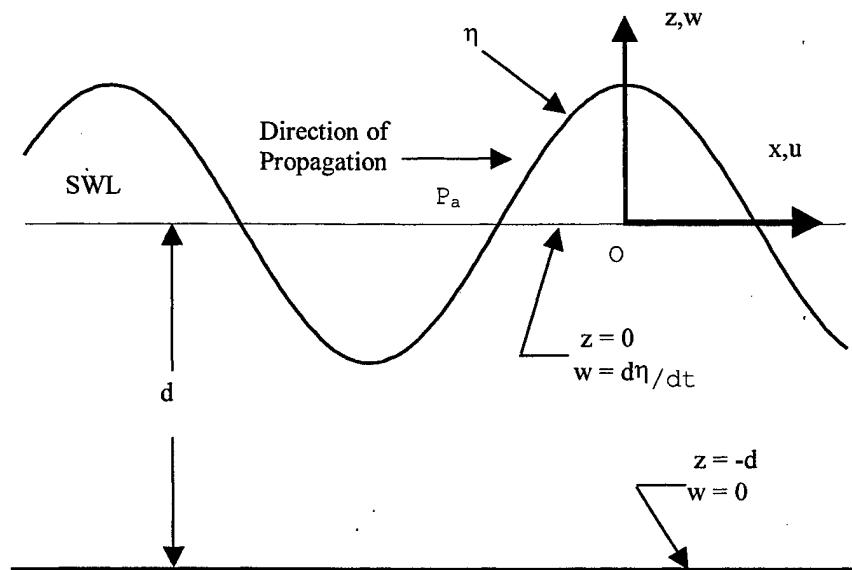

Figure 2.2: Schematic Representation of a Simple Harmonic Wave

The linear wave theory is also known as the small amplitude wave theory. The solution to the linear small amplitude wave theory can been summarized by the following equations (Wilson, 1984):

28

Surface profile	$\eta = A\cos(kx - \omega t)$	Eq(2.23)
Horizontal particle velocity	$u = \dfrac{2\pi A}{T}\dfrac{\cosh k(z+d)}{\sinh kd}\cos(kx - \omega t)$	Eq(2.24)
Vertical particle velocity	$w = \dfrac{2\pi A}{T}\dfrac{\sinh k(z+d)}{\sinh kd}\sin(kx - \omega t)$	Eq(2.25)
Horizontal particle acceleration	$\overset{0}{u} = \dfrac{4\pi^2 A}{T}\dfrac{\cosh k(z+d)}{\sinh kd}\sin(kx - \omega t)$	Eq(2.26)
Vertical particle acceleration	$\overset{0}{w} = \dfrac{-4\pi^2 A}{T}\dfrac{\sinh k(z+d)}{\sinh kd}\cos(kx - \omega t)$	Eq(2.27)
Dynamic pressure	$p = \rho g A\dfrac{\cosh k(z+d)}{\cosh kd}\cos(kx - \omega t)$	Eq(2.28)
Wave celerity	$c = \left[\dfrac{g}{k}\tanh kd\right]^{\frac{1}{2}}$	Eq(2.29)
Group velocity	$c_g = c * \dfrac{1}{2}\left[1 + \dfrac{2kd}{\sinh(2kd)}\right]$	Eq(2.30)

2.7.3 Wave Loading

Wave loading is a case where the fluid structure interaction involves a free surface. Of the number of techniques have been proposed for calculating wave loads on offshore structures, the most comprehensive of these involves three dimensional models for both the fluid and structure with full interaction (Riggs, 1991). These are computationally enormous and simplified methods are present for design purposes. One such method is the Morison's Equation approach (Morison, 1950) applicable to vertical cylinders subject to surface wave loading. It assumes that the force acting

29

transverse to the cylinder axis is made up of two components: a drag force, analogous to the drag on a body subjected to steady flow of a real fluid associated with wake formation behind the body; and an inertia force, analogous to that on a body subjected to a uniformly accelerated flow of an ideal fluid. For a circular cylinder of diameter D, Morison's Equation is expressed as

$$F = \frac{1}{2}\rho D C_D u|u| + \frac{1}{4}\rho\pi D^2 C_m \frac{du}{dt} \qquad Eq(2.31)$$

where F is force per unit length, u is fluid velocity, C_D is a drag coefficient, C_m is an inertia coefficient, and r is the fluid density. The first term in this equation corresponds to the drag force and the second term represents the inertia force. In general the coefficients C_D and C_m vary with time and space with average values of 0.9 and 1.94 (Sarpkaya, 1981).

2.7.4 Wave Spectrums

For the scale model testing, the waves are generated using the Bretschneider and Ochi formulas. The Bretschneider Double Height Spectra formula is an empirical spectral density function with significant wave height, H_s, significant wave period, T_s, arbitary time period, T, and component wave height, S, as parameters (Berteaux, 1976) and is given as

$$S_{2H}(T) = \frac{4200 * H_S^2}{T_S^4 * (\frac{2\pi}{T})^5} * e^{-\frac{1050}{T_S^4 * (\frac{2\pi}{T})^4}} \qquad Eq(2.32)$$

An example of the Bretschneider Double Height Spectra is shown below (Figure 2.3 – see appendix B for MathCAD sheet)
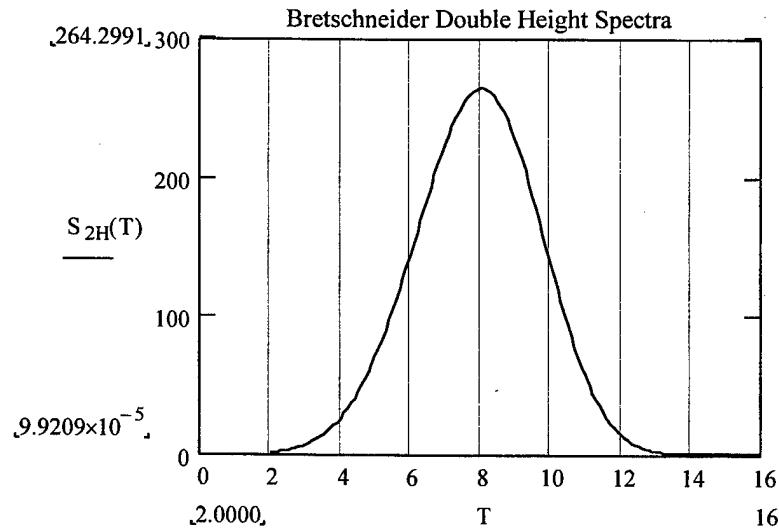
Figure 2.3: Bretschneider Double Height Spectra

Ochi and Hubble (1976) combined two sets of three-parameter spectra, one representing low frequency components and the other the high frequency components of the wave energy and derived the following Six-Parameter OCHI spectral representation

$$S(\omega) = \frac{1}{4}\sum_j \frac{\left(\dfrac{4\lambda_j+1}{4}\omega_{mj}\right)^{\lambda_j}}{\Gamma(\lambda_j)} \frac{\zeta_j^2}{\omega^{4\lambda_j+1}} * e^{-\left(\frac{4\lambda_j+1}{4}\right)\left(\frac{\omega_{mj}}{\omega}\right)^4} \qquad Eq(2.33)$$

An example of the OCHI Six-Parameter Spectra is shown below (Figure 2.4 – see appendix B for MathCAD sheet)

31
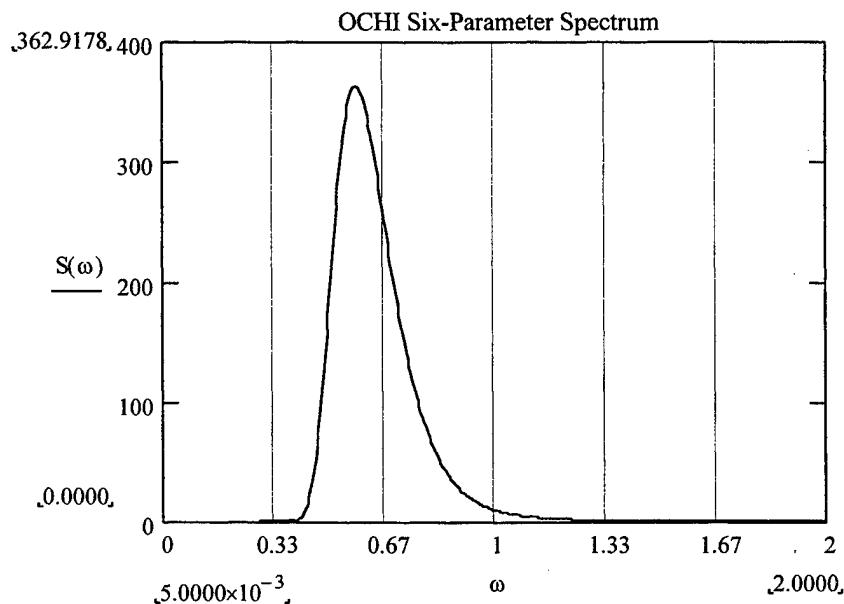
Figure 2.4: OCHI Six-Parameter Spectrum

where j=1,2 stands for the lower and higher frequency components. The six parameters ζ_1, ζ_2, ω_{m1}, ω_{m2}, λ_1, and λ_2 are determined numerically such that the difference between theoretical and observed spectra is minimal and Γ is the Gamma function.

2.7.5 Wave Conditions

Wave conditions can be primarily classified into small and large waves. Random seas are further classified by three different unidirectional representations, namely, head seas, beam seas and bow quartering seas (Figure 2.5).
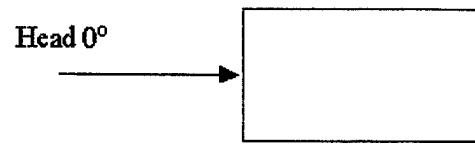
(a) Head Sea
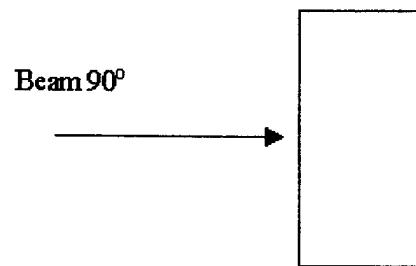
(b) Beam Sea
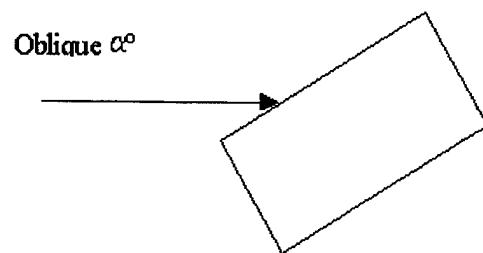
(c) Quartering Sea

Figure 2.5: Three Unidirectional Random Seas

Chapter 3

Physical Scale Model, Data Reduction, and Visualization Technique

3.1 Physical Scale Model

The design of the physical scale hydroelastic model (Figure 3.1) is based on the test

objectives, facility size and capability (Sikora, 1998). The test was based on the

assumption that the response of the structure affects the loads on the structure. Due to

conflicting non-dimensional requirements (e.g., Froude and Reynolds numbers), the

focus has been on using a structural scaling of the model. The elastic properties of the

scale model are designed such that the natural frequencies, flexibilities, and

displacements are within a range that could be expected of a fully scaled MOB.
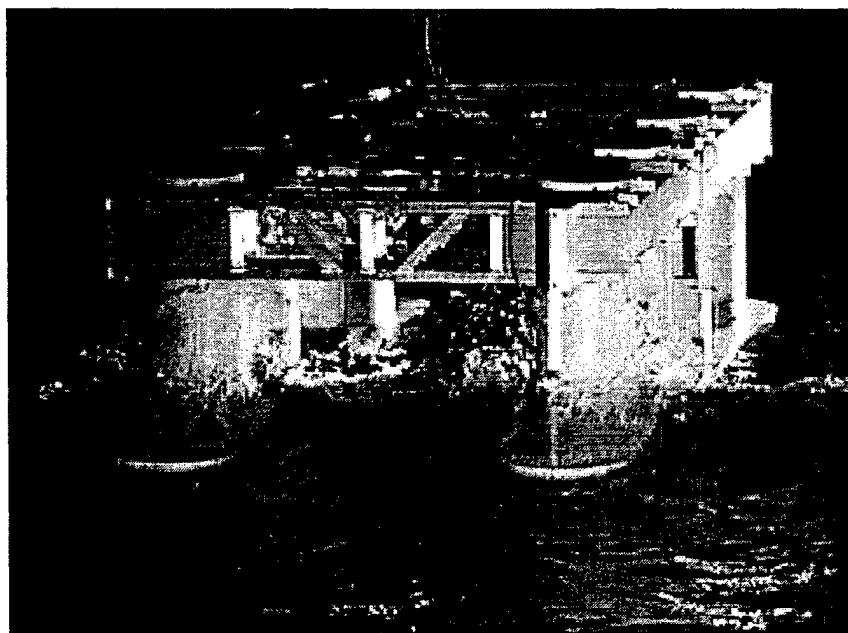
(a) Single Module Scale Model Test
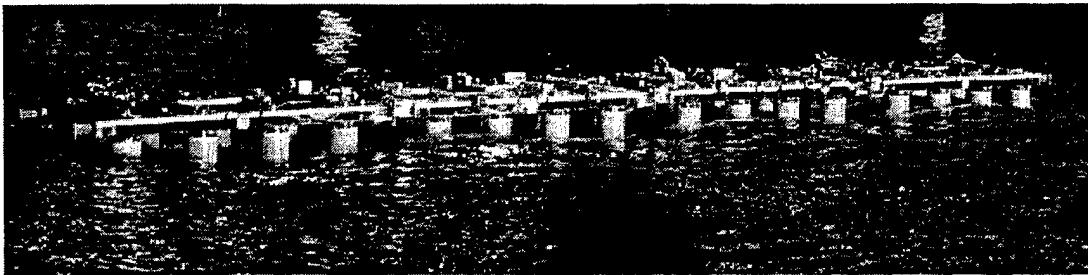
(b) Four Module Scale Model Test

Figure 3.1: Scale Models under Testing

3.1.1 Wave Tank

In designing the physical scale model, the following concerns are taken into account:

- The largest possible physical scale model should be used for testing to minimize model scale effects and maximize measurement signal to noise (S/N) ratio. This would also minimize frictional force effects (Reynolds) as opposed to inertial force effects (Froude).

- The wave tank should be large enough to avoid blockage or wall effects at head, following and oblique wave headings.

- Wave makers must be able to generate good quality waves.

From the above it has been determined that the NSWCCD Maneuvering and Seakeeping (MASK) Facility (Figure 3.2) meets all these requirements. The physical characteristics of the MASK basin are 350 feet long by 240 feet wide. Based on using the NSWC MASK, a model scale ratio of 60 was chosen for the MOB model. At this model scale factor the total model length of a four module unit is just over 100 feet long, which will avoid wall effects in the NSWC MASK facility.
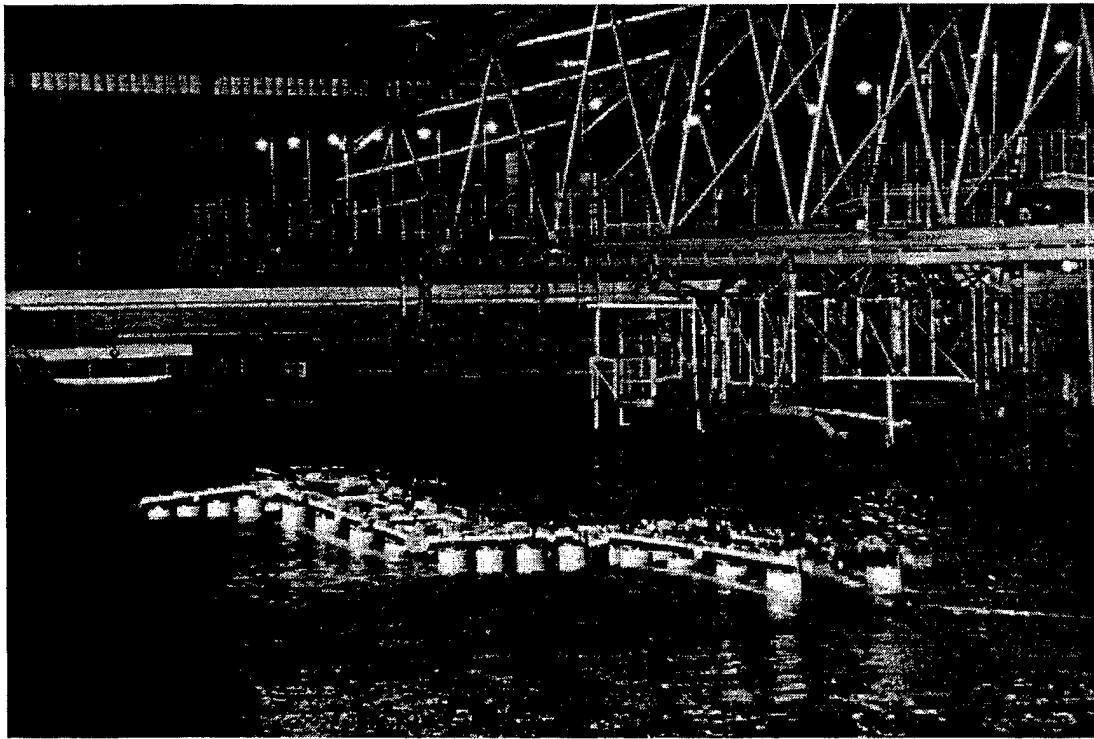
Figure 3.2: NSWC MASK Test Facility

3.1.2 Hull Form

The scale dimensions of each module hull are approximately 240 inches long, 100 inches wide, 48 inches high. It displaces 5253 pounds. This translates into a full scale MOB module 1200 feet long, 500 feet wide, displacing roughly 50,700 tons. The pontoons, or lower hulls, will be 216 inches long by 28 inches wide by 10 inches deep with a volume of 56,394 in^3. The pontoon has elliptical end pieces 34 inches long, leaving 148 inches of parallel middle body. The body plan and back lines are rectangular cross sections 10 inches high. The pontoon is thus designed to be perfectly wall sided. The corners are given a small radius to avoid a sharp edge. The columns are designed as cylinders 40 inches tall with 20-inch diameters. There are four columns per pontoon located symmetrically about midships. The column centers are

27 and 81 inches fore and aft of midships. There is no special shaping where the column meets the pontoon or upper box. The columns on each side are connected with 3 inch square PVC cross braces. These provide structural support for prying and squeezing. The centers of the cross brace will be 14 inches above the baseline, or 4 inches above the top of the pontoon. Model structural segmentation is achieved by attaching segments representing the hull attached to the continuous space frame connected by cross pieces. The pontoon will be made of four segments of equal length each. Each segment has a column. The modules will not be self-powered nor be remotely controlled. Bungee chords maintain the heading relative to the waves.

3.1.3 Internal Structure

NSWCCD has primarily considered three approaches for designing elastic models. In the first approach, all the scantlings, decks, and bulkheads of the prototype are scaled in a fully structural model. This will result in correctly scaled overall structural properties. Small models, usually constructed with polyvinyl chloride (PVC) measure the structural behavior as well as seaway loads of larger metal scales, the structural members conforming to external geometry. The major disadvantage of such a model is that it requires detailed prototype design and construction drawings, which is difficult to achieve with a notional MOB scale model. This model is more applicable when detailed MOB design has been established and can be used to evaluate the distribution of the connector loads into the support structure in the box.

In the second approach, a flexible beam (backspline) model is used to measure vertical bending, vertical shear, lateral bending, lateral shear, and torsion. This model is appropriate for monohull ships that can be idealized as a simple beam in bending and measures only loads. In reality, however, the load paths from the pontoons through the columns into the box are three dimensional in nature and cannot be modeled by a simple flexible beam. This is the major disadvantage of this model.

In the third approach, a three-dimensional space frame is designed to represent the overall rigidity of each module to measure the responses of interest. The upper hull consists of a structural ladder containing two rails that are aligned over the columns and correspond to the primary load path from the end connectors. The rails of the ladder provide the stiffness for vertical and lateral bending of the box while the number, size and stiffness of the rungs determine the torsional properties. Vertical bars attached to the rails of the ladder model the stiffness properties of the columns. The stiffnesses of each of the lower hulls are also modeled by rails attached to the column members. Structural foils connecting port and starboard columns complete the three-dimensional space frame. Non-load bearing segments, corresponding to the external geometry, are attached to the structural members. The major advantages of this model are cost and the ability to model the structural properties, modal shapes and frequencies.

Of the above three approaches, the third was selected due to its obvious advantages. A notional MOB model with a conceptual ladder (Figure 3.3) was chosen as the most appropriate structure for measuring seaway loads on the box. The structural members are built up plastic (PVC) box beams, tubing or I-beams. Finite

element analyses of the designs were performed to confirm that all of the desired stiffnesses were actually present. The complete model of each MOB module is obtained by encasing the structural members with the lower hulls, columns, and upper box composed of an appropriate shell material such as fiberglass, wood, or plastic.
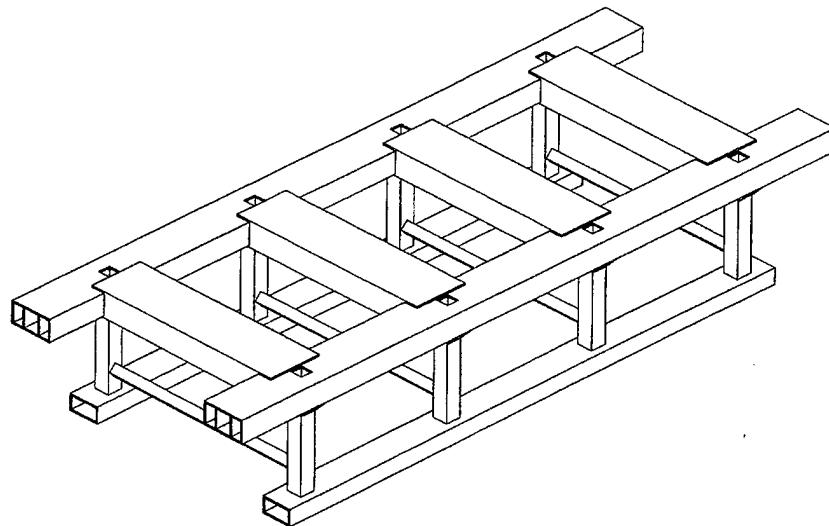
(a) Structural Space Frame
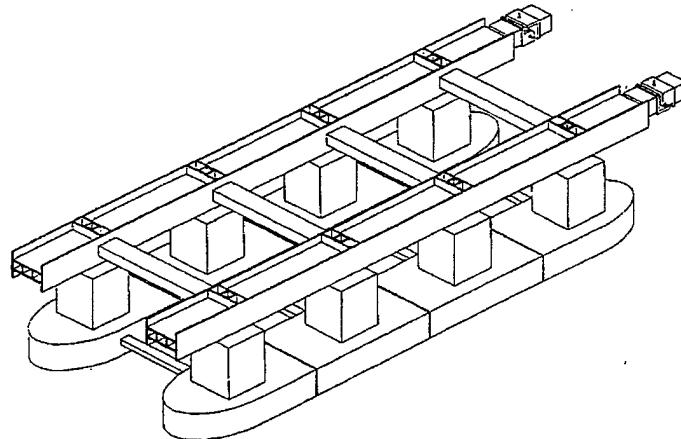
(b) Lower Hulls and Columns Encasing Structural Members

Figure 3.3: MOB Structural Model

39

3.1.4 End Connectors

The connection of the modules to each other is achieved through a notional connector (Figure 3.4). The connector represents a realistic stiffness for the axial loads that cause vertical bending, lateral bending, and torsion in the modules. For these model tests, multi-parameter load cells will be used to measure the connector forces.

(a) MOB connector attached to rail end   (b) 34" MOB Model Connector
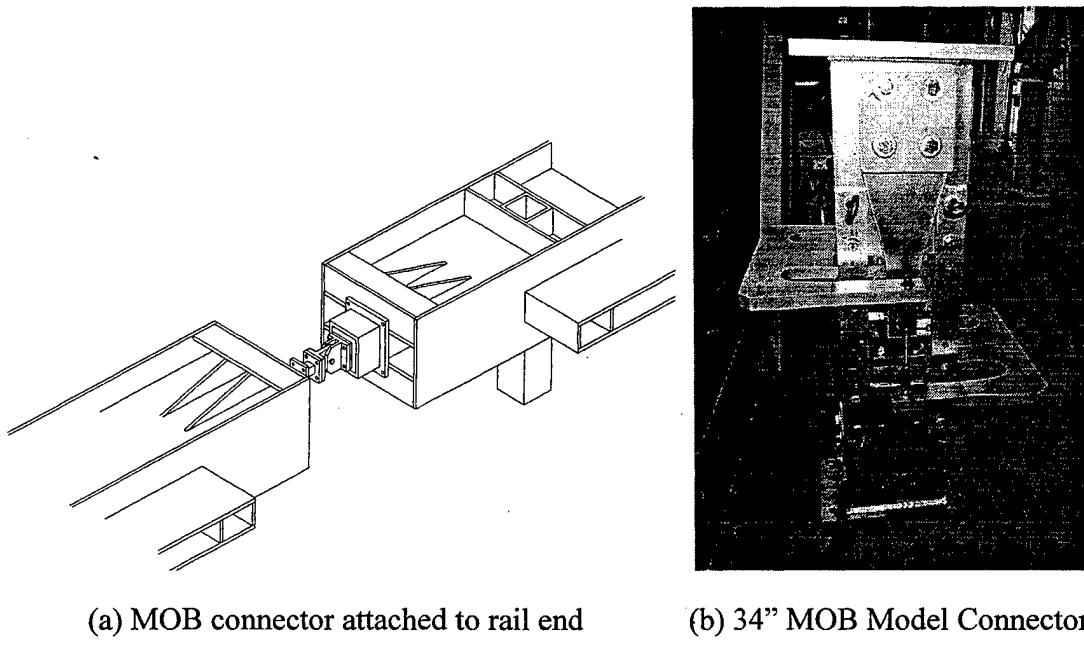
Figure 3.4: MOB Connector

3.1.5 Ballasting

In order to maintain the possible motion and period values of a full-scale model, each module is ballasted using a combination of lead weight and floodable space. To float at a 23-inch draft, the model displaces 5253 lbf. The model (structure and shell) and data measurement system weigh approximately 2000 lbf. The lead weight (989 lbfs) is used to adjust the draft up to 11 inches. The remaining 2255 lbfs of ballast is in floodable ballast tanks in the pontoons. These tanks are completely flooded to avoid

any sloshing. Each tank has plugs on the top and bottom and sloping sides to ensure complete flooding and drainage.

3.1.6 Instrumentation

The primary instrumentation on the model consists of load cells for measuring inter-modular connector loads. The space frame is instrumented with strain gages for the measurements of internal module loads and mode shapes. Pressure gauges and panel sized pressure sensors are also installed to provide measurements of the hydrostatic pressure fields and local wave impacts. The first order six degree of freedom motions are measured or calculated for each module by use of triaxial accelerometers (Figure 3.5). Connector responses were measured through a specially designed force transducer. This device isolated the vertical, longitudinal and transverse forces and moments using a set of four pins at each connector location. Video and photographic documentation of the tests have been conducted. The far and near field wave measurements will be used as the inputs and outputs for analysis.

(a) Single Module

41

Port Connector

| 16 | 15 | 14 | 13 | | 8 | 7 | 6 | 5 |

Y ← ⌐
     ↓
     X

Bow

| 12 | 11 | 10 | 9 | | 4 | 3 | 2 | 1 |

Starboard Connector

(b) Two-Module

Port Connector

| 32 | 31 | 30 | 29 | | 24 | 23 | 22 | 21 | | 16 | 15 | 14 | 13 | | 8 | 7 | 6 | 5 |

Y ← ⌐
     ↓
     X

Bow

| 28 | 27 | 26 | 25 | | 20 | 19 | 18 | 17 | | 12 | 11 | 10 | 9 | | 4 | 3 | 2 | 1 |

Starboard Connector
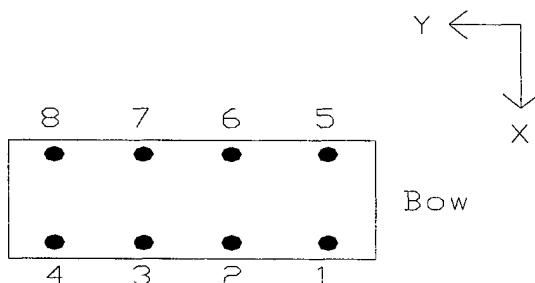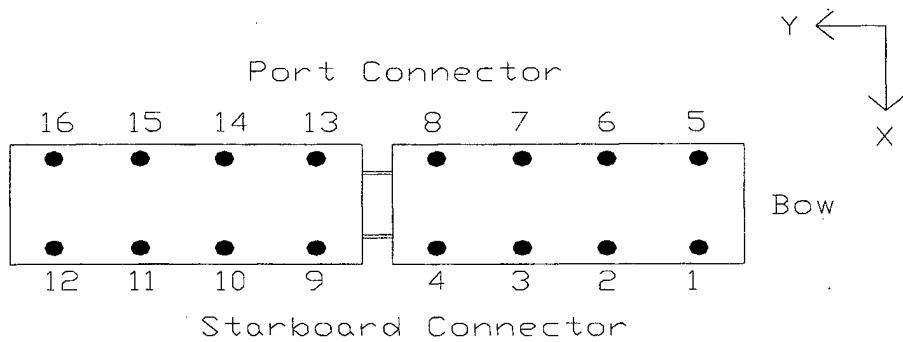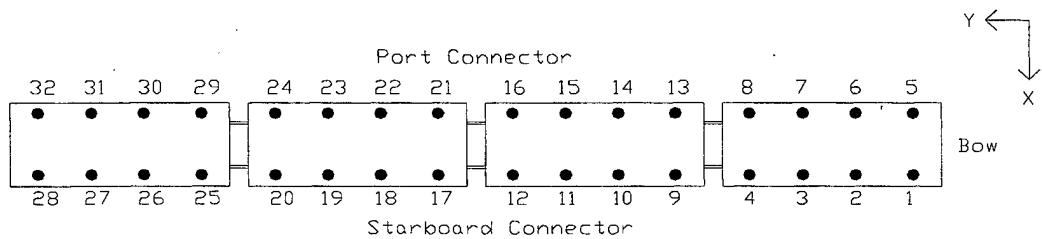
(c) Four-Module

Figure 3.5: Location of tri-axial accelerometers

3.2 Data Reduction

In order to perform a dynamic data analysis, a program, Integrated Test and Analysis Processor (ITAP™) distributed by Measurements Analysis Corp. was chosen which runs as a subset of MATLAB™ and is currently distributed by Measurements Analysis Corp. Importing of large sets of data into MATLAB™ is very time-consuming and inefficient. Hence efficient data reduction techniques are required.

The MOB data sets were oversampled to allow for post test digital filtering. Also, many more channels were recorded than are required to meet the objectives of the current analysis. To alleviate the processing difficulties, an application program called DynamicData (Figure 3.6) was written at the University of Maine in DELPHI™.

The purpose of this program is to read in the large MOB data set, reduce the data set to a subset of selected channels, filter the data, decimate the data, compute the power spectra, the FRF, the phase and the coherence based upon a selected reference channel. It also allows channels to be averaged. This is particularly useful in averaging the Z accelearations to obtain the heave acceleration response in the absence of a heave sensor. It also provides a graphical visualization of the results. Multiple records can be processed utilizing different windows and overlapping of records. This program writes a reduced data set for faster processing with MATLAB™ and EXCEL™.
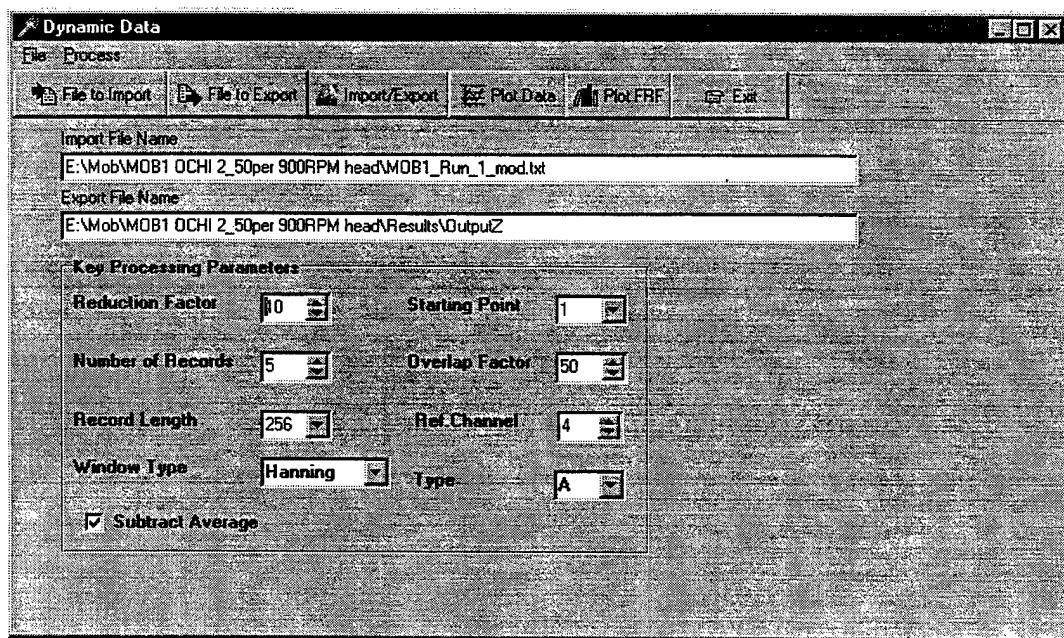

Figure 3.6: DynamicData Program

3.2.1 Differentiation and Integration Scheme

In order to perform analysis of the experimental data, the heave motion response is to be extracted from the averaged Z acceleration measurements from the accelerometers on the scale model. The velocity of the wave response $w(t)$, $\overset{o}{w}(t)$ is obtained using the built in differentiation tools of MATLAB™. MATLAB™ does not have built in integration tools for integration based on random data vectors. In order to obtain the heave motion, the average heave acceleration needs to be integrated twice. This integration is achieved using the constant acceleration method.

The constant average acceleration method uses an initial velocity condition and calculates the velocity based on the area under the curve (Figure 3.7) between two points on the time history of the acceleration data.
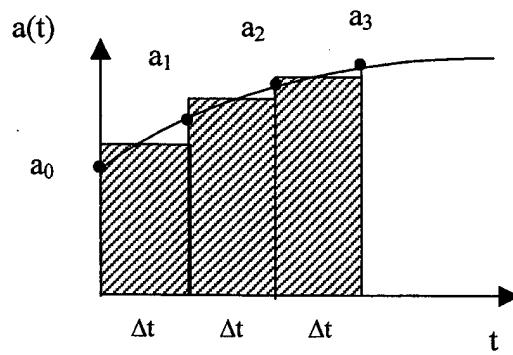

Figure 3.7: Constant Acceleration Method of Integration

The change in velocity, Δv, is given by the area of the curve given by the following equation

$$\Delta v = a_0 * t + \frac{a_1 - a_0}{2} * \Delta t$$

Eq(3.1)

44

The velocity is given by the following equation

$$V_{i+1} = V_i + \Delta v \qquad\qquad Eq(3.2)$$

The MATLAB™ code for the above is given below (given an acceleration vector 'a' of size 'm' with time step 'dt'):

```
v = zeros(m,1);
for i=1:(m-1)
        dt = Time(i+1,1)-Time(i,1);
        da = a(i+1,1) - a(i,1);
        dv = a(i,1)*dt + 0.5*da*dt;
        v(i+1,1) = v(i,1) + dv;
end
```

3.2.2 Noise Removal (Filtration)

Using the integration scheme discussed above, the acceleration time history profile shown in Figure 3.8(a) yields the corresponding velocity time history profile shown in Figure 3.8(b). It can be seen from the velocity profile, that the integration scheme has introduced a low frequency noise that needs to be removed. Applying filters directly to the time history velocity profile introduces changes to the amplitude and phase of the integrated velocity profile. Hence noise removal is achieved in the frequency domain. The Fast Fourier Transform (FFT) of the velocity obtained is shown in Figure 3.8(c) and the low frequency noise is removed from the profile, shown in Figure 3.8(d). The high pass frequency cut-off limit is determined through visual inspection of noise and in this analysis is determined to be 0.1 Hz, i.e., all frequencies of 0.1 Hz or lower are removed as being noise. The inverse of the filtered velocity FFT gives the required time history profile of the velocity, shown in Figure 3.8(e). To obtain the displacement time profile, the technique is repeated on the velocity time history data.
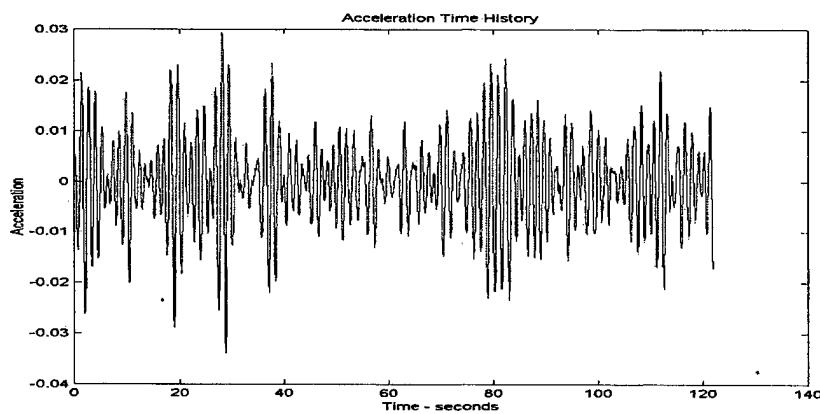
(a) Acceleration Time History
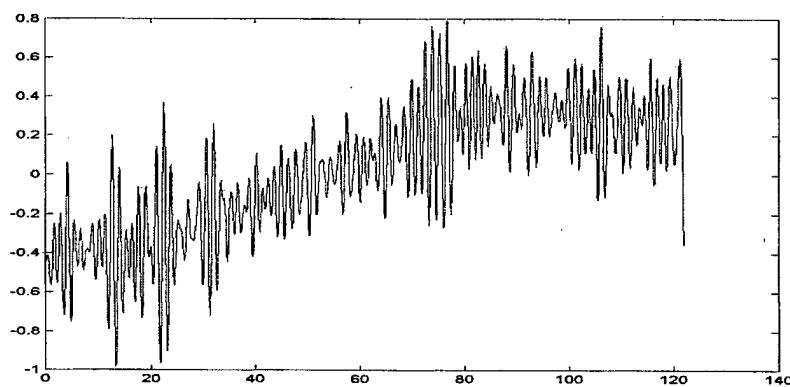
(b) Integrated Acceleration (Velocity) Time History
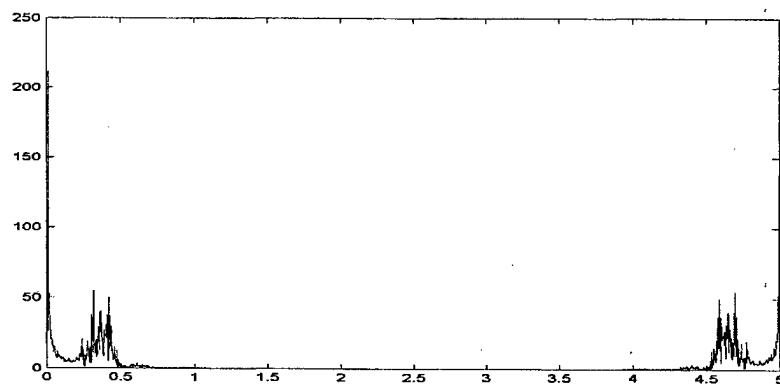
(c) Frequency Spectrum of Velocity Time History
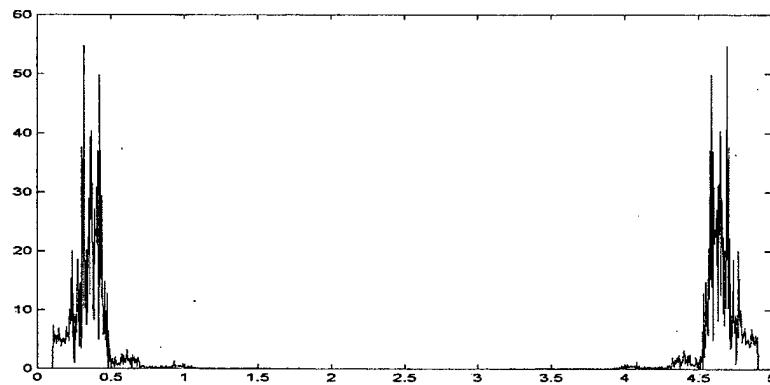
(d) Filtered Frequency Spectrum
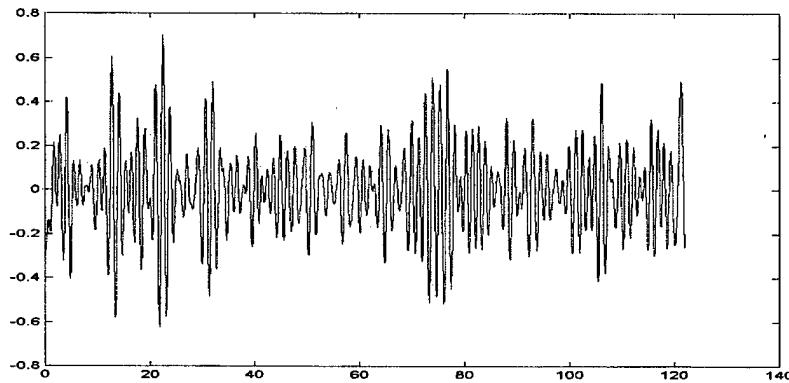
(e) Inverse FFT – Filtered Velocity

Figure 3.8: Noise Filtration Technique

The above procedure is designed as a function *dsp_diff* for differentiation and

dsp_int for integration (code listed in appendix C) with the following syntax

$$[y, v, a] = dsp\_diff(a\_t, sfreq, FMax, Wn)$$
$$[y, v, a] = dsp\_int(a\_t, sfreq, FMax, Wn)$$

where y, v, a = the displacement, velocity and acceleration
       a_t   = input time history data for acceleration (a = at)
       sfreq   = sampling frequency
       FMax   = max frequency range
       Wn   = high pass frequency value (freq < Wn = noise)

3.3 Visualization Technique

To get a better understanding of response of the MOB scale model, an animation program called MOB_Animate was written at the University of Maine in DELPHI™ (Figure 3.9). This program reads one, two and four module data containing the X, Y and Z acceleration data of all the sensors in the frequency domain along with the phase information. It accounts for the time lag in response of sensors located at different points along the MOB scale model and animates the response of the model at different frequencies. This allows for better visual understanding of the MOB structure response. The front, side, top and isometric views of the structure can be seen and the response amplitude can be scaled. There are 8 triaxial accelerometers for each module which are represented by black lines and the connectors are shown using red lines. The connectors simply connect the ends of the modules and are not constrained in any way.
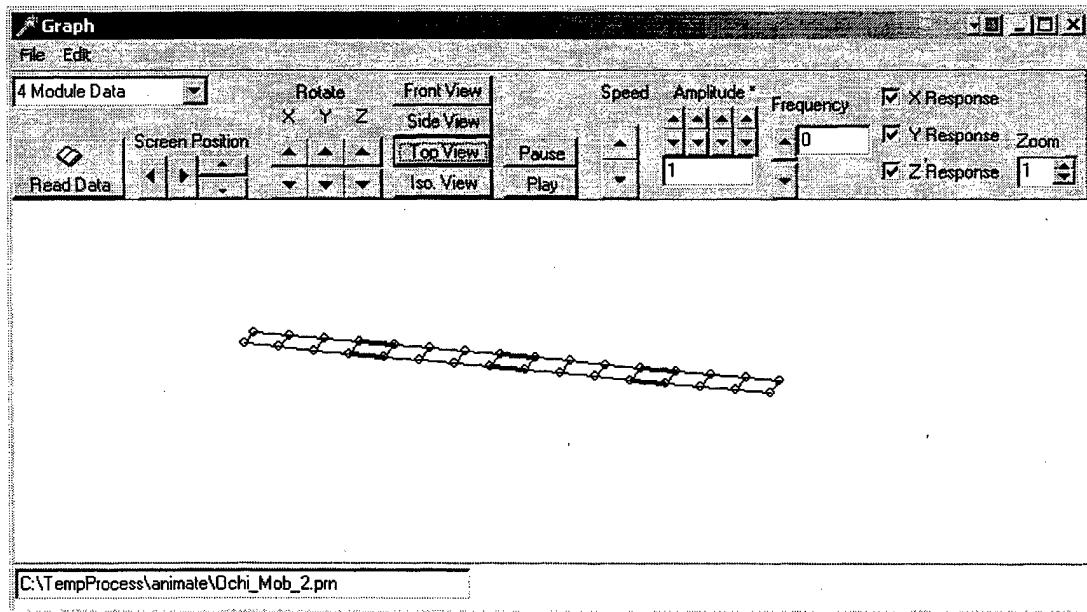
Figure 3.9: MOB_Animate Animation Program

48

To assess the vibration mode shape at a particular frequency the relative FRF amplitude and phase information are used to reconstruct the shape based upon the expression:

$$x_i = A_i \sin(2\pi f_i t + \phi_i) \qquad \text{Eq}(3.3)$$

At a particular frequency, the time parameter can be chosen to correlate to a particular degree of phase shift. In doing so, the change in shape of a particular mode over one period of oscillation can be ascertained.

Chapter 4

Frequency Response Functions, SI/SO and MI/SO Analysis

4.1 Frequency Response Functions

Frequency response functions (FRF) are used to describe the input-output (e.g., wave-heave) relationship of a given system (Alleman, 1995). For experimental modal analysis, the frequency response function is the most important measurement to be made. For linear or nearly linear systems, the FRF is assumed to be linear. For nonlinear systems, the measurement of the FRF may also be dependent upon the independent variables. In this way, a conditional frequency response function is measured as a function of the input amplitude and of the other independent variables in addition to frequency. Before estimating the FRF the following important aspects need to be remembered:

- The dynamic properties of the system determines the frequency response functions for given input/output parameters.

- It is important to eliminate or minimize all errors (aliasing, leakage, noise, calibration, etc.) when collecting data.

- If all noise terms are identically zero, the assumption concerning the source/location of the noise does not matter. Hence eliminating the source of noise is important.

- Modal parameters are only as accurate as the FRF they are estimated from.

FRF's can be based on four different configurations of input and outputs: (a) Single input/single output (SI/SO), (b) Single input/multiple output (SI/MO), (c) Multiple input/single output (MI/SO), and (d) Multiple input/multiple output (MI/MO). The SI/SO is used for time invariance problems between measurements. The SI/MO is applied in time invariance problems between measurements from different inputs. The MI/SO detects repeated roots and is used where there are more than one input in a measurement cycle. The MI/MO is generally the best overall testing scheme with consistent frequency and damping for all data acquired simultaneously.

The estimation of the FRF is based on the transformation of data from the time domain to the frequency domain. Computationally, a fast Fourier transform (FFT) is used to convert a time history data into the frequency domain. The frequency response function(s) satisfy the following single [Eq(4.1)] and multiple [Eq(4.2)] input relationships where X is the input, F is the output and H is the FRF function

Single Input Relationship

$$X_P * H_{PQ} = F_Q$$

Eq(4.1)

Multiple Input Relationship

$$\begin{bmatrix} X_1 \\ X_2 \\ \cdot \\ \cdot \\ X_P \end{bmatrix}_{N_o \times 1} * \begin{bmatrix} H_{11} & \cdot & \cdot & \cdot & H_{1Q} \\ H_{21} & & & & \cdot \\ \cdot & & & \cdot & \cdot \\ \cdot & & & \cdot & \\ H_{P1} & \cdot & \cdot & \cdot & H_{PQ} \end{bmatrix}_{N_o \times N_i} = \begin{bmatrix} F_1 \\ F_2 \\ \cdot \\ \cdot \\ F_Q \end{bmatrix}_{N_i \times 1}$$

Eq(4.2)

A sample FRF generated by the Dynamic Data program for a single input and single output is shown (Figure 4.1). For a multiple input case, the FRF has two values, component FRF value and cumulative FRF value.

(a) Frequency Composition of Input (Wave Input)

(b) Frequency Composition of Output (Heave Output)

(c) FRF Function from Input to Output
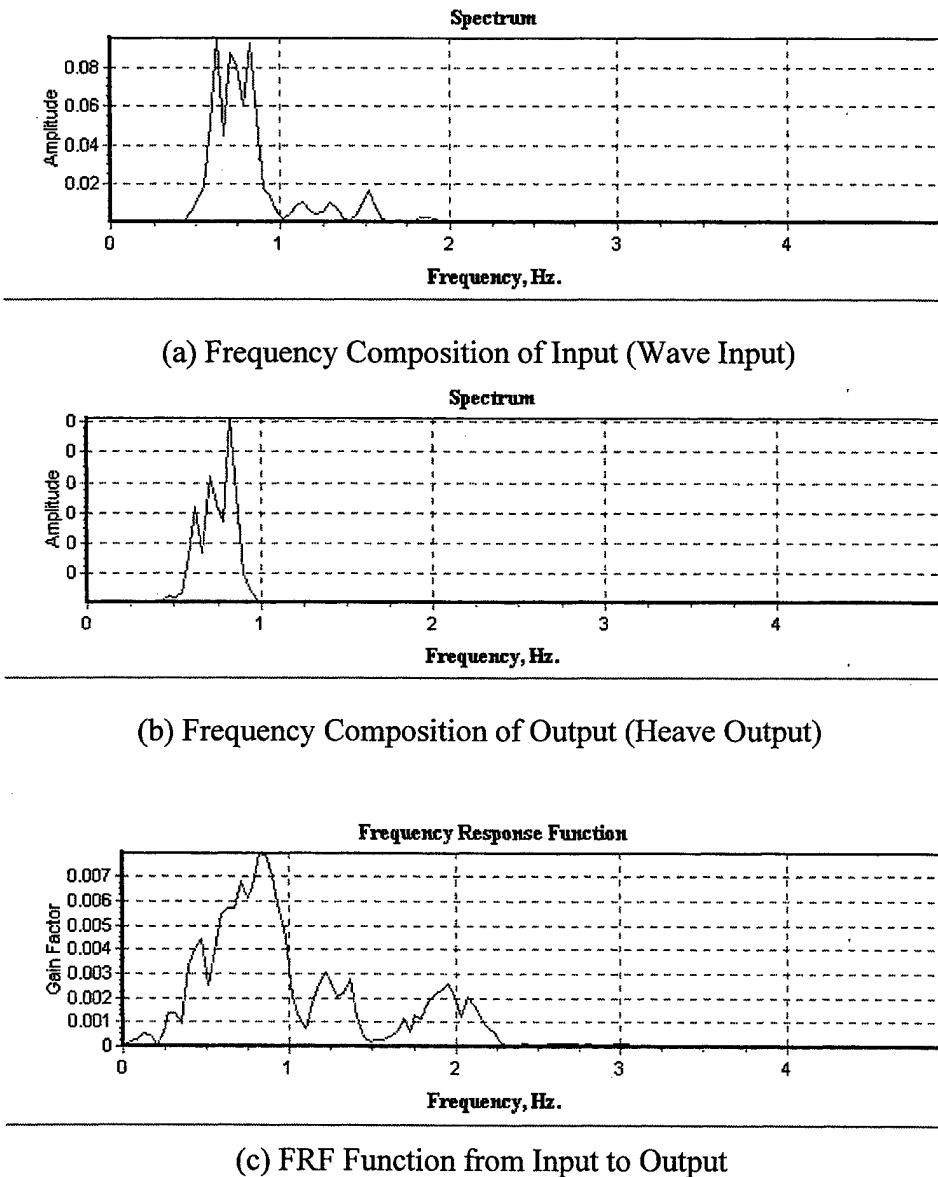
Figure 4.1: Sample FRF for a SI/SO Function

4.1.1 Coherence Function

The scalar or ordinary coherence function is a frequency dependent function carrying a real value between zero and one. The ordinary coherence function indicates the degree of causality in a frequency response function. If the coherence is equal to one at any specific frequency, the system is said to have perfect causality at that frequency. In other words, the measured response power is caused totally by the measured input power. A coherence value less than unity at any frequency indicates that the measured response power is greater than that due the measured input. This could possibly be the extraneous noise contributing to the output power or nonlinearity in the system. Low coherence does not necessarily imply poor estimates of the frequency response function, but suggests more averaging for reliable results. The ordinary coherence function (for the system depicted by Eq(4.1) is computed as follows:

Cross Power Spectra

$$GXF_{PQ} = \sum_{1}^{N_{avg}} X_P F_Q^*$$ Eq(4.3)

$$GXF_{QP} = \sum_{1}^{N_{avg}} F_Q X_P^*$$ Eq(4.4)

N_{avg} is the number of averages used to minimize the random errors (variance), F^* is the complex conjugate of $F(\omega)$ and X^* is the complex conjugate of $X(\omega)$. Using the above, the ordinary coherence function is given by:

$$COH_{PQ} = \gamma^2_{PQ} = \frac{|GXF_{PQ}|^2}{GFF_{QQ} \ GXX_{PP}} = \frac{GXF_{PQ} \ GFX_{PQ}}{GFF_{QQ} \ GXX_{PP}}$$ Eq(4.5)

53

In general, the coherence can be a measure of the degree of noise contamination in a measurement. With more averaging, the coherence may contain less variance, giving a better estimate of the noise energy in the measured signal if there are no bias errors. The coherence function corresponding to the FRF shown above (Figure 4.1) generated by the Dynamic Data program for a single input and single output is shown (Figure 4.2)
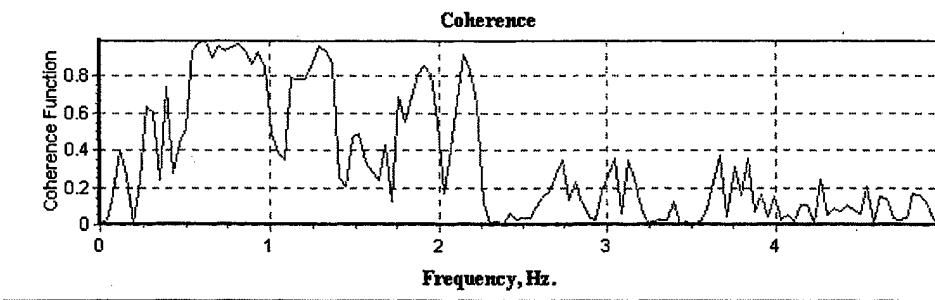

Figure 4.2: Coherence Function for a SI/SO FRF shown in Figure 4.1

Comparing the coherence function to the FRF, it can be observed that the coherence function is high between the range of 0.4-1 Hz, and the FRF also shows a significant response in the same frequency band. Similarly, the coherence shows good causality in the region between 1.75-2.25 Hz excluding 2 Hz, which is supported by the FRF.

Two special cases of low coherence are particularly important. The first case of low coherence is due to *leakage error* occurring in one or both of the input and output measurements. This causes the coherence in the area of the peaks of the frequency response to be less than unity. This can be reduced by the use of weighting functions or cyclic averaging. The second case occurs when a significant *propagation time delay* occurs between the input and the output. If a propagation delay of length *t* is compared

to a sample function length of T, a low estimate of coherence will be estimated as a function of the ratio t/T. This propagation delay causes a bias error in the frequency response and should be removed prior to computation.

4.1.2 Phase

The phase of the FRF is the shift of a periodic signal (output) compared to a reference (input) signal of the same frequency. It is obtained by computing the angle using the four-quadrant arc tangent of the division of the imaginary over the real values of the FRF.

$$\theta = \arctan\left(\frac{imag(FRF)}{real(FRF)}\right)$$ Eq(4.6)

The phase function corresponding to the FRF and coherence functions shown above (Figures 4.1 and 4.2) is shown below (Figure 4.3).
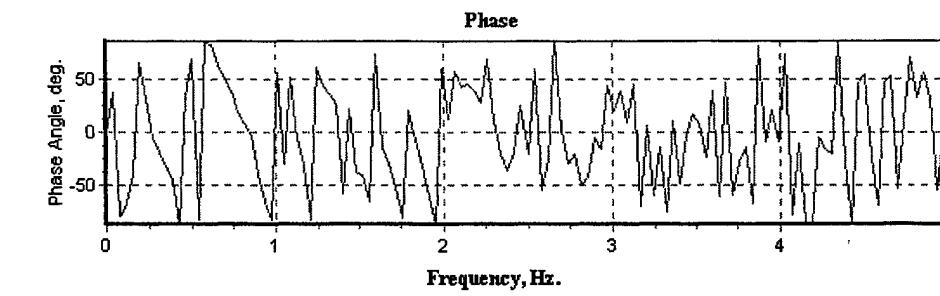

Figure 4.3: Phase Function for a SI/SO FRF

4.2 SI/SO & MI/SO Analysis

The dynamic response of a single module scale model can be best analyzed using the SI/SO technique for linear response characteristics and MI/SO technique for nonlinear

55

characteristics. Tests with small waves are expected to yield linear results only and tests with large waves are expected to yield both linear and nonlinear results. The main objective of the analysis is to identify appropriate linear and nonlinear integrodifferential equations of motion that can describe the scale model motions in waves. The SI/SO and MI/SO analyses are performed using the direct and reverse techniques. The MI/SO direct and reverse techniques are carried out using two-input/single-output and three-input/single-output models. The following important conclusions were drawn up regarding SI/SO and MI/SO analysis (Bendat, 1998):

- For SDOF linear systems, the SI/SO linear method can correctly identify the system frequency response functions.

- For SDOF nonlinear systems, the Reverse MI/SO Technique can correctly identify the system frequency response functions.

- For SDOF nonlinear systems, SI/SO based optimum linear frequency response function estimates can give erroneous results compared to Reverse MI/SO techniques.

- Serious mistakes can occur when nonlinear effects are undetected between SI/SO and Reverse MI/SO results.

In order to develop the theoretical basis for the response of the single module scale model, its response can be characterized by a six degree of freedom motion model shown below (Figure 4.4).

56
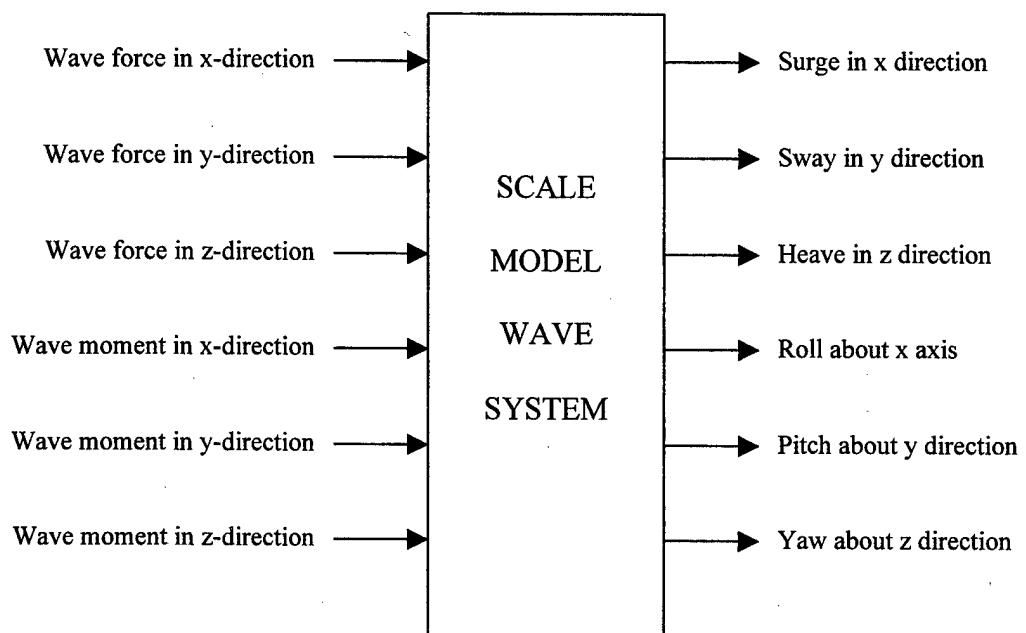
(a) Physical Input/Output Model
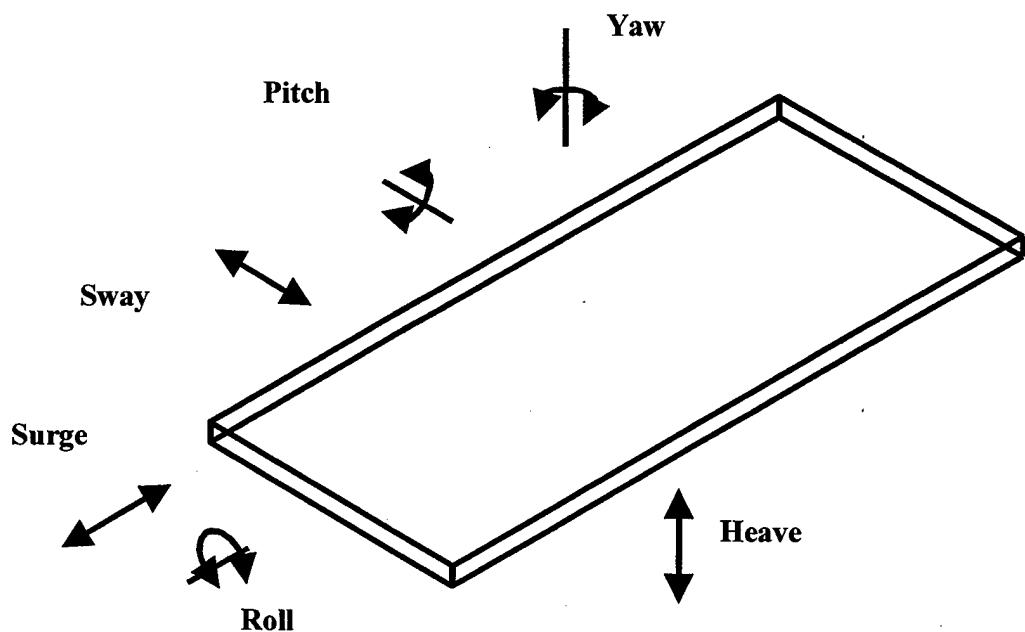
(b) Sea Motion

Figure 4.4: Six-DOF Sea Motion

4.2.1 Linear SI/SO Model

Three independent SI/SO models corresponding to the heave motion, roll angular rotation and the pitch angular rotation can be proposed. For small waves, a linear relationship can be assumed between the wave amplitudes and the resulting motions and rotations of the scale model

The heave differential equation of motion with constant damping and stiffness coefficients is given by

$$(m + a_{33})\ddot{z}(t) + c_{33}\dot{z}(t) + k_{33}z(t) = w(t) \qquad \text{Eq(4.7)}$$

where $z(t)$ is the physical heave motion output, $w(t)$ is the wave amplitude input, m is the mass of the scale model, and a_{33}, c_{33}, k_{33} are constants. Eq(4.7) can be extended to cover frequency-dependent damping and stiffness coefficients by using the heave linear integrodifferential equation of motion

$$(m + a_{33})\ddot{z}(t) + \int c_{33}(\tau)\dot{z}(\tau)(t-\tau)d\tau + \int k_{33}(\tau)z(t)(t-\tau)d\tau = w(t) \quad \text{Eq(4.8)}$$

where $c_{33}(\tau)$ and $k_{33}(\tau)$ are weighting functions. Taking the Fourier transforms of both sides of Eq(4.8) yields the simple mathematical formula

$$X(f)A(f) = Y(f) \qquad \text{Eq(4.9)}$$

58

where X(f) is the Fourier transform of mathematical input z(t) , Y(f) is the Fourier transform of mathematical output w(t) and A(f) is the frequency response function from z(t) to w(t) and is given by:

$$A(f) = K_{33}(f) - (2\pi f)^2 (m + a_{33}) + j(2\pi f)C_{33}(f) \qquad \text{Eq}(4.10)$$

where $K_{33}(\tau)$ and $C_{33}(\tau)$ are Fourier transforms of $c_{33}(\tau)$ and $k_{33}(\tau)$ respectively. Eq(4.9) is a reverse dynamic SI/SO model with the single mathematical input z(t) defined by X(f), and single mathematical output w(t) defined by Y(f). A(f) defines the linear system (Figure 4.5).

X(F) ⟶ A(F) ⟶ Y(F)
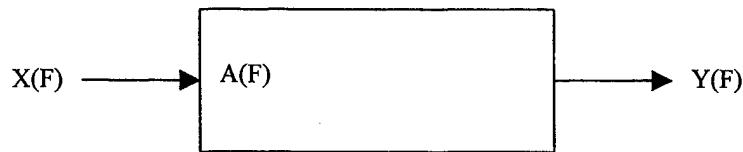
Figure 4.5: Reverse Dynamic Single-Input/Single-Output System

When X(f) represents the Fourier transform of the physical input x(t) = w(t), and when Y(f) represents the Fourier transform of the physical output y(t) = z(t), the direct dynamic data model is obtained (Figure 4.6). In reality, noise is present in the system which is represented by N(f) in the system. The reciprocal of A(f) gives the optimum linear frequency function H(f) for a direct system [Eq(4.11)]

$$H(f) = [A(f)]^{-1} \qquad \text{Eq}(4.11)$$
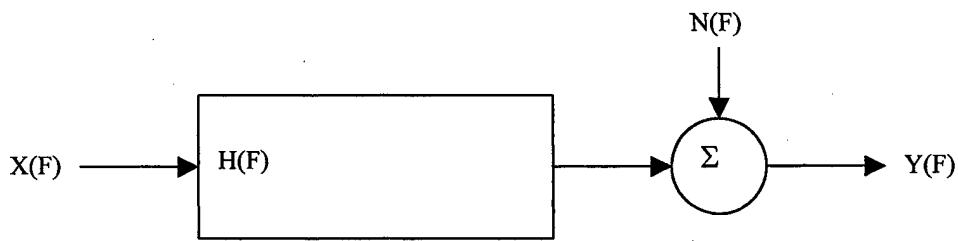
Figure 4.6: Direct Dynamic Single-Input/Single-Output Linear Model

Similarly the roll rotation differential equation of motion with constant damping and stiffness coefficients is given in Eq 4.12. The roll angular moment k(t) has been replaced by an appropriate linearly equivalent w(t).

$$(m + a_{44})\ddot{\phi}(t) + c_{44}\dot{\phi}(t) + k_{44}\phi(t) = w(t) \qquad \text{Eq(4.12)}$$

The pitch rotation linear differential equation of motion with constant damping and stiffness coefficients is given below. The pitch angular moment M(t) has been replaced by an appropriate linearly equivalent w(t).

$$(m + a_{55})\ddot{\theta}(t) + c_{55}\dot{\theta}(t) + k_{55}\theta(t) = w(t) \qquad \text{Eq(4.13)}$$

Eq(4.12) and Eq(4.13) can be extended to generate the model discussed by Eq(4.8-11).

4.2.2 Nonlinear MI/SO Model

Many MI/SO models can be proposed out of which special models relating to heave, roll and pitch motions occurring in head, beam and quartering seas are considered. These models have one linear input term and one or two parallel nonlinear input terms, where the first nonlinear term represents a nonlinear relative hydrodynamic damping force and the second nonlinear term represents a nonlinear restoring force. Both, Direct MI/SO and Reverse MI/SO techniques are proposed.

4.2.2.1 Direct MI/SO Nonlinear Model

The *direct* MI/SO two-input/single-output nonlinear integrodifferential equation of motion can be represented by

$$X_1(f)H_1(f) + X_2(f)H_2(f) = Y(f) \qquad \text{Eq(4.14)}$$

where $X_1(f)$ is the Fourier transform of the first physical input, $X_2(f)$ is the Fourier transform of second physical (nonlinear) input, $Y(f)$ is the Fourier transform of physical output, $H_1(f)$ is the frequency response function from $X_1(f)$ to $Y(f)$, and $H_2(f)$ is the frequency response function from $X_2(f)$ to $Y(f)$. This model is pictured below (Figure 4.8) with a noise term $N(f)$ representing deviations from the ideal model.

61
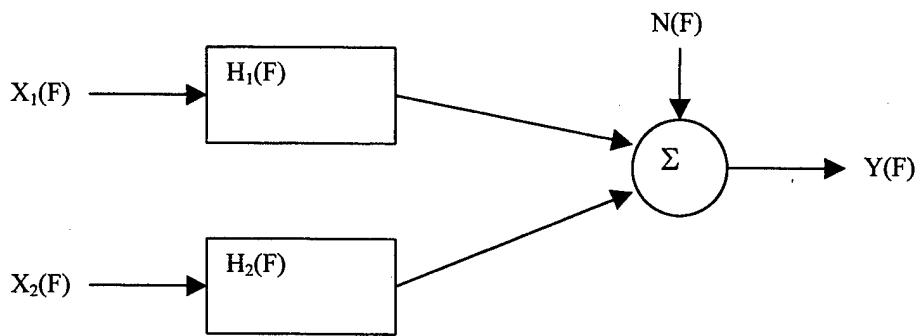
Figure 4.8: Direct Dynamic Two-Input/Single-Output Linear Model

The two-input model can be extended to a three-input model given by

$$X_1(f)H_1(f) + X_2(f)H_2(f) + X_3(f)H_3(f) = Y(f) \qquad \text{Eq(4.15)}$$

where $X_3(f)$ is the Fourier transform of the third physical (nonlinear) input. This model is pictured below (Figure 4.9) with a noise term N(f) representing deviations from the ideal model
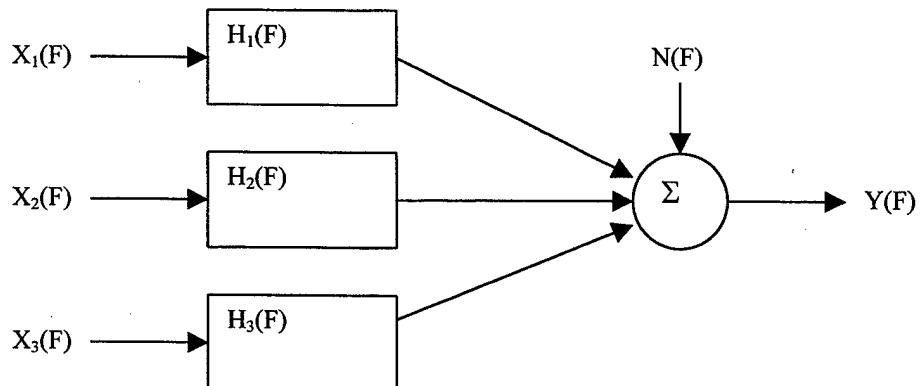

Figure 4.9: Direct Dynamic Three-Input/Single-Output Linear Model

The above two-input and three-input/single-output models can be extended to nonlinear models both in the time and frequency domain. In the time domain W and $\overset{o}{W}$ represent the wave motion w(t) and its derivative respectively. In the frequency domain they represent the Fourier transforms of the wave motion w(t) and the Fourier transform of its derivative respectively. Similarly, Z and $\overset{o}{Z}$ represent the heave motion z(t), P represents the pitch angle $\theta(t)$ and R represents the roll angle $\phi(t)$. The first input $X_1(f)$ is taken as the physical input from the wave w(t) and is given by

$$X_1(f) = W \qquad \text{Eq(4.16)}$$

The second input term $X_2(f)$ is a physical input for a nonlinear relative hydrodynamic damping force related to the relative velocity represented by:

$$X_2(f) = (\overset{o}{Z} - \overset{o}{W})^* \, | \, \overset{o}{Z} - \overset{o}{W} \, | \qquad \text{Eq(4.17)}$$

For three-input models the third input model $X_3(f)$ is a physical input for a nonlinear restoring force that varies for each case of interest. The output Y(f) is a physical output that varies for each case. For given input and output records, the cumulative coherence function and the associated values of the frequency response functions $H_1(f)$, and $H_2(f)$ in the two-input models and $H_1(f)$, $H_2(f)$, and $H_3(f)$ in the three-input models should be computed. The following two-input and three-input direct models are proposed for the direct MI/SO analysis:

63

Model D1: *Heave Motions in Head Seas Using Large Wave Data*

	Direct Two-Input Model	Direct Three-Input Model
X_1	W	W
X_2	$(\overset{o}{Z}-\overset{o}{W})^*\,|\,\overset{o}{Z}-\overset{o}{W}\,|$	$(\overset{o}{Z}-\overset{o}{W})^*\,|\,\overset{o}{Z}-\overset{o}{W}\,|$
X_3	0	$P^*\,|\,P\,|$
Y	Z	Z

Model D2: *Pitch Motions in Head Seas Using Large Wave Data*

	Direct Two-Input Model	Direct Three-Input Model
X_1	W	W
X_2	$(\overset{o}{Z}-\overset{o}{W})^*\,|\,\overset{o}{Z}-\overset{o}{W}\,|$	$(\overset{o}{Z}-\overset{o}{W})^*\,|\,\overset{o}{Z}-\overset{o}{W}\,|$
X_3	0	$P^*\,|\,P\,|$
Y	P	P

Model D3: *Heave Motions in Beam Seas Using Large Wave Data*

	Direct Two-Input Model	Direct Three-Input Model
X_1	W	W
X_2	$(\overset{o}{Z}-\overset{o}{W})^*\,|\,\overset{o}{Z}-\overset{o}{W}\,|$	$(\overset{o}{Z}-\overset{o}{W})^*\,|\,\overset{o}{Z}-\overset{o}{W}\,|$
X_3	0	$R^*\,|\,R\,|$
Y	Z	Z

Model D4: *Roll Motions in Beam Seas Using Large Wave Data*

	Direct Two-Input Model	Direct Three-Input Model
X_1	W	W
X_2	$(\overset{o}{Z}-\overset{o}{W})^*\,\lvert\overset{o}{Z}-\overset{o}{W}\rvert$	$(\overset{o}{Z}-\overset{o}{W})^*\,\lvert\overset{o}{Z}-\overset{o}{W}\rvert$
X_3	0	$R^*\,\lvert R\rvert$
Y	R	R

Model D5: *Heave Motions in Quartering Seas Using Large Wave Data*

	Direct Two-Input Model
X_1	W
X_2	$(\overset{o}{Z}-\overset{o}{W})^*\,\lvert\overset{o}{Z}-\overset{o}{W}\rvert$
Y	Z

Model D6: *Roll Motions in Quartering Seas Using Large Wave Data*

	Direct Two-Input Model
X_1	W
X_2	$(\overset{o}{Z}-\overset{o}{W})^*\,\lvert\overset{o}{Z}-\overset{o}{W}\rvert$
Y	R

Model D7: *Pitch Motions in Quartering Seas Using Large Wave Data*

Direct Two-Input Model

X₁	W
X₂	$(\overset{o}{Z}-\overset{o}{W})^{*}\,\lvert\,\overset{o}{Z}-\overset{o}{W}\,\rvert$
Y	P

4.2.2.2 Reverse MI/SO Nonlinear Model

The *reverse* MI/SO two-input/single-output nonlinear integrodifferential equation of motion can be represented by:

$$X_1(f)\,A_1(f)+X_2(f)\,A_2(f)=Y(f) \qquad\qquad \text{Eq(4.18)}$$

where $X_1(f)$ is the Fourier transform of the first mathematical input, $X_2(f)$ is the Fourier transform of second mathematical (nonlinear) input, $Y(f)$ is the Fourier transform of mathematical output, $A_1(f)$ is the frequency response function from $X_1(f)$ to $Y(f)$, and $A_2(f)$ is the frequency response function from $X_2(f)$ to $Y(f)$. This model is pictured below (Figure 4.10) with a noise term $N(f)$ representing deviations from the ideal model
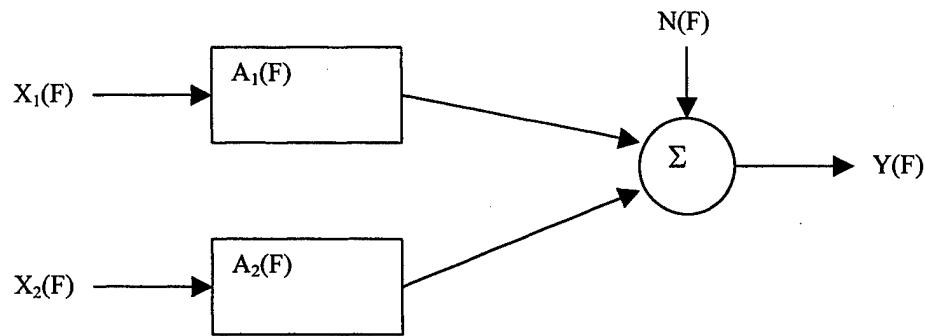
Figure 4.10: Reverse Dynamic Two-Input/Single-Output Linear Model

The two-input model can be extended to a three-input model given by

$$X_1(f)A_1(f) + X_2(f)A_2(f) + X_3(f)A_3(f) = Y(f) \qquad \text{Eq(4.19)}$$

where $X_3(f)$ is the Fourier transform of the third mathematical (nonlinear) input. This model is pictured below (Figure 4.11) with a noise term $N(f)$ representing deviations from the ideal models
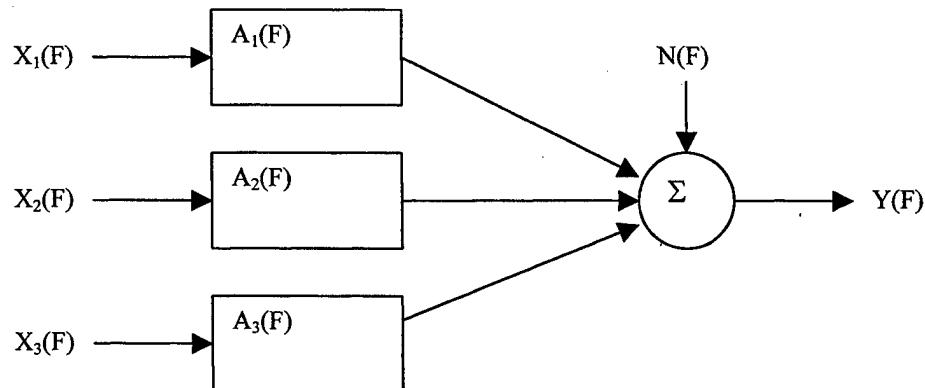

Figure 4.11: Reverse Dynamic Three-Input/Single-Output Linear Model

The above two-input and three-input/single-output models can be extended to nonlinear models both in the time and frequency domain. In the time domain W and $\overset{o}{W}$ represent the wave motion w(t) and its derivative respectively. In the frequency domain they represent the Fourier transforms of the wave motion w(t) and the Fourier transform of its derivative respectively. Similarly, Z and $\overset{o}{Z}$ represent the heave motion z(t), P represents the pitch angle $\theta(t)$ and R represents the roll angle $\phi(t)$. The first input $X_1(f)$ is taken as the mathematical input that varies with each case of interest. The second input term $X_2(f)$ is the same mathematical input for a nonlinear relative hydrodynamic term given in Eq 4.17 represented by:

$$X_2(f) = (\overset{o}{Z} - \overset{o}{W})^* | \overset{o}{Z} - \overset{o}{W} | \qquad \text{Eq(4.20)}$$

For three-input models the third input model $X_3(f)$ is a mathematical input for a nonlinear restoring force that varies for each case of interest. The output Y(f) is a mathematical output from the wave w(t) given by

$$Y(f) = W \qquad \text{Eq(4.21)}$$

For given input and output records, the cumulative coherence function and the associated values of the frequency response functions $A_1(f)$, and $A_2(f)$ in the two-input models and $A_1(f)$, $A_2(f)$, and $A_3(f)$ in the three-input models should be

computed. The following two-input and three-input direct models are proposed for the reverse MI/SO analysis:

Model R1: *Heave Motions in Head Seas Using Large Wave Data*

	Direct Two-Input Model	Direct Three-Input Model
X_1	Z	Z
X_2	$(\overset{o}{Z}-\overset{o}{W})^*\,\lvert \overset{o}{Z}-\overset{o}{W}\rvert$	$(\overset{o}{Z}-\overset{o}{W})^*\,\lvert \overset{o}{Z}-\overset{o}{W}\rvert$
X_3	0	$P^*\,\lvert P\rvert$
Y	W	W

Model R2: *Pitch Motions in Head Seas Using Large Wave Data*

	Direct Two-Input Model	Direct Three-Input Model
X_1	P	P
X_2	$(\overset{o}{Z}-\overset{o}{W})^*\,\lvert \overset{o}{Z}-\overset{o}{W}\rvert$	$(\overset{o}{Z}-\overset{o}{W})^*\,\lvert \overset{o}{Z}-\overset{o}{W}\rvert$
X_3	0	$P^*\,\lvert P\rvert$
Y	W	W

Model R3: *Heave Motions in Beam Seas Using Large Wave Data*

	Direct Two-Input Model	Direct Three-Input Model
X_1	Z	Z
X_2	$(\overset{o}{Z}-\overset{o}{W})*\mid\overset{o}{Z}-\overset{o}{W}\mid$	$(\overset{o}{Z}-\overset{o}{W})*\mid\overset{o}{Z}-\overset{o}{W}\mid$
X_3	0	$R*\mid R\mid$
Y	W	W

Model R4: *Roll Motions in Beam Seas Using Large Wave Data*

	Direct Two-Input Model	Direct Three-Input Model
X_1	R	R
X_2	$(\overset{o}{Z}-\overset{o}{W})*\mid\overset{o}{Z}-\overset{o}{W}\mid$	$(\overset{o}{Z}-\overset{o}{W})*\mid\overset{o}{Z}-\overset{o}{W}\mid$
X_3	0	$R*\mid R\mid$
Y	W	W

Model R5: *Heave Motions in Quartering Seas Using Large Wave Data*

	Direct Two-Input Model
X_1	Z
X_2	$(\overset{o}{Z}-\overset{o}{W})*\mid\overset{o}{Z}-\overset{o}{W}\mid$
Y	W

Model R6: *Roll Motions in Quartering Seas Using Large Wave Data*

Direct Two-Input Model

X_1	R
X_2	$(\overset{o}{Z}-\overset{o}{W})^*\|\overset{o}{Z}-\overset{o}{W}\|$
Y	W

Model R7: *Pitch Motions in Quartering Seas Using Large Wave Data*

Direct Two-Input Model

X_1	P
X_2	$(\overset{o}{Z}-\overset{o}{W})^*\|\overset{o}{Z}-\overset{o}{W}\|$
Y	W

4.3 SI/SO and MI/SO Analysis using the ITAP MATLAB Toolbox

The ITAP toolbox (M.A.Corp., 2000) provides several tools to perform random data processing. The version used runs on MATLAB version 5.3. Out of these, the following tools are used in the SI/SO and MI/SO analysis:

- *pre1* - Generate a single channel time history snapshot

    Syntax: pre1(X,dt,NFFT,namfil ,namch);

    A descriptive display of a single channel time history array, X, sampled over uniform time increments dt, is generated. Four plots appear in the display, namely, (1) a time-frequency spectrogram, (2) time history trace, (3)

71

autospectrum, (4) probability density. A window length, NFFT, is specified for spectrogram and autospectrum calculations. Alphanumeric names "namfil" (the data file name) and "namch" (the channel name) are specified for display labeling. This routine is used within the ITAP-T function module prelim.

- *sisogen* - Perform SI/SO analysis computations

    Syntax: [frq,HYX,COH,GYY,GXX,GYX] =

    sisogen(X,Y,dt,nwin,novl);

This ITAP-T function module performs SI/SO computations for one specific input time history channel (columns of the matrix, X) and one specific output time history channel (columns vector, Y), where the data is sampled over uniform time increments, dt. The FFT window length, nwin, and overlap processing index, novl, are specified as input parameters. Output arrays resulting from the MI/SO analysis consist of a frequency vector, frq, FRF array, HYX, and ordinary coherence array, COH. Additional output arrays consist of the output autospectrum, GYY, input autospectra, GXX, and output/input cross-spectra, GYX. This function module should only be used if GYY, GXX, and/or GYX are desired. Otherwise, use mimogen. This module performs computations using the MATLAB Signal Processing Toolbox function spectrum.

- *misogen* - Perform MI/SO Computations

      Syntax: [frq,HYX,COH,GYY,GXX,GYX] =

                              misogen(X,Y,dt,nwin,novl,iout);

This ITAP-T function module performs MI/SO computations for an arbitrary
number of input time history channels (columns of the matrix, X) and one
specific output time history channel (columns vector, Y), where the data is
sampled over uniform time increments, dt. The FFT window length, nwin, and
overlap processing index, novl, are specified as input parameters. The integer
parameter, iout, is used by a "waitbar" display to inform the user of
computation progress during MI/MO analyses. Output arrays resulting from
the MI/SO analysis consist of a frequency vector, frq, FRF array, HYX, and
ordinary or cumulative coherence array, COH. Additional output arrays consist
of the output autospectrum, GYY, input autospectra, GXX, and output/input
cross-spectra, GYX.

- *pwrspec* - Calculate and display the autospectrum or power spectral density of
a single channel time history array

      Syntax: [freq,gxx,stx]=pwrspec(tdata,dt,NFFT,namfil,namch);

This ITAP-T function routine calculates the autospectrum or power spectral
density of a single channel time history array X, sampled over uniform time
increments, dt. The user specifies a desired window length "NFFT" for the
spectral calculation. Alphanumeric names "namfil" (the data file name) and
"namch" (the channel name) are specified for display labeling. The output

arrays, freq, gxx and stx represent the frequency array, autospectrum, and tstandard deviation, respectively.

Chapter 5

Analysis of Single Module MOB Scale Model

This section presents the analysis of DynamicData sensors from testing of a single module MOB at NSWC-Caderock MASK facility. The MOB data sets consists of numerous sets predominantly of regular waves with several sets containing spectrally dispersed waves characterized by OCHI and Bretschneider spectra. The focus of this effort centers upon OCHI and Bretschneider data only.

From the data sets that have been made available, two wave spectrum cases listed below (Table 5.1) are analyzed:

Table 5.1: Single Module MOB Data Sets Analyzed

Data Set	Wave Spectrum	Specifications	Sea Condition
1	OCHI	2_50per 900RPM	Head Sea
2	Bretschneider	2_58per 1125RPM	Bow Quartering Sea (66°)

No wave spectra – type beam sea data was available for analysis. Each of the above data sets had the following data channels for analysis (Table 5.2)

Table 5.2: Summary of the Analyzed Hydrodynamic Data Channel Designations

Response Designation	Description	Ch. No.
PITCH_ANGLE	Pitch Angle	49
ROLL_ANGLE	Roll Angle	50
FWD WHT	Forward Wave Height - STBD	51
ACC1 X,Y,Z	X,Y,Z Accelerometer 1	137-39
ACC2 X,Y,Z	X,Y,Z Accelerometer 2	140-42
ACC3 X,Y,Z	X,Y,Z Accelerometer 3	143-45
ACC4 X,Y,Z	X,Y,Z Accelerometer 4	146-48
ACC5 X,Y,Z	X,Y,Z Accelerometer 5	149-51
ACC6 X,Y,Z	X,Y,Z Accelerometer 6	152-54
ACC7 X,Y,Z	X,Y,Z Accelerometer 7	155-57
ACC8 X,Y,Z	X,Y,Z Accelerometer 8	158-60

The eight Z accelerations were averaged and double interpolated using the DynamicData program to obtain the Heave response, as there is no heave sensor data. The heave response was obtained using the integration techniques discussed in Chapter 3. The velocity of the forward wave motion is obtained using the differentiation technique discussed in the same chapter. The original data set contains 272 channels sampled at 100 Hz. Since invalid data may be present in this time frame, a preliminary scan of the data is conducted to find the useful range of data. Once the range is determined, a reduction analysis routine was devised so that data from different data sets would be processed in a consistent manner. The following reduction scheme was applied:

- Filter data – a 30 pole FIR filter is used with cutoff of 1/10 of the sampling frequency. The average value is calculated and subtracted from the data set.

- Decimate data by a factor of 10, resulting in an effective sampling rate of 10 Hz and a Nyquist frequency of 5 Hz.

- Compute the power spectral density (PSD) using a 256 point FFT, a Hanning window, and an overlap of 50%. The final number of records depends on the useful range of data determined.

- Compute FRF – the frequency response functions were computed. Reference channel selected was the wave height sensor FWD_WHT, a Hanning window, and an overlap of 50%. The final number of records depends on the useful range of data determined.

During the data import process, the Z accelerations are averaged. The program automatically performs a SI/SO analysis on all the channels with respect to the reference channel (FWD_WHT). The reduced data is then exported to be further processed by MATLAB™ and EXCEL™.

5.1 SI/SO Analysis – Comparison between DynamicData and ITAP™

A comparison of SI/SO analysis between the DynamicData and ITAP™ analysis is carried out to validate the analyses and also to study the differences in the two analysis schemes. For this purpose a SI/SO analysis is performed on Data Set 1 (see Table 5.1) with the input as the FWD_WHT sensor and the output as the Average Z acceleration which is the average of all the eight Z accelerometers for the module.

Frequency Response Function
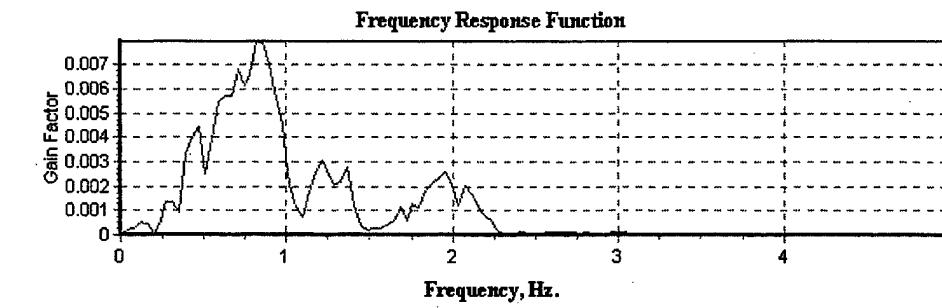
(a) Frequency Response Function
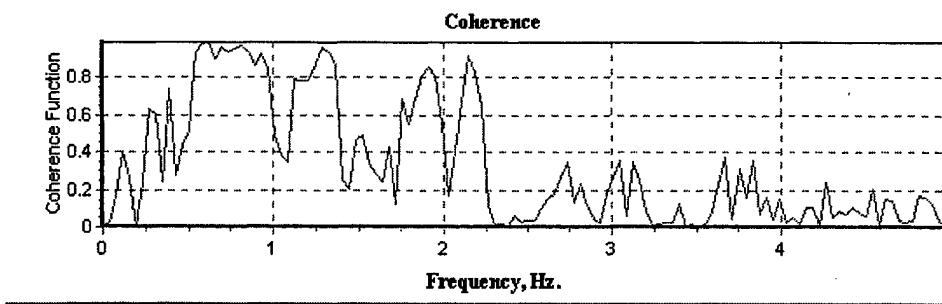
Coherence

(b) Coherence Function
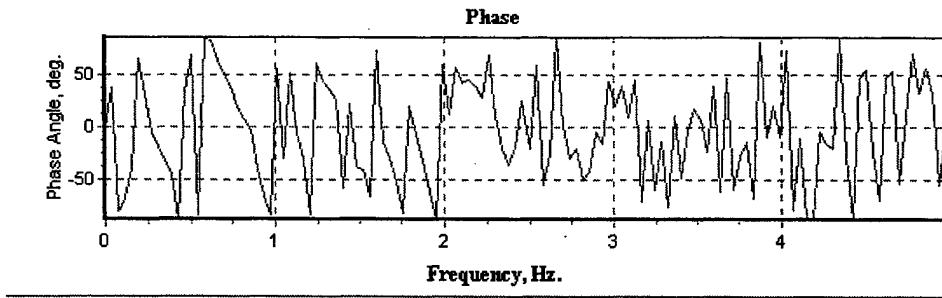
Phase

(c) Phase

Figure 5.1: SI/SO Analysis using the DynamicData Program
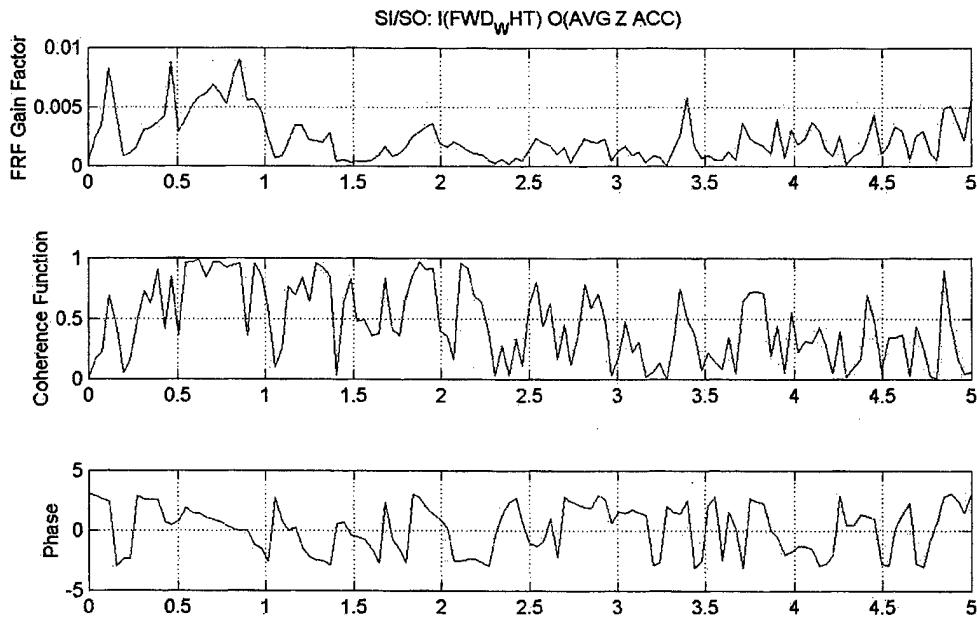
Figure 5.2: FRF, Coherence, and Phase from the ITAP™ program

The results from the DynamicData program (Figure 5.1) and the ITAP™ (Figure 5.2) is shown below. Comparing the results of the DyanamicData and the ITAP™ programs it can be seen that the SI/SO results show similar frequency response function, coherence and phase with one major exception in the FRF. In the regions of 0.2Hz, 0.5Hz, and 3.4Hz, the DynamicData program hardly shows a response in the FRF whereas the ITAP™ FRF peaks out sharply in these regions. The reason for this discrepancy is due to the different division techniques that are used in calculating the FRFs. The ITAP™ program divides the input over the output without any modification. Hence when the input signal is very low, the division leads to a high value of the FRF and results in peaks seen in the result. This occurs in regions of low coherence. The DynamicData program, on the other hand, adds a small constant value to the denominator so that in the absence of an appreciable input signal the division

79

does not lead to a large spike. This prevents the FRF plot from being cluttered with spikes in regions where the output signal is negligible.

5.2 Results of Analysis of a Single Module MOB Scale Model

The motion response of the single module data is first studied using the MOB_Animate animation program. The significant frequencies of the six DOF system is first visually determined. Then SI/SO and MI/SO techniques with appropriate MI/SO models, discussed in Chapter 4, are applied to the two data sets using the ITAP™. Table 5.3 lists the MI/SO models that were applied to each of the data sets.

Table 5.3: MI/SO Models Applied to the Data Sets

Data Set	Wave Spectrum	Sea Type	Nonlinear Models applied	
			Direct	Reverse
1	OCHI	Head	D1,D2	R1,R2
2	Bretschneider	Quartering	D5,D6,D7	R5,R6,R7

Preliminary analysis of the wave data consists of time history plots, plots from the MOB_Animate program, probability density function plots, and autospectral density function plots. SI/SO and MI/SO analyses results are presented in terms of the frequency response functions, coherence functions and phases. For the SI/SO and the MI/SO analyses results, the frequencies extracted are for the peaks where the corresponding coherence function is greater than or equal to 0.75. At these frequencies, the random errors in estimating associated frequency response functions

are not as low. The initial points in the data set are ignored to exclude data corresponding to the rampup section in the time history, where waves are allowed to build up in amplitude.

5.2.1 Results for OCHI Head Sea 2_50per 900 RPM Data Set

The time history of the wave input and its frequency response is shown (Figure 5.3). It can be seen from the time history that the input power is in the region of 0.45Hz to 2Hz with peaks at 0.625 and 0.781Hz. There is no significant input power below or beyond this range.
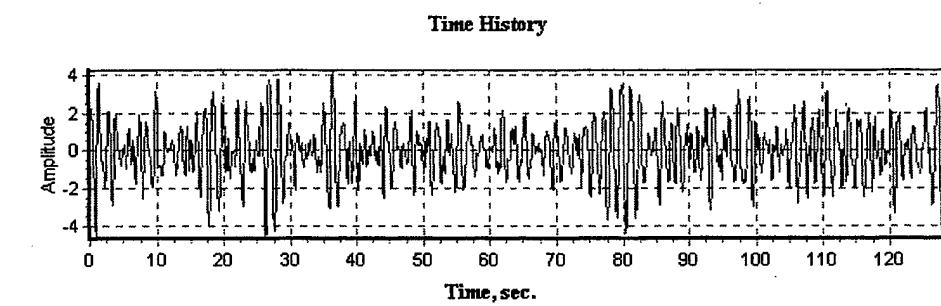
(a) OCHI Wave Time History
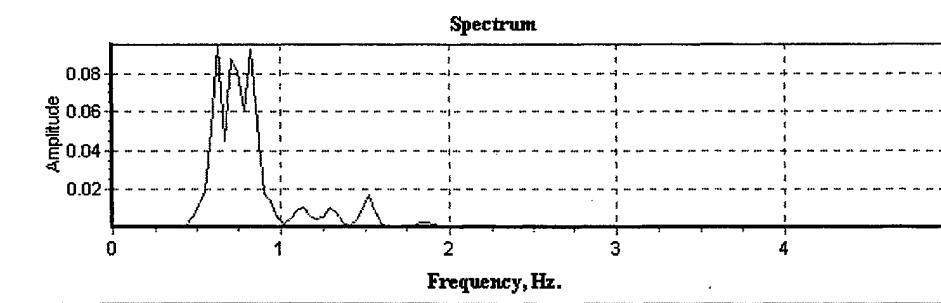
(b) OCHI Wave Frequency Response

Figures 5.3: OCHI Wave for Single Module Test

81

Using the MOB_Animate program, the response of the OCHI Head Sea data set is studied visually and the results are tabulated in Table 5.4 (Figure 5.5). These observations are based upon visual inspection of the acceleration data simultaneously. The corresponding coherence of the accelerations is shown in Figure 5.4.
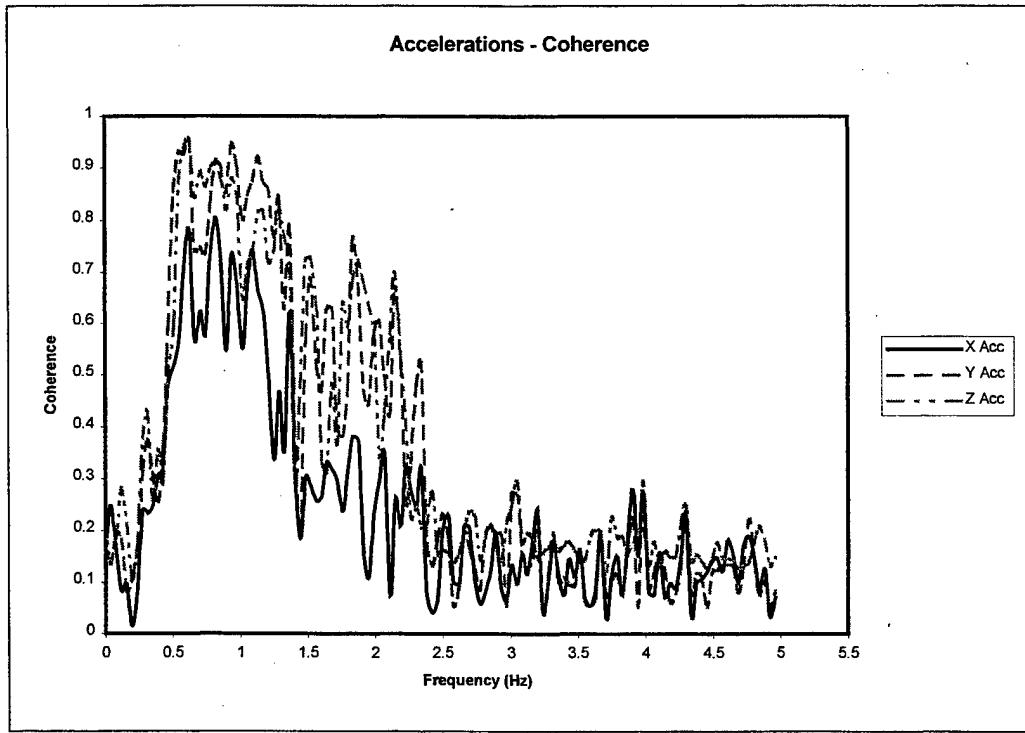
Figure 5.4: Coherence of Averaged X, Y and Z Accelerations for OCHI Single Module Data Set

Table 5.4: Summary of Results for the OCHI Single Module

Frequency (Hz)	Period (seconds)	Response			
		Significant Response	Faint Response	Type	Coherence
0.09749	10.25	Surge	Roll	Rigid response region (mild)	0 - 0.27 (poor)
0.15599	6.41	Sway, Surge	Roll, Heave		
0.23399	4.27	Pitch and Sway	*		
0.25349	3.95	Heave and Sway	*		
0.29 - 0.60	3.45 – 1.67	Heave and Sway	*	Elastic response region	0.25 – 0.95 (good)
0.64349	1.55	Heave and Sway	*	Rigid response region (pronounced)	0.6 – 0.95 (good)
0.70199	1.43	Pitch and Sway	*		
0.8 -1.28	1.38 – 0.78125	Pitch, Heave and Sway	*	Highly Elastic	0.3 – 0.95
1.28699	0.78	No response	*	No response	

It can be seen from Table 5.4 that sway and heave are the significant motions of the OCHI MOB single module model. As the orientation is head seas, there is poor roll response of the structure and absent yaw response. There is no significant response above 1.29 Hz. The structure shows elasticity in the 0.29-0.6 Hz and 0.8-1.28 Hz regions. This elastic behavior cannot be concluded as being that of the MOB model. It could also be due to the local elasticity of the plate or layer on which the accelerometers are mounted. As the MOB is designed to be elastic, it is desirable to avoid the MOB functioning in these ranges, specifically in the latter range. Surge and sway dominate the initial rigid response region at 0.09749 Hz and 0.15599 Hz

respectively, while heave and pitch have pronounced mode shapes at 0.64349 Hz and 0.70199 Hz respectively.
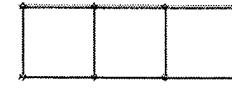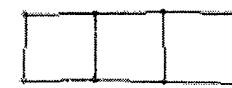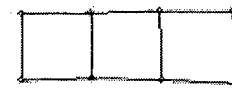

(a) Surge (0.09749 Hz)   (b) Surge and Sway (0.15599 Hz)
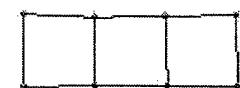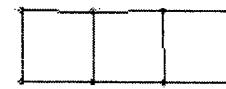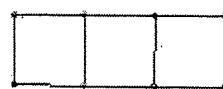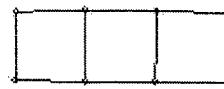
(c) Pitch and Sway (0.23399 and 0.70199 Hz)
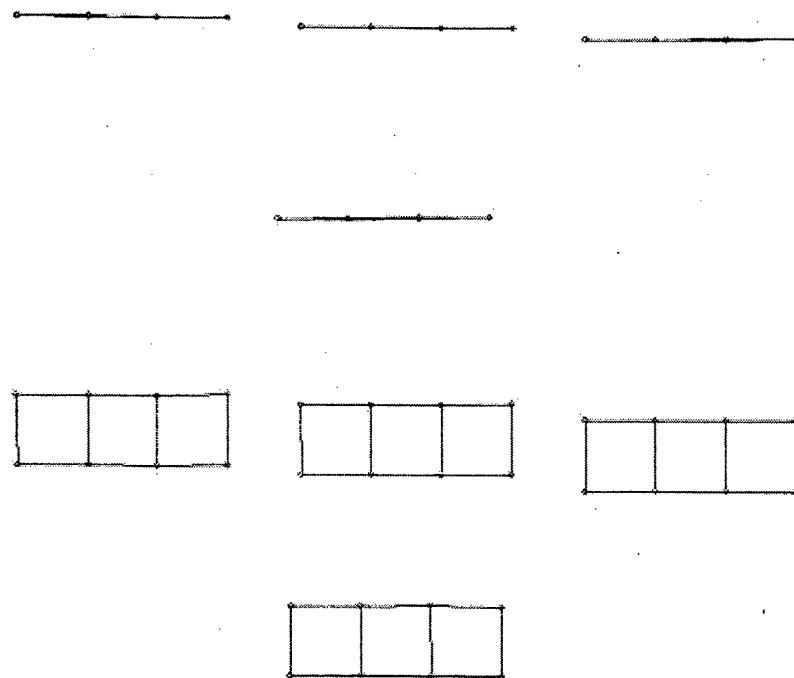
(d) Heave and Sway (0.25349 and 0.64349 Hz)
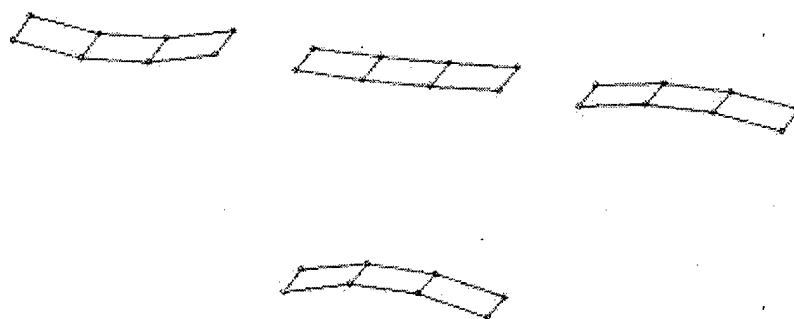
(e) Elastic Heave and Sway – first bending mode (0.29 - 0.60 Hz)

Figure 5.5: Mode Shapes of the Single Module OCHI MOB

Using the DynamicData program with a window length of 128 and an overlap of 50, there were 9 records available for SI/SO and MI/SO analysis. The sampling rate of the reduced data set is 10 Hz (period = 0.1sec). Sample SI/SO and MI/SO results are shown (Figure 5.6). See appendix D.1 for all SI/SO and MI/SO analysis results (Figures D.1-15). The summary of results is presented in Table 5.5.

Table 5.5: SI/SO and MI/SO Results for the OCHI Single Module MOB

Model	Response Range (Hz)	Single Module Response		Other significant Frequencies (Hz)
		Max Freq., F (Hz)*	Period, P (secs)*	
FWD_WHT	0.469 - 2.031	0.781	1.28	0.6250; 1.0938; 1.3281; 1.4844; 1.8750
Z	0.391 - 1.016	0.625	1.6	
P	0.000 - 1.250	0.781	1.28	0.0781; 0.3906
R	0.000 - 1.016	0.078	12.8	0.2344; 0.8594
SISO_W_Z	0.000 - 2.266	0.547	1.83	0.8594
SISO_W_P	0.000 - 2.266	0.859	1.16	1.4844
SISO_W_R	0.000 - 1.250	0.859	1.16	
D1 2-Input: (Y = Z)_1	0.000 - 2.266	0.703	1.42	
D1 2-Input: (Y = Z)_2	0.000 - 2.109	0.703	1.42	
D1 3-Input: (X3 = P; Y = Z)_1	0.000 - 2.188	0.703	1.42	
D1 3-Input: (X3 = P; Y = Z)_2	0.000 - 1.563	0.703	1.42	1.25
D2 2-Input: (Y = P)_1	0.000 - 2.891	0.625	1.6	0.8594; 1.4844
D2 2-Input: (Y = P)_2	0.000 - 1.719	0.781	1.28	
D2 3-Input: (X3 = P; Y = P)_1	0.000 - 4.844	0.859	1.16	
D2 3-Input: (X3 = P; Y = P)_2	0.000 - 2.031	0.859	1.16	
R1 2-Input: (X1 = Z)_1	1.250 - 5.000	1.328	0.75	
R1 2-Input: (X1 = Z)_2	0.000 - 4.766	0.703	1.42	1.0938; 1.4844; 1.8750
R1 3-Input: (X1 = Z; X3 = P)_1	1.250 - 5.000	1.328	0.75	
R1 3-Input: (X1 = Z; X3 = P)_2	0.000 - 4.375	0.703	1.42	0.9375; 1.4844; 1.8750
R2 2-Input: (X1 = P)_1	0.469 - 5.000	0.859	1.16	0.5469; 1.4844
R2 2-Input: (X1 = P)_2	0.000 - 4.453	0.703	1.42	0.9375; 1.2500; 1.5625; 1.8750
R2 3-Input: (X1 = P; X3 = P)_1	0.000 - 5.000	0.625	1.6	0.7813; 1.4844
R2 3-Input: (X1 = P; X3 = P)_2	0.000 - 4.375	0.703	1.42	0.9375; 1.3281; 1.5625; 1.8750

* Max frequency represents the peaks corresponding to maximum coherence where applicable; period is the inverse of the maximum frequency value

SI/SO: I(FWD WHT), O(*AVG Z 1-8)
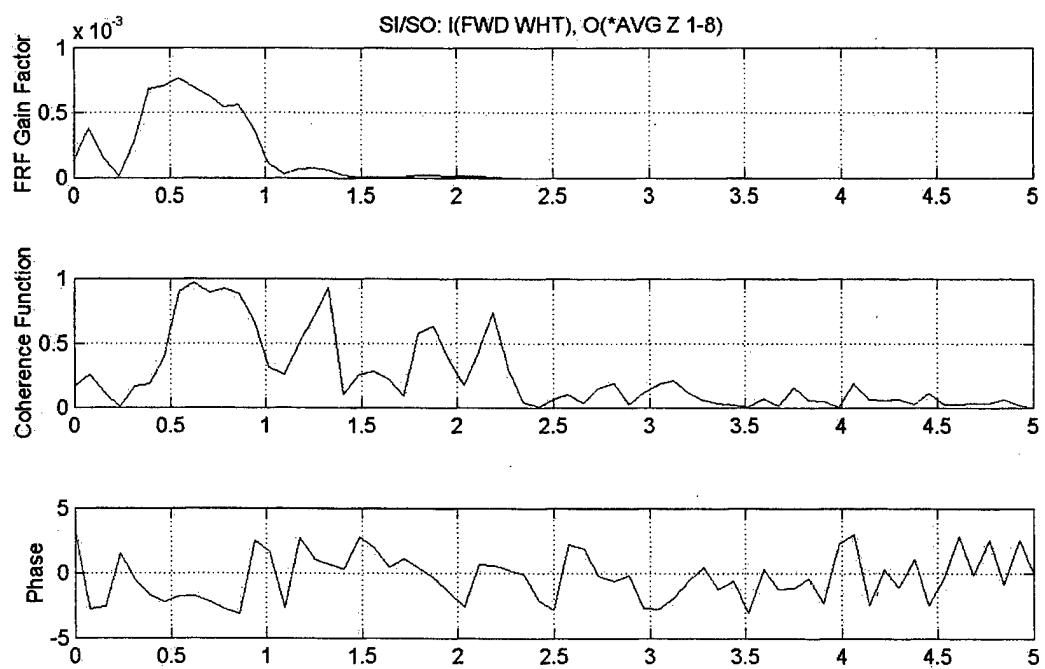
(a) Sample SI/SO Result – Input (FWD_WHT) and Output (Heave)
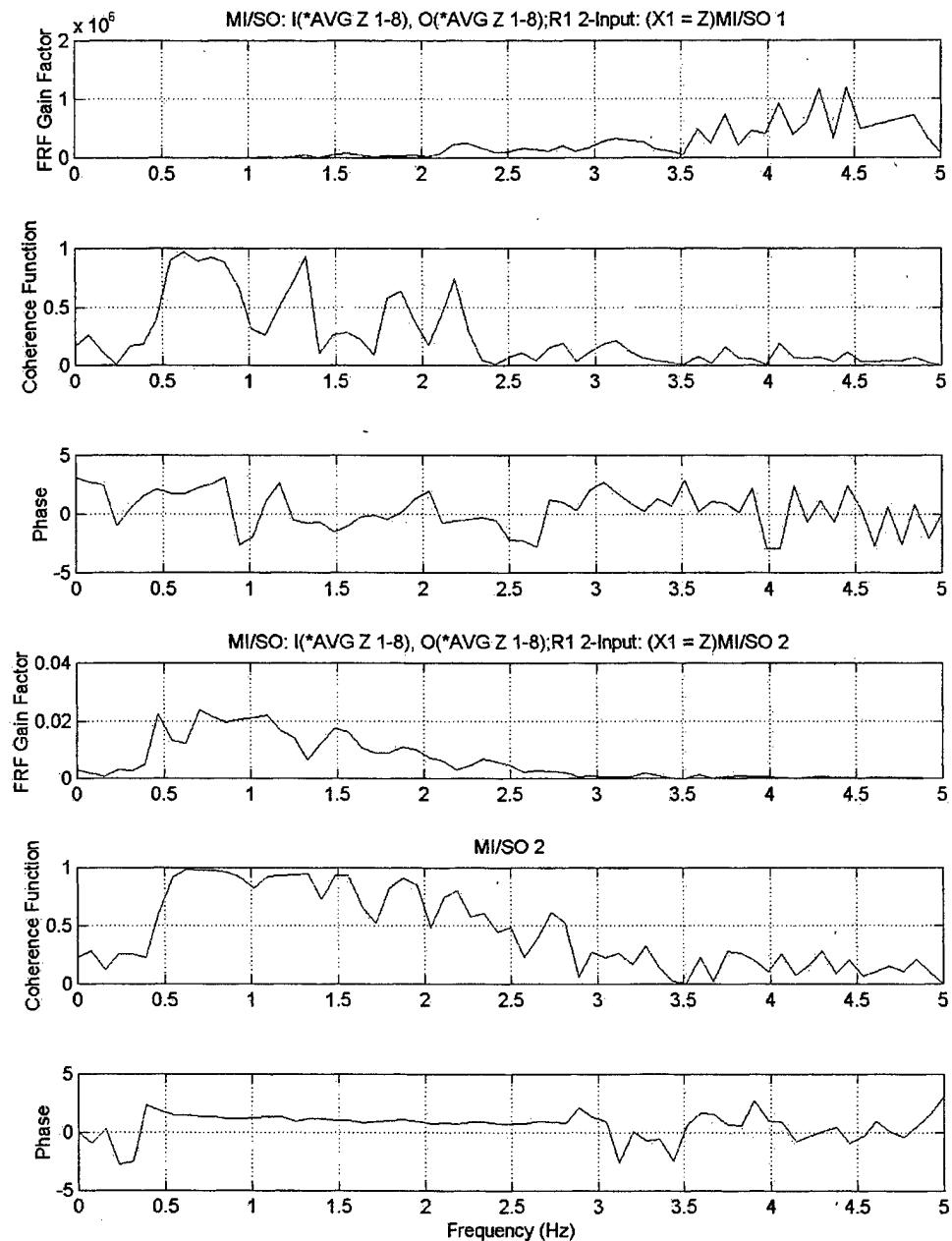
(b) Sample MI/SO Result – R1 2-Input Model

Figure 5.6: Sample SI/SO and MI/SO Result for OCHI Single Module MOB

The results in Table 5.5 can be seen to vary from the results obtained from the MOB_Animate program. The discrepancy is due to the fact that values obtained using the MOB_Animate program are visual and are based on dominant mode shapes at a particular frequency. The SI/SO and MI/SO analyses are a relationship between the input and output power. The roll response is below the 0.3 Hz range. Significant heave and pitch responses are above the 0.6 Hz range. Comparing this with Table 5.4, the heave and pitch have peak mode shapes at 0.64349 Hz and 0.70199 Hz respectively. The linear SI/SO results indicate that the heave is most influenced by the wave at 0.547 Hz, while the pitch is most influenced by the wave at 0.859 Hz. It is observed that the pitch response frequency is in a highly elastic response range. This undesirable response is created by the wave and is not a fundamental mode shape of the single MOB module. The SI/SO roll response is insignificant in the frequency indicated in Table 5.5.

Improvement in the coherence function after applying a nonlinear model is the indication of nonlinear behavior in the response. Studying the nonlinear characteristics using the Direct MI/SO results (see appendix D Figures D.8-D1.11), the wave-heave response does not show an improvement in the coherence when the difference in velocities is used as a nonlinear input term (model D1) in the MI/SO analysis in the region of 0.547 Hz. The same characteristic is also seen in the three-input model with pitch as the third input. Since there is no significant improvement in the coherence, it can be concluded that the wave-heave response does not have any significant nonlinear characteristics. Similarly there is no significant improvement is observed in the coherence for the wave-pitch response (model D2) in the region of 0.859 Hz.

The Reverse MI/SO results (see appendix D Figures D1.12-D1.15), there is significant improvement in the coherence value in the range of 0.5 Hz to 2.5 Hz for the reverse two models (models R1 and R2) suggesting a nonlinear damping force. The three input models do not show any further improvement to the two input models. Hence the reverse nonlinear models applied should be considered when defining the response of the MOB module in the range of 0.5 to 2.5 Hz range.

5.2.2 Results for Bretschneider BOW66 (b) Quartering Sea 2_58per 1125 RPM Data Set

The time history of the wave input and its frequency response is shown (Figure 5.7). It can be seen that the input power is in the region of 0.23Hz to 1.9Hz with peak at 0.781Hz. There is no significant input power below or beyond this range.

(a) Bretschneider Wave Time History

91

Spectrum
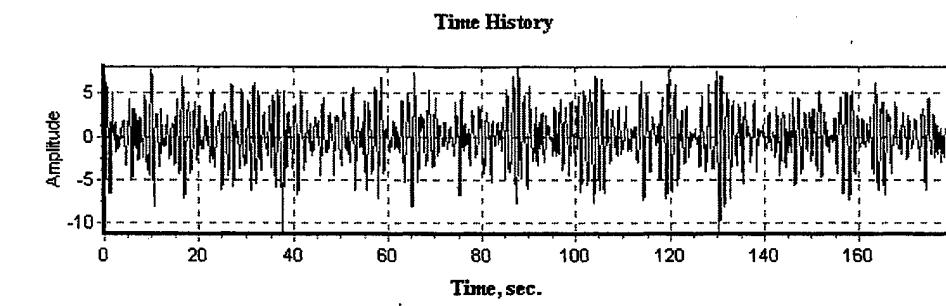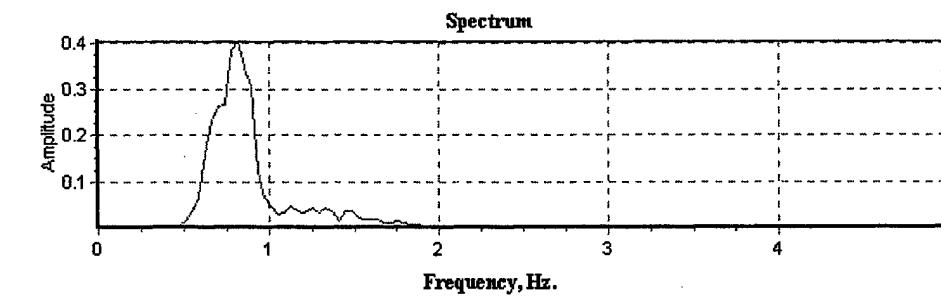
(b) Bretschneider Wave Frequency Response

Figure 5.7: Bretschneider Wave for Single Module Test

Using the MOB_Animate program, the response of the Bretschneider Head Sea data set is studied visually and the results are tabulated in Table 5.6 (Figure 5.9). The corresponding coherence for the accelerations is shown in Figure 5.8.
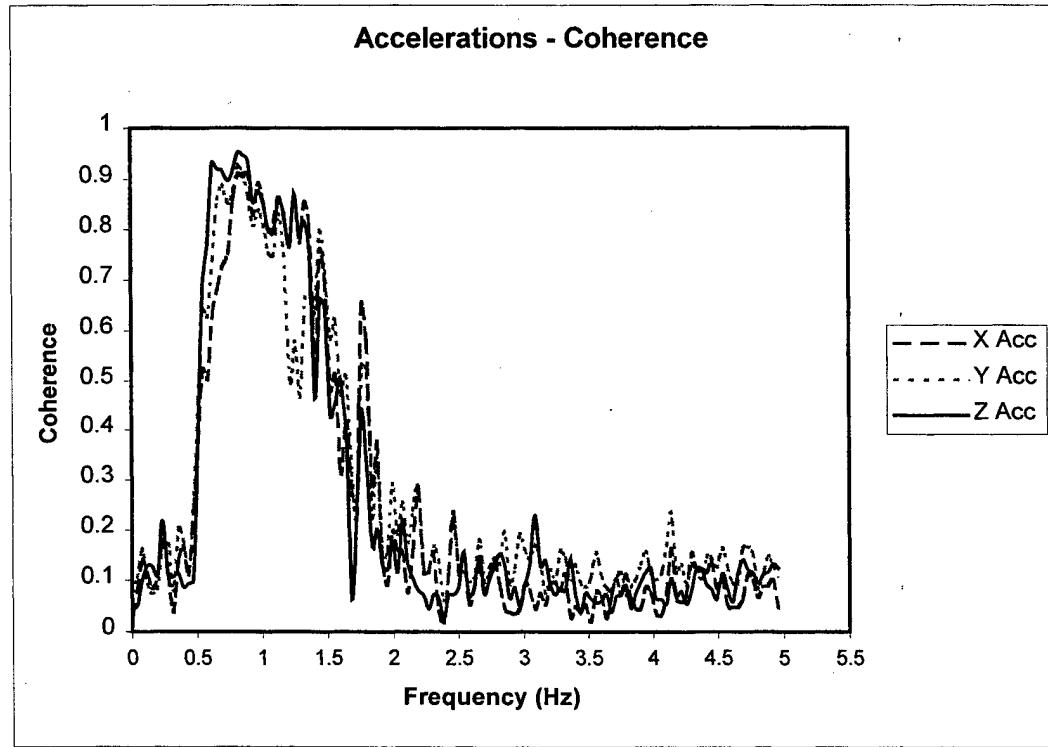
Figure 5.8: Coherence of Averaged X, Y and Z Accelerations for Bretschneider Single Module Data Set

92

Table 5.6: Summary of Results for the Bretschneider Single Module

Frequency (Hz)	Period (seconds)	Response			
		Significant Response	Faint Response	Type	Coherence
0.09749	10.25	Surge	*	Non-elastic response region (mild)	0-0.2 (poor)
0.23399	4.27	Sway and Roll	Surge		
0.27299	3.66	Heave and Surge	*		
0.29 - 0.60	3.45 – 1.67	Torsion, Surge and Heave	*	Elastic response region	0.2-0.6 (moderate)
0.66299	1.51	Heave, Roll and Surge	*	Non-elastic response region (pronounced)	0.95 (high)
0.7 -1.28	1.38 – 0.78125	Mixed	*	Highly Elastic	0.5-0.95 (high)
1.28699	0.78	No response	*	No response	0.75 (moderate)

It can be seen from Table 5.6 that surge, roll and heave are the significant motions of the Bretschneider MOB single module model. As the orientation is quartering seas, there is very good roll response of the structure, while the pitch and yaw response are not significant. There is no response above 1.29 Hz. The structure shows an elastic behavior in the 0.29-0.6 Hz and 0.8-1.28 Hz regions. This elastic behavior, as in the OCHI single module case, cannot be concluded as being that of the MOB model. Given the uniformity of the sensor motions it is highly probable that the response is elastic in those frequency ranges. Surge, roll and sway dominate the initial non-elastic response region at 0.09749 Hz and 0.23399 Hz. There is a prominent

93

torsion observed in the region of 0.29 to 0.6 Hz along with heave and surge. Heave, roll and surge have a pronounced mode shapes at 0.66299 Hz. Between 0.7 to 1.28 Hz the response is mixed with no response beyond 1.29 Hz.
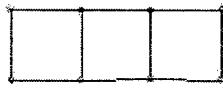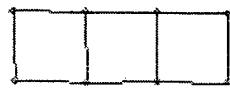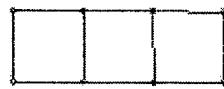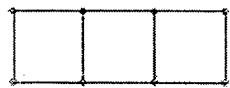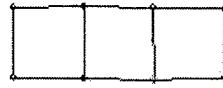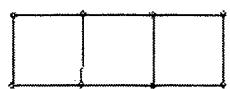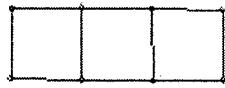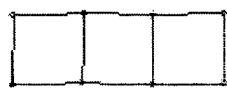

(a) Surge (0.09749 Hz)   (b) Sway and Roll (0.23399 Hz)

(c) Heave and Surge (0.27299 Hz)

94
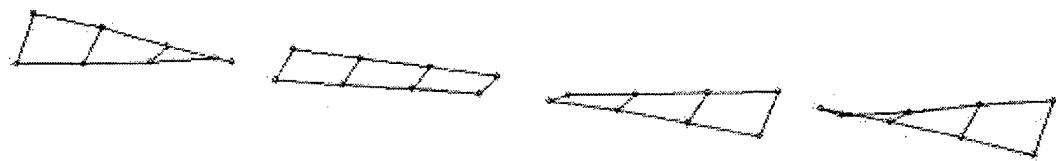
(d) Torsion (twist), Heave and Surge (0.29 - 0.60 Hz)
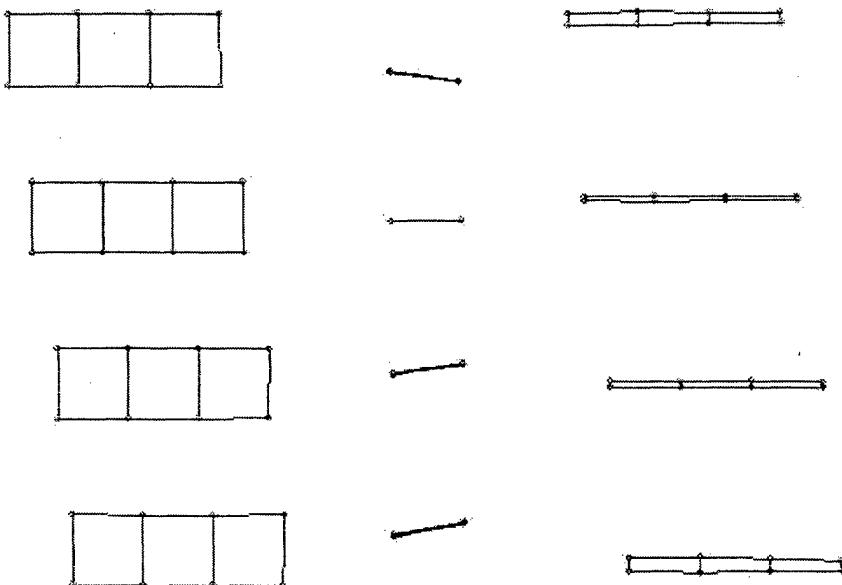

(e) Roll, Heave and Surge (0.66299 Hz)

Figure 5.9: Mode Shapes of the Single Module Bretschneider MOB

Using the DynamicData program with a window length of 128 and an overlap of 50, there were 13 records available for SI/SO and MI/SO analysis. The sampling rate of the reduced data set is 10 Hz (period = 0.1sec). Sample SI/SO and MI/SO results are shown (Figure 5.10). See appendix D2 for all figures related to SI/SO and MI/SO analysis. The summary of results is presented in Table 5.7.

Table 5.7: SI/SO and MI/SO Results for the Bretschneider Single Module MOB

Quantity	Response Range (Hz)	Single Module Response		Other significant Frequencies (Hz)
		Max Freq., F (Hz)*	Period, P (secs)*	
FWD_WHT	0.469 - 1.953	0.781	1.28	1.1719; 1.4844
Z	0.313 - 1.094	0.781	1.28	0.4688
P	0.000 - 1.328	0.859	1.16	0.0781; 0.3906
R	0.000 - 1.406	0.078	12.8	0.7813
SISO_W_Z	0.000 - 2.109	0.781	1.28	
SISO_W_P	0.000 - 3.203	0.938	1.07	
SISO_W_R	0.000 - 1.953	0.781	1.28	1.0156
D5 2-Input: (Y = Z)_1	0.000 - 2.188	0.781	1.28	
D5 2-Input: (Y = Z)_2	0.000 - 2.188	0.938	1.07	0.7813; 1.1719
D6 2-Input: (Y = R)_1	0.000 - 2.734	0.781	1.28	1.0156
D6 2-Input: (Y = R)_2	0.000 - 2.422	0.781	1.28	1.0156
D7 2-Input: (Y = P)_1	0.000 - 3.047	0.781	1.28	1.0156; 1.1719
D7 2-Input: (Y = P)_2	0.000 - 2.266	0.859	1.16	1.0156; 1.1719
R5 2-Input: (X1 = Z)_1	1.484 - 5.000	0		
R5 2-Input: (X1 = Z)_2	0.000 - 5.000	0.781	1.28	0.5469; 1.2500; 1.6406; 1.7969; 2.1094; 2.9688
R6 2-Input: (X1 = R)_1	0.391 - 5.000	0.859	1.16	0.6250; 1.0938
R6 2-Input: (X1 = R)_2	0.000 - 5.000	0.625	1.6	1.4844
R7 2-Input: (X1 = P)_1	0.547 - 5.000	0.859	1.16	0.6250; 1.1719
R7 2-Input: (X1 = P)_2	0.000 - 5.000	0.781	1.28	1.2500; 1.6406; 2.1094

Max frequency represents the peaks corresponding to maximum coherence where applicable; period is the inverse of the maximum frequency value
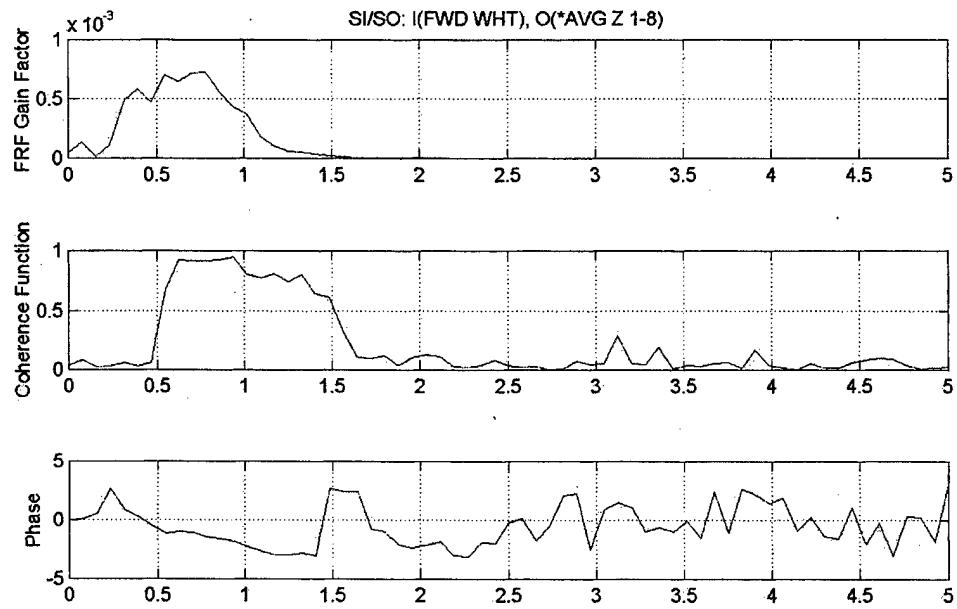
(a) SI/SO Input = FWD_WHT Output = Average Z
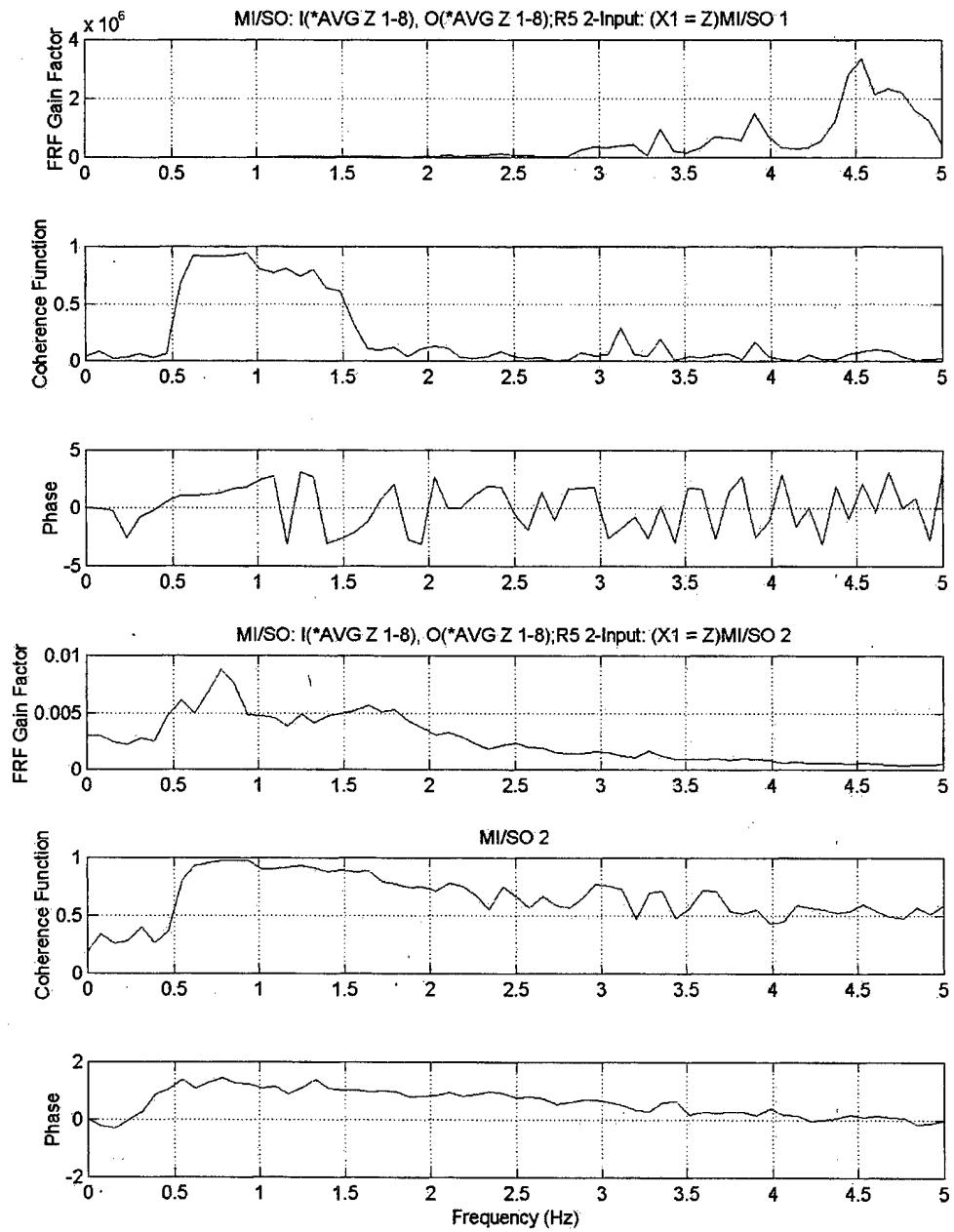
(b) Reverse Two-Input Model R5

Figure 5.10: Sample SI/SO and MI/SO Results for Bretschneider Single Module MOB

As in the case of the OCHI MOB module, the results in Table 5.7 can be seen to vary from the results obtained from the MOB_Animate program in Table 5.6. It can be seen that the significant heave and pitch responses above the 0.6 Hz range while the roll response is now both 0-0.3 Hz and in the 0.6-0.8 ranges. Both these ranges correspond to the non-elastic response region shown in Table 5.6. Therefore it can be concluded that the heave and roll have fundamental mode shapes at 0.66299 Hz. The linear SI/SO results indicate that the heave is most influenced by the wave at 0.781 Hz. The pitch is most influenced by the wave at 0.859 Hz as it is in the OCHI case, which again is in an undesirable highly elastic response range. The SI/SO roll response is significant in the 0.781 Hz shown in Table 5.7.

Studying the nonlinear characteristics using the Direct MI/SO results (see appendix D Figures D.23-D.25), the wave-heave response does not show an improvement in the coherence when the difference in velocities is used as a nonlinear input term (model D5) in the MI/SO analysis in the region of 0.781 Hz. Since there is no significant improvement in the coherence, it can be concluded that the wave-heave response does not have any significant nonlinear characteristics. Similarly, there is no significant improvement observed in the coherence for the wave-roll response (model D6) and wave-pitch response (model D7) in the region of 0.781 and 0.859 Hz respectively.

The Reverse MI/SO results (see appendix D Figures D.26-D.28) there is significant improvement in the coherence value after 0.5 Hz for all the three models (models R5, R6 and R7). As in the case of the OCHI, this suggests a nonlinear

damping force and the reverse nonlinear models have to be considered in analysis of

the Bretschneider data for frequencies greater than 0.5 Hz.

Chapter 6

Analysis of Two and Four Module MOB Scaled Model

This section presents the analysis of DynamicData sensors from testing of two and four module MOB at NSWC-Caderock MASK facility. Performing SI/SO and MI/SO analyses on the two and four module MOB models is complicated due to the involvement of connector dynamics. Hence the primary analysis of the response mode shapes of the two and four module setup is conducted using animations with the MOB_Animate program. The results are compared to those obtained for the single module. Due to non-availability of valid data sets, only one data set is analyzed for the two module and the four module tests.

6.1 Analysis of OCHI 1100 RPM Head Sea Two Module Data Set

Analysis of an OCHI two module has been conducted and reported earlier at the University of Maine (Caccese, 2000). A summary of the results along with comparisons with the single module response discussed in Chapter 5 is included.

The channel designations in the data set are shown in Table 6.1.

Table 6.1: Channel Designations in the OCHI Two Module Data Set

(a) Hydrodynamic Data Channel Designations

Response Designation	Description	Ch. No.
FWD_WVHT_2	Forward Wave Height - STBD	53
ACC1 X,Y,Z	X,Y,Z Accelerometer 1	137-39
ACC2 X,Y,Z	X,Y,Z Accelerometer 2	140-42
ACC3 X,Y,Z	X,Y,Z Accelerometer 3	143-45
ACC4 X,Y,Z	X,Y,Z Accelerometer 4 ·	146-48
ACC5 X,Y,Z	X,Y,Z Accelerometer 5	149-51
ACC6 X,Y,Z	X,Y,Z Accelerometer 6	152-54
ACC7 X,Y,Z	X,Y,Z Accelerometer 7	155-57
ACC8 X,Y,Z ·	X,Y,Z Accelerometer 8 ·	158-60
ACC9 X,Y,Z	X,Y,Z Accelerometer 9	261-63
ACC10 X,Y,Z	X,Y,Z Accelerometer 10	264-66
ACC11 X,Y,Z	X,Y,Z Accelerometer 11	267-69
ACC12 X,Y,Z	X,Y,Z Accelerometer 12	270-72
ACC13 X,Y,Z	X,Y,Z Accelerometer 13	249-51
ACC14 X,Y,Z	X,Y,Z Accelerometer 14	252-54
ACC15 X,Y,Z	X,Y,Z Accelerometer 15	255-57
ACC16 X,Y,Z	X,Y,Z Accelerometer 16	258-60

(b) Connector Force Data Channel Designations

Connector Designation	Description	Ch. No.
TLPin1_PORT	Top Longitudinal Pin, Port Side	201
BLPin5_PORT	Bottom Longitudinal Pin, Port Side	202
TransPin4_PORT	Transverse Pin, Port Side	203
VERTPin3_PORT	Vertical Pin, Port Side	204
VertPin9_STBD	Top Longitudinal Pin, Starboard Side	205
TransPin12_STBD	Bottom Longitudinal Pin, Starboard Side	206
BLPin2_STBD	Transverse Pin, Starboard Side	207
TLPin10_STBD	Vertical Pin, Starboard Side	208

The original data set contains 272 channels sampled at 100 Hz. for a total of 72,000 data points with a sampling period of 720 seconds. The following reduction scheme was applied:

- Filter data – a 30 pole FIR filter is used with cutoff of 1/20 of the sampling frequency. The average value is calculated and subtracted from the data set.

102

- Decimate data by a factor of 20, resulting in an effective sampling rate of 5 Hz and a Nyquist frequency of 2.5 Hz.

- Compute the power spectral density (PSD) using a 256 point FFT, a Hanning window, and an overlap of 50% to get 27 records.

- Compute FRF – the frequency response functions were computed. Reference channel selected was the wave height sensor FWD_WHT_2 (channel 53), a Hanning window, and an overlap of 50% resulting in 27 total records.

The reduced data is then exported to be further processed by EXCEL™ and MOB_Animate program. The input OCHI wave is shown (Figure 6.1). The input power response is between 0.25 to 1.25Hz with a peak response at 0.43Hz. The corresponding coherence for the output accelerations is shown in Figure 6.2. Using the MOB_Animate program, the response of the OCHI Head Sea data set is studied visually and the results are tabulated in Table 6.2 (Figure 6.3).

Time History

(a) OCHI Wave Time History

Spectrum
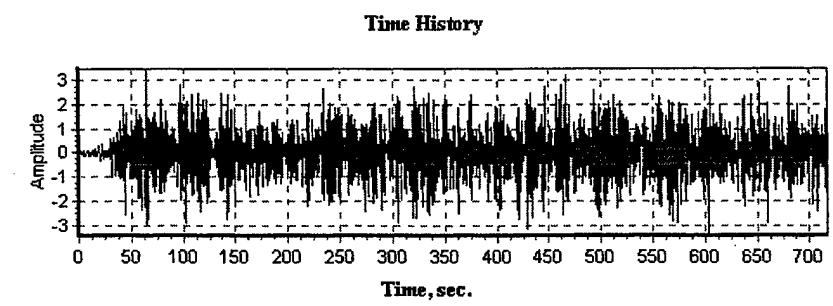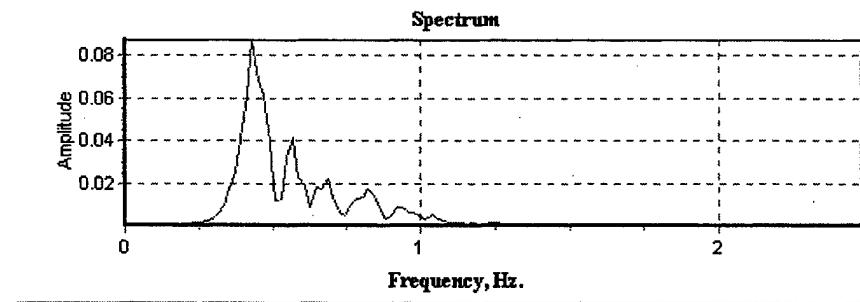
(b) OCHI Wave Frequency Response

Figure 6.1: OCHI Wave for Two Module Test
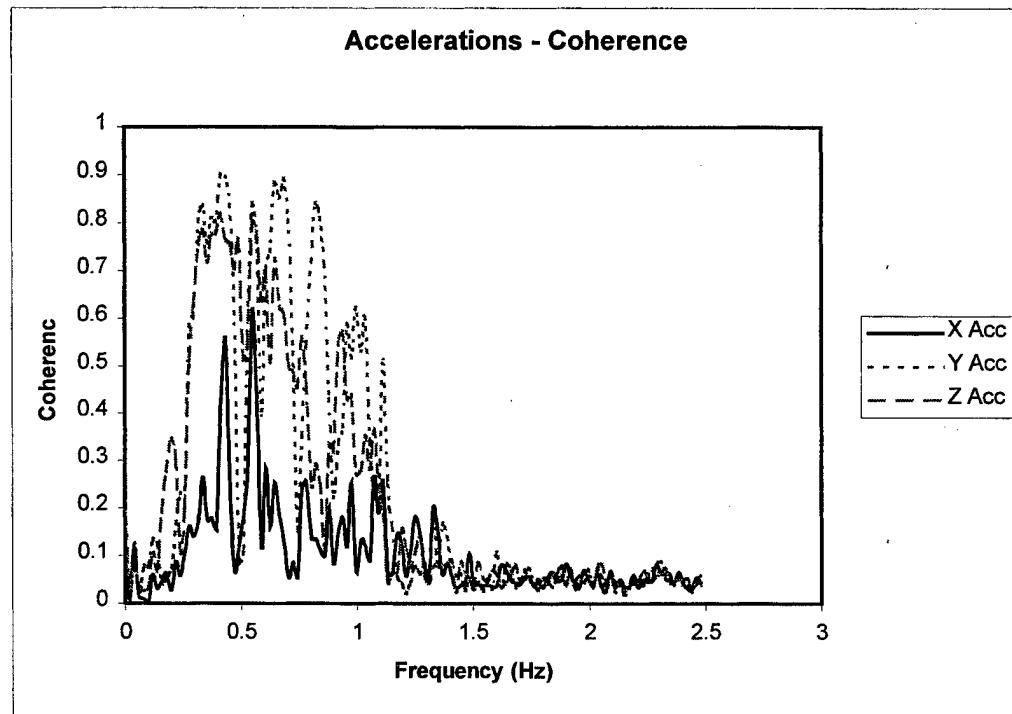
Figure 6.2: Coherence of Averaged X, Y and Z Accelerations for OCHI Two Module
Data Set

104

Table 6.2: Summary of Results for OCHI Two Module MOB

Frequency (Hz)	Period (seconds)	Response			
		Significant Response	Faint Response	Type	Coherence
0.13649	7.32	In-phase Surge	Sway	Irregular rigid response region (mild)	0-0.3 (poor)
0.17549	5.67	Off-phase, Surge	Roll		
0.21449	4.66	Pitch, Heave	Sway		
0.23399	4.28	Pitch and Sway	*		
0.25 - 0.60	4 – 1.67	Connector angle and out-of-phase Sway	Heave	Rigid response	0.1-0.9 (good)
0.66299	1.51	Sway	Pitch and Heave		
0.74099	1.35	Connector angle and in-phase Sway	*		
0.99 – 1.13	1.01 – 0.86	Torsion	*	Elastic response	0.1-0.6 (moderate)
1.28699	0.78	No significant response	*	No significant response	0.15 (poor)

It can be seen from Table 6.2 that sway is the significant motion of the OCHI
MOB two module model. As the orientation is head seas, there is poor roll response of
the structure and absent yaw response. There is no significant response above 1.29 Hz.
The structure shows elasticity in the 0.99-1.13 Hz region. Comparing this to the single
module, it is observed that the two module configuration shows less elasticity than the
single module. This could be due to the flexibility offered by the connectors. The
primary mode shape of surge is between 0.13-0.17 Hz with faint swaying or rolling.
There is a combined pitch and heave response at 0.22 Hz. There is a sway response

105

(in-phase and out-of-phase) over a wide range from 0.23 to 0.75Hz. At 0.23Hz it is combined with pitch. Between 0.25 and 0.6Hz the surge is out-of-phase and is combined with the connector angle mode shape. At 0.66Hz the response is dominated by the sway with faint pitch and heave response. At 0.74 Hz there is a in-phase sway response with connector angle. Between 0.99 Hz and 1.13 Hz, the model shows a high elastic response with out-of-phase torsion (twisting) of the two modules constrained by the connectors.
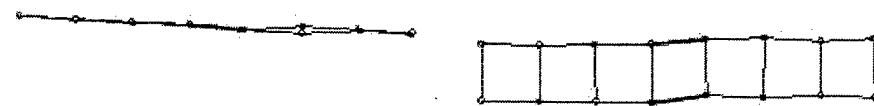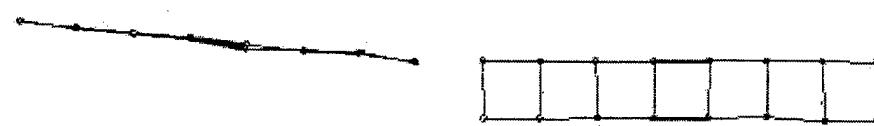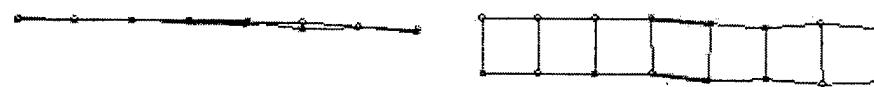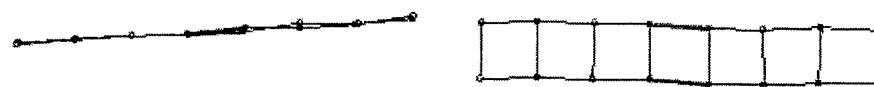
(a) In Phase Pitch and Sway (0.23399 Hz)
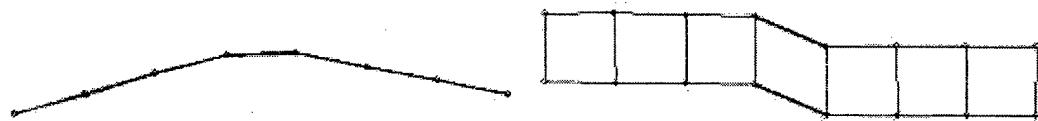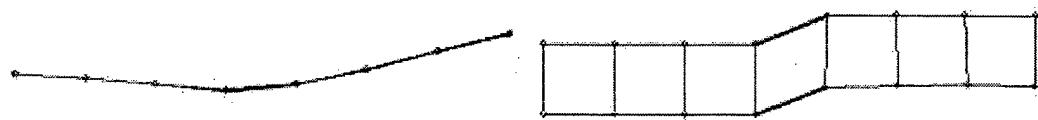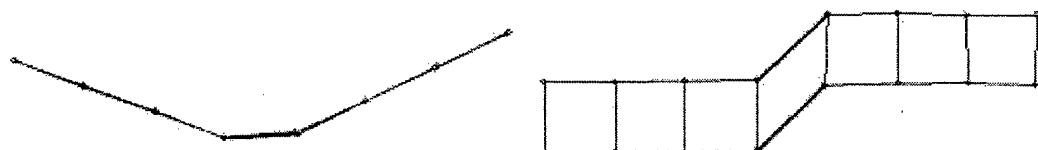
(b) Connector Angle and Out-of-Phase Sway (0.42899 Hz)
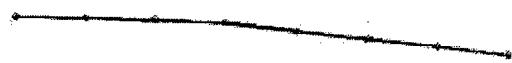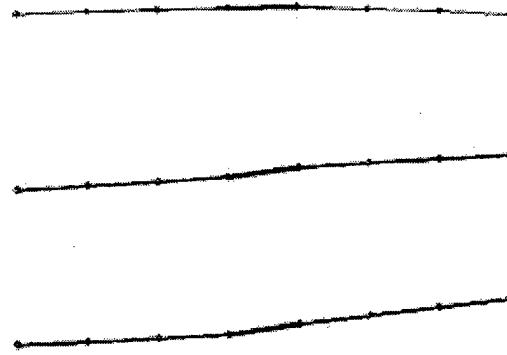
(c) Pitch and Heave Response Combined (0.50699 Hz)
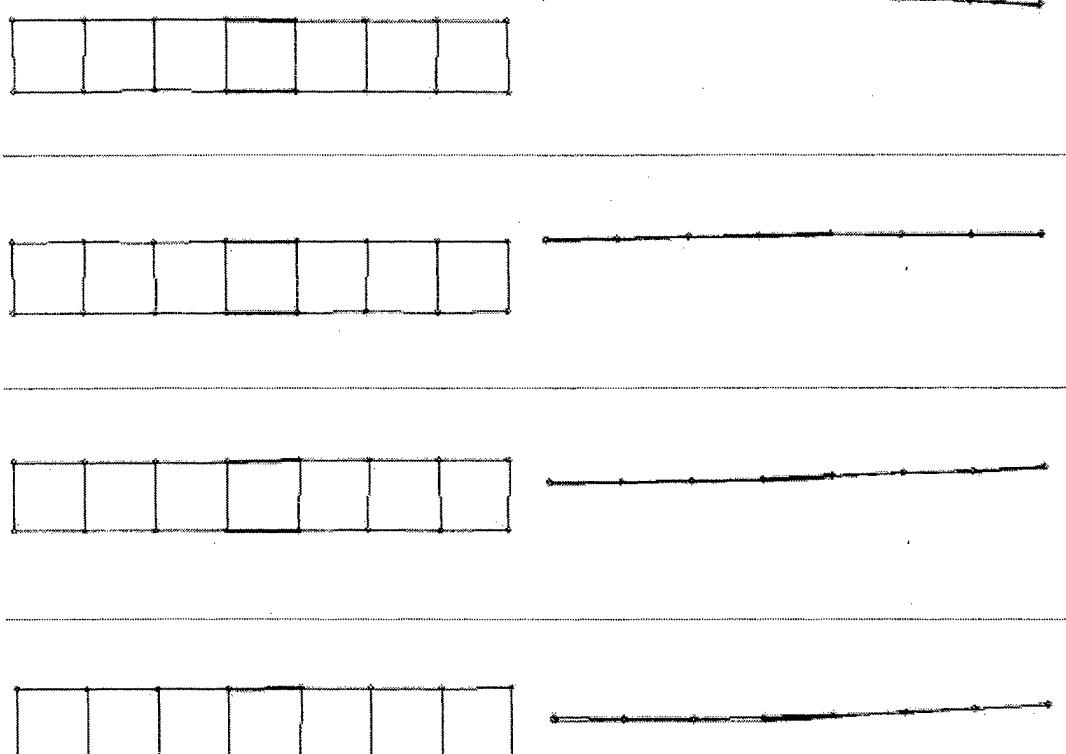
(d) Sway Response with Mild Pitch or Heave (0.66299 Hz)
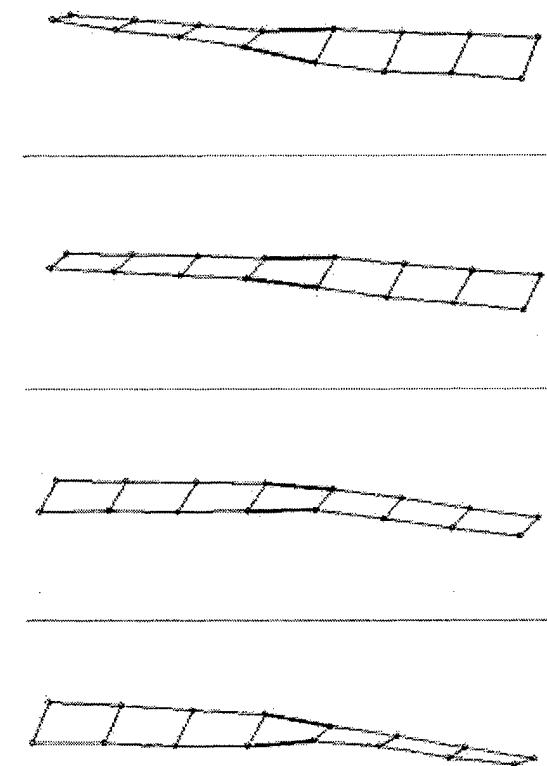
(e) Out of Phase Torsion Constrained by the Connectors (0.99 Hz)

Figure 6.3: Mode Shapes of OCHI Two Module Test

Figure 6.4 show the connector response on the port side and starboard side. It can be seen that connector response range is dominant between 0.1 to 0.7 Hz with maximum force between 0.23Hz to 0.5Hz and a peak at 0.43Hz. This corresponds to the peak of the wave height frequency response (Figure 6.1) and the in-phase and out-of-phase sway and connector angle response (Table 6.2).
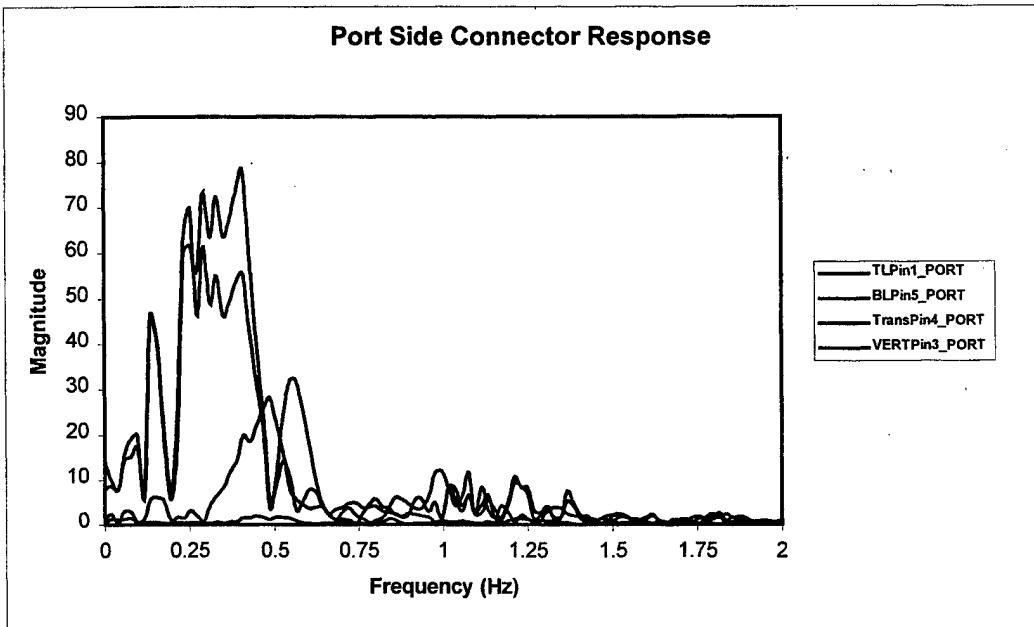
(a) Port Side Connector Response
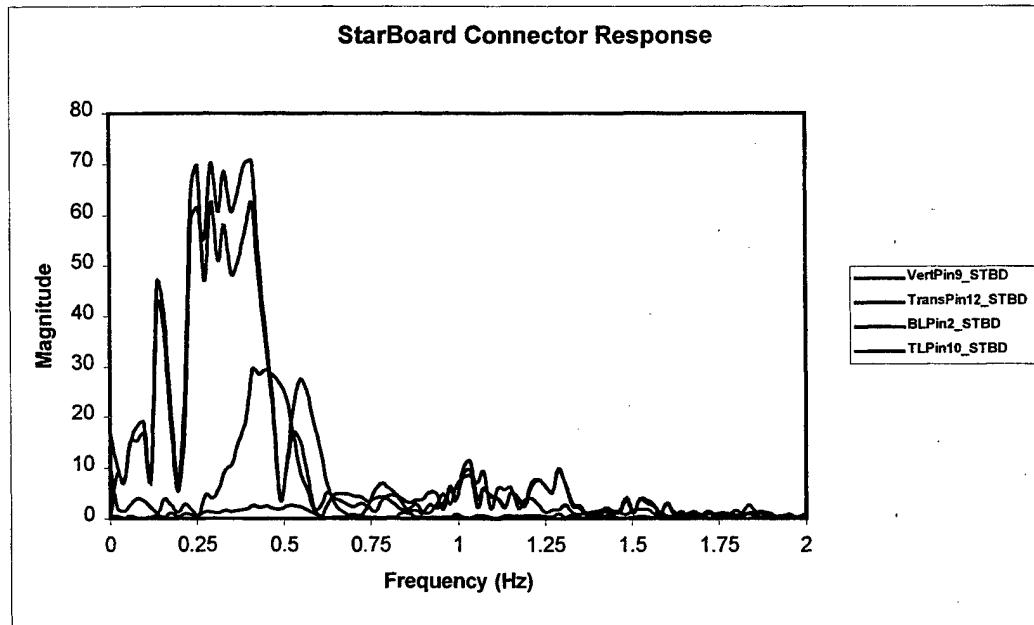
(b) Star Board Side Connector Response

Figure 6.4: Connector Response of the OCHI Two Module Test

6.2 Analysis of Bretschneider 1125 RPM 85DEG Quartering Sea Four Module Data Set

The channel setup for the Bretschneider quartering sea data is shown in Table 6.3.

Table 6.3: Channel Designations in the Bretschneider Quartering Sea Data

(a) Hydrodynamic Data Channel Designations

Response Designation	Description	Ch. No.
FWD_WVHT_2	Forward Wave Height - STBD	53
ACC1 X,Y,Z	X,Y,Z Accelerometer 1	137-39
ACC2 X,Y,Z	X,Y,Z Accelerometer 2	140-42
ACC3 X,Y,Z	X,Y,Z Accelerometer 3	143-45
ACC4 X,Y,Z	X,Y,Z Accelerometer 4	146-48
ACC5 X,Y,Z	X,Y,Z Accelerometer 5	149-51
ACC6 X,Y,Z	X,Y,Z Accelerometer 6	152-54
ACC7 X,Y,Z	X,Y,Z Accelerometer 7	155-57
ACC8 X,Y,Z	X,Y,Z Accelerometer 8	158-60
ACC9 X,Y,Z	X,Y,Z Accelerometer 9	261-63
ACC10 X,Y,Z	X,Y,Z Accelerometer 10	264-66
ACC11 X,Y,Z	X,Y,Z Accelerometer 11	267-69
ACC12 X,Y,Z	X,Y,Z Accelerometer 12	270-72
ACC13 X,Y,Z	X,Y,Z Accelerometer 13	249-51
ACC14 X,Y,Z	X,Y,Z Accelerometer 14	252-54
ACC15 X,Y,Z	X,Y,Z Accelerometer 15	255-57
ACC16 X,Y,Z	X,Y,Z Accelerometer 16	258-60
ACC17 X,Y,Z	X,Y,Z Accelerometer 17	41-43
ACC18 X,Y,Z	X,Y,Z Accelerometer 18	44-46
ACC19 X,Y,Z	X,Y,Z Accelerometer 19	47-49
ACC20 X,Y,Z	X,Y,Z Accelerometer 20	50-52
ACC21 X,Y,Z	X,Y,Z Accelerometer 21	53-55
ACC22 X,Y,Z	X,Y,Z Accelerometer 22	56-57
ACC23 X,Y,Z	X,Y,Z Accelerometer 23	59-61
ACC24 X,Y,Z	X,Y,Z Accelerometer 24	62-64
ACC25 X,Y,Z	X,Y,Z Accelerometer 25	9-11
ACC26 X,Y,Z	X,Y,Z Accelerometer 26	15-17
ACC27 X,Y,Z	X,Y,Z Accelerometer 27	12-14
ACC28 X,Y,Z	X,Y,Z Accelerometer 28	18-20
ACC29 X,Y,Z	X,Y,Z Accelerometer 29	21-23
ACC30 X,Y,Z	X,Y,Z Accelerometer 30	24-26
ACC31 X,Y,Z	X,Y,Z Accelerometer 31	27-29
ACC32 X,Y,Z	X,Y,Z Accelerometer 32	30-32

(b) Connector Force Data Channel Designations

Connector Designation	Description	Ch. No.
TLPin1_PORT	Top Longitudinal Pin, Port Side	201
BLPin5_PORT	Bottom Longitudinal Pin, Port Side	202
TransPin4_PORT	Transverse Pin, Port Side	203
VERTPin3_PORT	Vertical Pin, Port Side	204
VertPin9_STBD	Top Longitudinal Pin, Starboard Side	205
TransPin12_STBD	Bottom Longitudinal Pin, Starboard Side	206
BLPin2_STBD	Transverse Pin, Starboard Side	207
TLPin10_STBD	Vertical Pin, Starboard Side	208

The original data contains two files. One set containing 272 channels sampled at 100 Hz. for a total of 46,080 data points with a sampling period of 460 seconds. The other data set contains 64 channels sampled at 100 Hz with the same number of data points and sampling period. The following reduction scheme was applied:

- Filter data – a 30 pole FIR filter is used with cutoff of 1/20 of the sampling frequency. The average value is calculated and subtracted from the data set.

- Decimate data by a factor of 20, resulting in an effective sampling rate of 5 Hz and a Nyquist frequency of 2.5 Hz.

- Compute the power spectral density (PSD) using a 256 point FFT, a Hanning window, and an overlap of 50% to get 9 records.

- Compute FRF – the frequency response functions were computed. Reference channel selected was the wave height sensor FWD_WHT_2 (channel 53), a Hanning window, and an overlap of 50% resulting in 9 total records.

The reduced data is then exported to be further processed by EXCEL™ and MOB_Animate program. The input Bretschneider wave is shown (Figure 6.5). The input power response is between 0.25 to 0.9Hz with a peak response at 0.43Hz. The

acceleration data across the different data sets had different scaling factors. A scaling scheme was used to normalize the data (see appendix E for scaling technique adopted). The corresponding coherence for the accelerations is shown in Figure 6.6. Using the MOB_Animate program, the response of the Bretschneider quartering sea data set is studied visually and the results are tabulated in Table 6.4 (Figure 6.7).

Time History

(a) Bretschneider Wave Time History

Spectrum
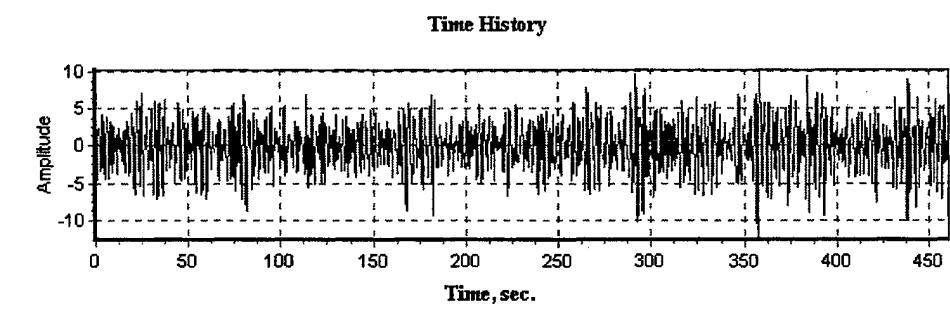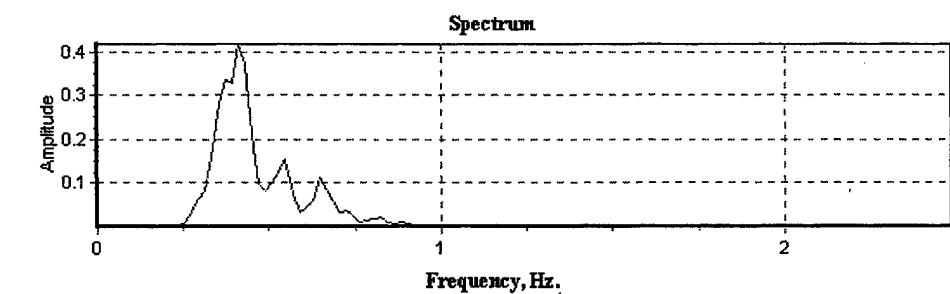
(b) Bretschneider Wave Frequency Response

Figure 6.5: Bretschneider Wave for Four Module Test

113
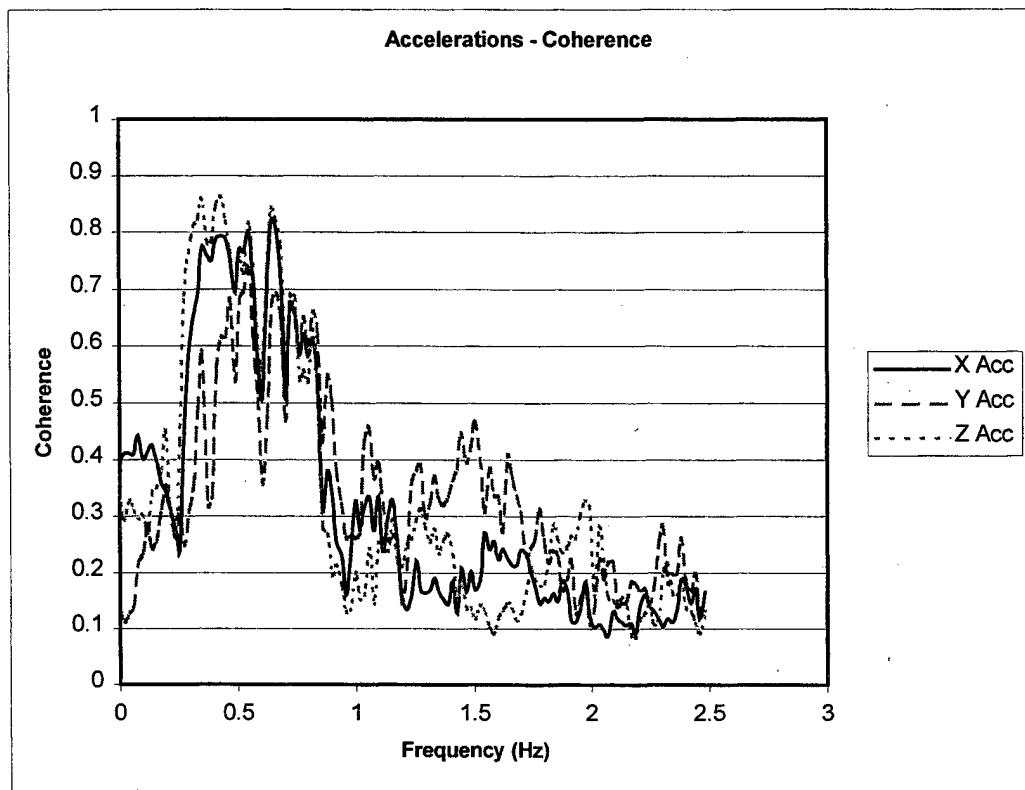
Figure 6.6: Coherence of Averaged X, Y and Z Accelerations for Bretschneider Four
Module Data Set

Table 6.4: Summary of Results for Bretschneider Four Module MOB Data Set

Frequency (Hz)	Period (seconds)	Response			
		Significant Response	Faint Response	Type	Coherence
0.09749	10.23	In-phase Surge	Roll	Irregular rigid response region	0.1 – 0.4 (poor)
0.23399	4.28	Sway, Heave, Roll	Pitch, Surge		
0.272999	3.66	Heave, Roll	Sway		
0.31 - 0.60	3.23 – 1.67	Surge, Heave, Roll, Torsion	*	Elastic response	0.3-0.85 (high)
0.72149	1.39	In-phase Roll	Heave and Surge	Rigid response	0.75 (hight)
0.79949	1.25	Out-of-phase Roll (Twist)	*	Elastic response	0.2-0.65 (moderate)
0.76 – 1.56	1.32 – 0.64	Surge (with or without Roll)	*		
1.56 and above	0.64	No significant response	*	No significant response	0.2 (poor)

It can be seen from Table 6.4 that surge is the significant motion of the Bretschneider MOB four module model. As the orientation is quartering seas, there is good roll and torsion response of the structure. There is no significant response above 1.56 Hz, which is higher than the response range seen in the one and two module cases. The structure shows elasticity in the 0.3-0.6 Hz and 0.7-1.56 Hz regions. The primary mode shape in the initial frequency range is the in-phase surge at 0.0975Hz. A combined sway, heave and roll response is observed at 0.234Hz. A heave and roll combination is observed at 0.273Hz. The frequency range between 0.3 to 0.6 Hz is dominated by a combination of surge, heave, roll and torsion, which is in the primary frequency response region of the wave. There is significant roll response with in-phase

roll at 0.72Hz and out-of-phase roll at 0.799Hz. There is a significant surge response between 0.76-1.56Hz frequency range. There is no significant response above 1.56Hz.
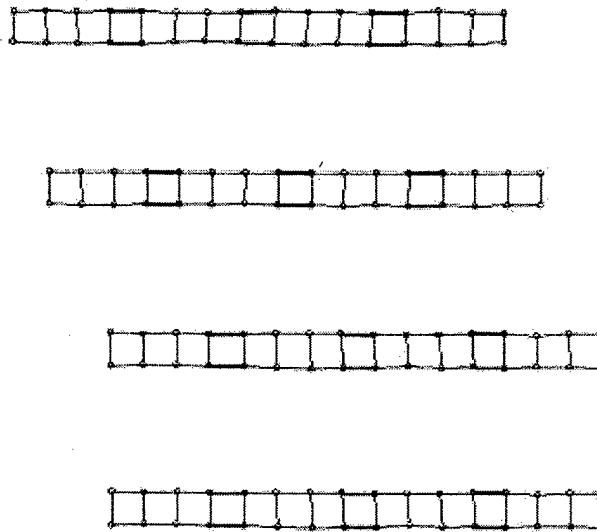
(a) In-phase Surge (0.09749 Hz)
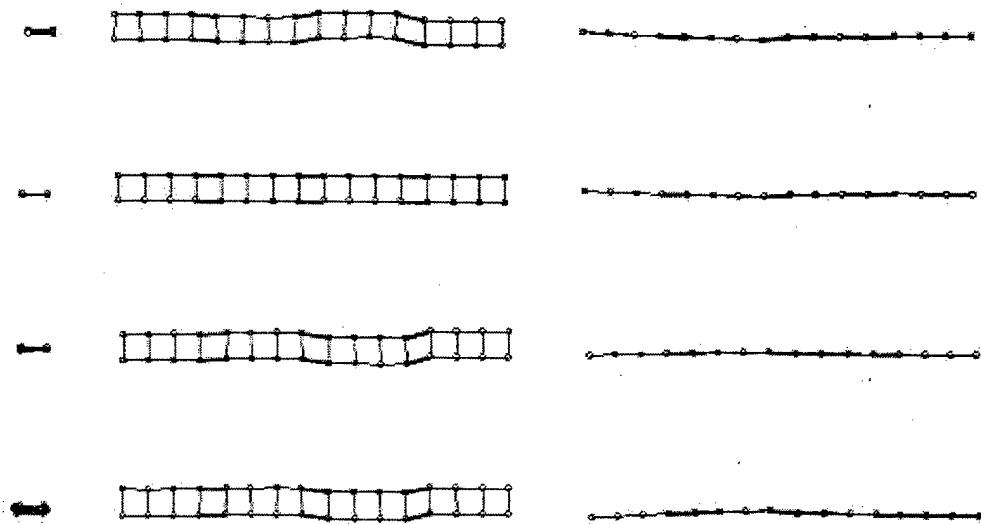
(b) Roll, Sway and Heave (0.23399 Hz)
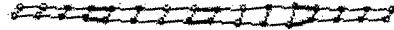
(c) Surge, Roll, and Heave (0.42899 Hz)
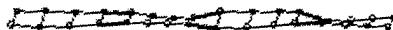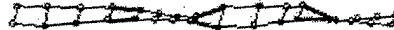
(d) Out-of-Phase Roll (0.79949 Hz)

117
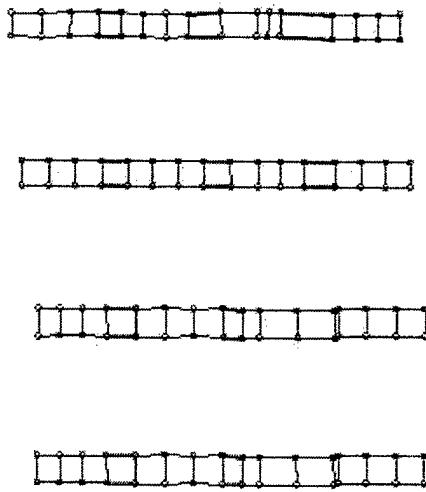
(e) Out-of-phase Surge (0.87749 Hz)

Figure 6.7: Mode Shapes of the Bretschneider Four Module MOB

There is only one set of connector force sensors available in the data set. Figure 6.8 shows the connector response on the port and starboard side. It can be seen that connector response range is dominant between 0.1 to 1 Hz with maximum force around 0.43Hz. This corresponds to the peak wave frequency (Figure 6.5) and elastic response region dominated by surge, roll and heave in a torsion motion (Table 6.4).
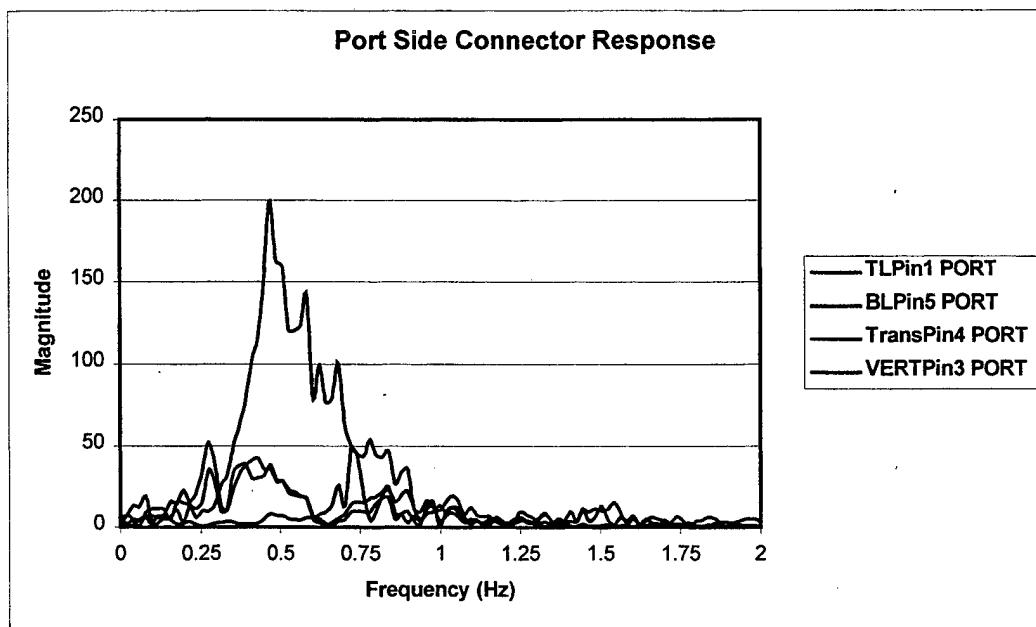
(a) Port Side Connector Response
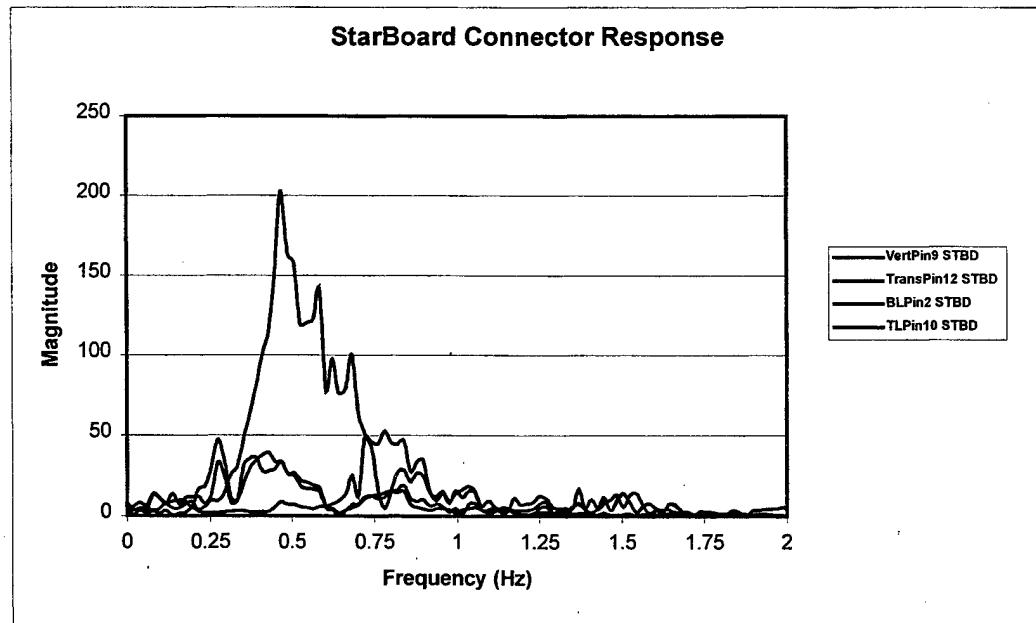
(b) Star Board Connector Response

Figure 6.8: Connector Response of a Bretschneider Four Module Test

119

Chapter 7

Summary, Conclusions, and Future Work

This chapter summarizes the thesis work and presents conclusions. The future directions for research based on this work are highlighted with recommendations.

7.1 Summary

The overall goal of this thesis was to provide necessary validation data to develop hydrodynamic and hydroelastic computer models for the analysis of critical MOB aspects. The response frequency mode shapes are analyzed and provided for the single, two and four module hydrodynamic scale model tests for available data sets. Results indicate the response of the MOB scale module to be elastic in nature. The nonlinear characteristics of the single module are also investigated. MI/SO results indicate the development of a nonlinear damping force in the MOB module.

7.2 Conclusions

The following conclusions are outcome of this thesis work:

- At any given frequency, the response of a module is generally described by a combination of mode shapes. The motion is rarely described using one particular mode shape alone.

- The response of the module is elastic. Significant torsion is observed in the Bretschneider single module, OCHI two module and Bretschneider four module configurations that depict the elastic motion response.

120

- The response of the modules is highly dependent on the kind on input wave. Poor roll response is observed in OCHI head seas, while the Bretschneider quartering seas show significant roll response at specific frequencies.

- High roll response is observed in quartering seas in the region of 0.6 to 0.8 Hz for single module Bretschneider case and 0.6 to 1.2 Hz region for the multi module case. This can be combined with a torsion response.

- In-phase and out-of-phase torsion is observed to be significant in both the two and four module case.

- Sway is observed to be the significant response type of a two module OCHI configuration.

- Surge is observed to be the significant response type of a four module Bretschneider configuration.

- A higher response range is observed in the four module case compared to the single and two module configurations.

- While no nonlinearity is observed in Direct MI/SO models (wave influence on the module), good nonlinearity is present in Reverse MI/SO models that suggest the presence of a nonlinear damping force.

7.3 Future Work

This section reviews the future work that the efforts of this thesis can lead:

- *Development of hydrodynamic and hydroelastic models*

  In keeping with the objectives of this thesis, the frequency mode shape values can be used to develop hydrodynamic and hydroelastic computational models. Several

commercial finite element analysis programs, namely ABAQUS® and Algor®, have built in hydroelastic elements that can be used in creating the models. The input wave can be specified and the output response for a particular finite element model can be made to match the values provided by this research work.

- *Conducting further scale model testing*

  One of the primary constraints in the analysis of a MOB scale model response was the lack of sufficient data sets. Further testing can be carried out for different wave models for the single, two and four model configurations. In designing future tests, the following aspects need special attention:

  o Run lengths should be sufficient so that the initial transient effects can be removed from the time history, while having enough records for better averaging of results. At the same time, care should be taken to prevent lengthy data collection that might be affected by wave reflections.

  o Proper calibration data for all the sensors should be available. This study did not concern itself with the amplitudes of the responses. In order to facilitate the study of the amplitudes of the response, properly scaled and referenced acceleration data need to be made available.

  o Sufficient runs must be made for head, beam and quartering seas.

  o Wider random spectra should be utilized for three sets of seas – head, beam and quartering at different amplitudes.

BIBLIOGRAPHY

[1]   Taylor, R.L. and Zueck, R.F., "Mobile Offshore Base – A Self Propelled Logistics Platform", Logistics Spectrum, SOLE, Vol. 35, Issue 1, January – March 2001.

[2]   Weybrant, E., 1999, "A computational study of connector force dynamics in a mobile offshore base (MOB)", dissertation at the University of Maine, Orono.

[3]   Remmers, G., Zueck, R., Palo, P., and Taylor, R., "Mobile Offshore Base", presented at ISOPE, Montreal, May 1997.

[4]   Sikora, J., and Smith, T., 1998, "Test plan for MOB Model Tests", NSWCCCD, Third Draft.

[5]   Zueck, R., Taylor, R. and Palo, P. "Development Options for Mobile Offshore Base Technology", The 11th International Offshore and Polar Engineering Conference, Stavanger, Norway, June 2001.

[6]   Smith, T.C., O'Dea, J., and Lewis, R., January, 1998, "Mobile Offshore Base Motions and Connector Loads Data Reduction", Naval Surface Warfare Center Report CRDKNSWC/HD-0279-10.

[7]   Blevins, R.D., 1977, "Flow-induced vibration", Van Nostrand Reinhold Company.

[8]   Blevins, R.D., 1979, "Structural Vibrations in a Fluid", Chapter 14 from "Formulas for Natural Frequency and Mode Shapes", Van Nostrand Reinhold Company.

[9]   Barr, R.A., November 10, 1999, "Review of NSWCCD Mask Wave Test Data for use in MOB Tests", Technical Note 9920-1, Hydronautics Research, Inc.

[10]   McCormick, M.E., 1973, "Ocean Engineering Wave Mechanics", Wiley-Interscience Publication.

[11]   Wilson, J.F., 1984, "Dynamics of Offshore Structures", Wiley-Interscience Publication.

[12]   Ochi, M.K., 1998, "Ocean Waves: The Stochastic Approach", Cambridge University Press.

[13] Zhang, J., 1998, "Ocean Wave Kinematics, Dynamics and Loads on Structures", *Proc.* of the 1998 International OTRC Symposium, ASCE.

[14] Berteaux, H., "Buoy Engineering", UMI Books on Demand, 1994, originally published by John Wiley & Sons, 1976.

[15] Caccese, V., February 2000, "Dynamic Response of the Mobile Offshore Base Hydroelastic Test Model", Technical Progress Report, Department of Mechanical Engineering, University of Maine, Orono, USA.

[16] Riggs, H. R., "Current Efforts in Technology Development for Very Large Floating Structures", First International Workshop on Very Large Floating Structures, Honolulu, April 1991.

[17] Sarpkaya, T., and Isaacson, M., 1981 "Mechanics of Wave Forces on Offshore Structures", Van Nostrand Reinhold Company.

[18] Ochi, M. K., and Hubble, E. N., 1976, On six-parameter wave spectra. *Proc. 15th Coastal Engineering Conf., A.S.C.E.*, 321-328.

[19] Allemang, R. J., 1995, Vibrations: Experimental Modal Analysis; Structural Dynamics Research Laboratory; University of Cincinnati; UC-SDRL-CN-20-263-663/664; Cincinnati, Ohio.

[20] National Instruments, "Phase" and "Phase Measurements", Measurement Glossary.

[21] Bendat, J.S., 1998, "Nonlinear systems techniques and applications", John Wiley and Sons, Inc.

[22] Marven, C. and Ewers, G., 1996, "A Simple Approach to Digital Signal Processing", John Wiley and Sons.

[23] Morgan, D., 1994, "Practical DSP – Modeling, Techniques, and Programming in C", John Wiley and Sons.

[24] Bendat, J.S., and Piersol, A.G., 1986, "Random Data: Analysis and Measurement Procedures", John Wiley and Sons.

[25] Wiener, N., 1949, "Extrapolation, Interpolation, and Smoothing of Stationary Time Series", published jointly by MIT Press and John Wiley and Sons.

[26] Bendat, J.S., and Piersol, A.G., 1980, "Engineering Applications of Correlation and Spectral Analysis", John Wiley and Sons.

[27] Bendat, J.S., 1990, "Nonlinear system analysis and identification from Random Data", John Wiley and Sons.

[28] MathWorks, 1999, "MATLAB Signal Processing Toolbox", Ver. 4, User's Guide.

[29] M.A. Corp, 2000, "Integrated Test Analysis Processor Toolbox User's Guide".

Appendix A

Non-Dimensional Parameters of a Two-Dimensional, Spring-Supported, Damped Structural Model Exposed to a Steady Flow (Blevins, 1977)

A.1 Fineness ratio (non-dimensional geometry parameter)

$$\text{Fineness ratio} = \frac{L}{D} = \frac{\text{Length}}{\text{Width}} \qquad \text{Eq(A.1)}$$

Width (D) – side normal to the free stream surface.

Length (L) – characteristic length along the free stream surface

A.2 Reduced Velocity (non-dimensional velocity parameter)

$$\text{Reduced Velocity} = \frac{U}{fD} = \frac{\text{path length per cycle}}{\text{Model width}} \qquad \text{Eq(A.2)}$$

U – free stream velocity

f - frequency of vibration (of structure in fluid)

The non-dimensional frequency is the inverse of reduced velocity.

A.3 Dimensionless Amplitude

$$\text{Dimensionless Amplitude} = \frac{A_y}{D} = \frac{\text{vibration amplitude}}{\text{model width}} \qquad \text{Eq(A.3)}$$

A.4. Mass Ratio

$$\text{Mass ratio} = \frac{m}{\rho D^2} = \frac{\text{mass per unit length of model}}{\text{fluid density x model dimension}} \qquad \text{Eq(A.4)}$$

'm' includes structural and "added" mass

126

The mass ratio term is commonly used to measure the susceptibility of lightweight structures to flow-induced vibration.

A.5 Reynold's Number (Re)

$$Re = \frac{UD}{v} = \frac{\text{inertial force}}{\text{viscous force (kinematic viscosity)}} \qquad \text{Eq(A.5)}$$

This ratio is used to determine the transition from laminar to turbulent fluid flow and the boundary layer thickness.

A.6 Mach Number

$$\text{Mach Number} = \frac{U}{c} = \frac{\text{fluid velocity}}{\text{velocity of sound}} \qquad \text{Eq(A.6)}$$

A.7 Damping Factor/Ratio (ζ)

$$\zeta = \frac{\text{energy dissipated per cycle}}{4\pi * \text{total energy of the structure}} \qquad \text{Eq(A.7)}$$

A.8 Reduced Damping (δ_r)

$$\frac{2m(2\pi\zeta)}{\rho D^2} = \delta_r \qquad \text{Eq(A.8)}$$

A.9 Application of the non-dimensional parameters

The dimensionless amplitude is a function of fineness ratio, reduced velocity, Reynolds's number, damping ratio, mass ratio.

$$\frac{A_y}{D} = F(\frac{L}{D}, \frac{UD}{v}, \frac{U}{fD}, \frac{m}{\rho D^2}, \zeta) \qquad Eq(A.9)$$

A.10 Strouhal Number (S)

The Strouhal number is the non-dimensional frequency parameter. At low Mach number flows it is a function of geometry and Reynold's number. Expression for Strouhal's number is:

$$f_s = \frac{SU}{D} \qquad Eq(A.10)$$

f_s – frequency of vortex shedding (dominant)

U – free stream velocity

D – width (normal to free stream surface)

S – Strouhal number

Strouhal numbers for specific geometries are available. "Bluff sections" have lower Strouhal numbers.

A.11 Froude Number (Fr)

Froude number is proportional to the inertial force over the gravitational force and is used in momentum transfer in general and open channel flow and wave and surface behavior calculations in particular. It is normally defined in one of the following forms

$$Fr = \underline{V^2} \quad (or) \quad \underline{V^2} \qquad Eq(A.11)$$

$$a*L \qquad g*L$$

where a   -   Acceleration
       g   -   Gravitational acceleration
       L   -   Characteristic Length
       V   -   Fluid Velocity

Appendix B

Wave Spectrums

B.1 Bretschnieder Wave Spectrum Example

$H_s := 12$ Significant wave height (ft)

$T_s := 6.9$ Significant wave period (sec.)

$$S_{2H}(T) := \frac{4200 \, H_s^2}{T_s^4 \cdot \left(\frac{2 \cdot \pi}{T}\right)^5} \cdot e^{-\frac{1050}{T_s^4 \cdot \left(\frac{2 \cdot \pi}{T}\right)^4}}$$ Bretschnieder Formula ft^2-sec

$T := 2.0, 2.1 .. 16$

Bretschneider Double Height Spectra
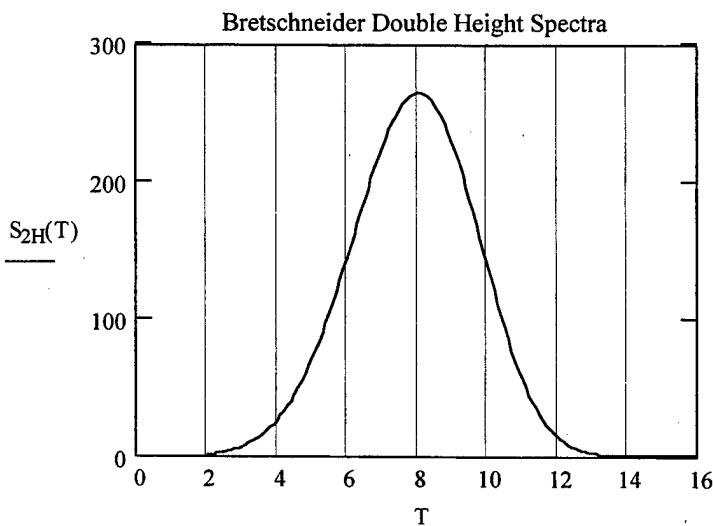
B.2 OCHI Wave Spectrum Example

$$\zeta := \begin{pmatrix} 13.59\,\text{ft} \\ 10.73\,\text{ft} \end{pmatrix} \qquad \omega m := \begin{pmatrix} 0.58 \\ 1.00 \end{pmatrix} \qquad \lambda := \begin{pmatrix} 2.67 \\ 1.37 \end{pmatrix}$$

$$\omega := 0, 0.005 .. 2.00$$

$$S(\omega) := \frac{1}{4} \cdot \sum_{j=1}^{2} \frac{\left(\dfrac{4 \cdot \lambda_j + 1}{4} \cdot \omega m_j \right)^{\lambda_j}}{\Gamma(\lambda_j)} \cdot \frac{(\zeta_j)^2}{\omega^{(4 \cdot \lambda_j + 1)}} \cdot e^{-\left(\dfrac{4 \cdot \lambda_j + 1}{4} \right) \cdot \left(\dfrac{\omega m_j}{\omega} \right)^4}$$

OCHI Six-Parameter Spectrum

131
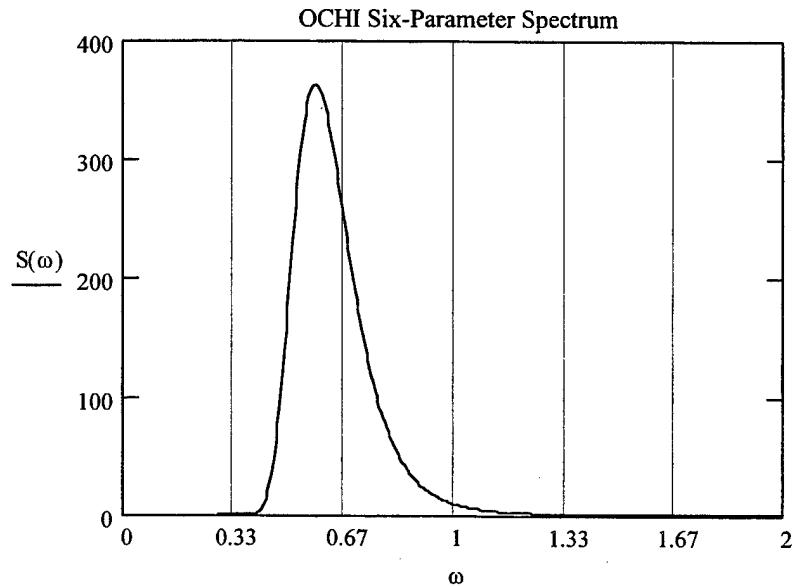
Appendix C

Integration and Differentiation Functions - MATLAB® Code Listing

C.1 dsp_diff.m

```
%
% DSP_DIFF() - Function to Perform Differentiation
%

function [yf, vf, af] = dsp_diff(y, sfreq, FMax, Wn)

dt = 1/sfreq;
[m,n] = size(y);
Time = [0:dt:m*dt-dt]';

% Get velocity
v   = diff(y)/dt;
[p,q] = size(v);

% FFT filter the velocity
[vnew] = fftfil(v,FMax,Wn);
[r,s] = size(vnew);

% Get acceleration
a   = diff(vnew)/dt;
[t,u] = size(a);

% Normalize the acceleration
[anew] = fftfil(a,FMax,Wn);
[e,f] = size(anew);

% Final results
yf   =      y(1:e);
vf   =   vnew(1:e);
af   =   anew(1:e);
```

C.2 dsp_int.m

```
%
% Dsp_int() - Function to perform integration of data
% Integration technique - constant acceleration method
%

function [yf, vf, af] = dsp_int(a, sfreq, FMax, Wn)

dt = 1/sfreq;
[m,n] = size(a);
Time = [0:dt:m*dt-dt]';

% Obtain the velocity
v = zeros(m,1);
for i=1:(m-1)
      dt = Time(i+1,1)-Time(i,1);
      da = a(i+1,1) - a(i,1);
      dv = a(i,1)*dt + 0.5*da*dt;
      v(i+1,1) = v(i,1) + dv;
end

% FFT filter the velocity
[vnew] = fftfil(v,FMax,Wn);
[p,q] = size(vnew);

% Obtain the displacement from the filtered velocity
y = zeros(p,1);
for i=1:(p-1)
    dt = Time(i+1,1)-Time(i,1);
    dvnew = vnew(i+1,1) - vnew(i,1);
    dy = vnew(i,1)*dt + 0.5*dvnew*dt;
    y(i+1,1) = y(i,1) + dy;
end

% FFT filter the displacement
[ynew] = fftfil(y,FMax,Wn);
[r,s] = size(ynew);

% Return result
af =    a(1:r);
vf = vnew(1:r);
yf = ynew(1:r);
```

C.3 fftfil.m

```
%
% fft_fil() - Function to perform FFT filtering
%
function [v_new] = fftfil(v, maxfreq, remfreq)

m = length(v);
fdt = maxfreq/m;
freq = [fdt:fdt:m*fdt];
v_fft = fft(v);
v_fft_new = zeros(m,1);
rmlen = (maxfreq/remfreq)/2;
v_fft_new(rmlen+1:(m-rmlen)) = v_fft(rmlen+1:(m-rmlen));
v_new = real(ifft(v_fft_new));
```

Appendix D

Time History, SI/SO and MI/SO Results for Single Module MOB Scale Model Tests

D.1 Bretschneider BOW66 (b) Quartering Sea 2_58per 1125 RPM Data Set

File: Ochi$_h$d Chan:FWD WHT   [dt=0.1, N$_w$=128, df=0.078, N$_{av}$=9, Mean=0.0015, Std=1.4] 02-Jul-2001 11:53 PM
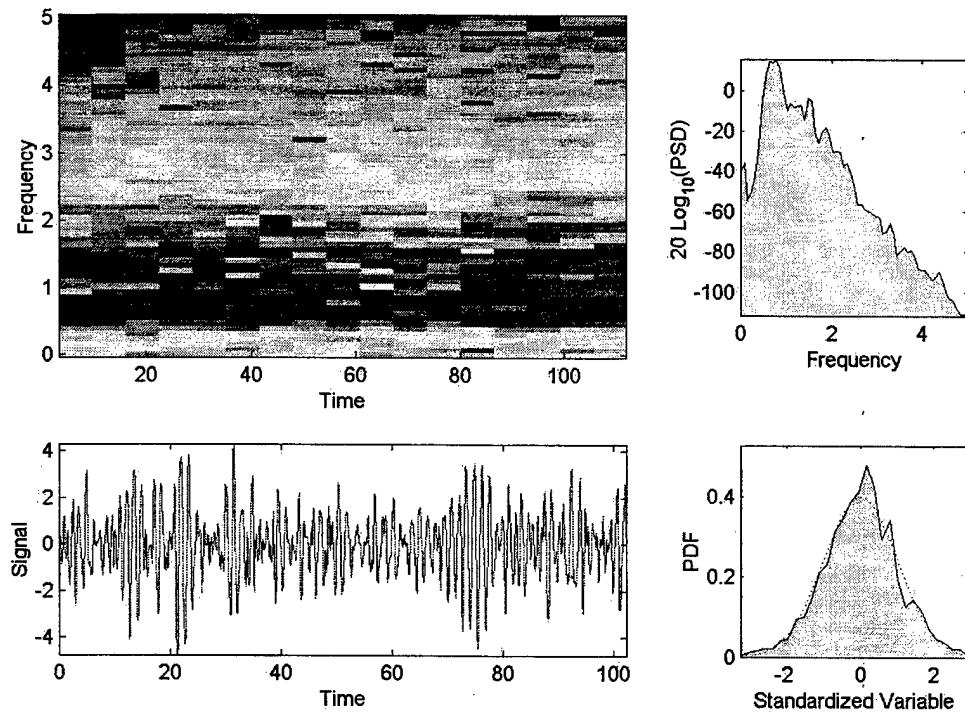
Figure D.1: FWD_WHT Time History (Input Power)
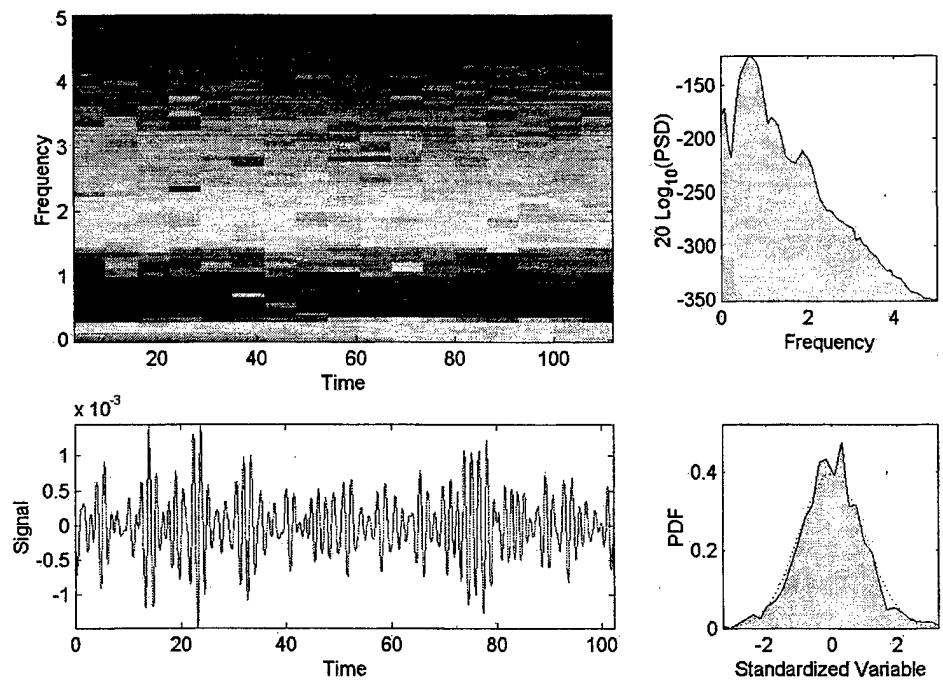
Figure D.2: Heave (Average Z) Time History (Output Power)
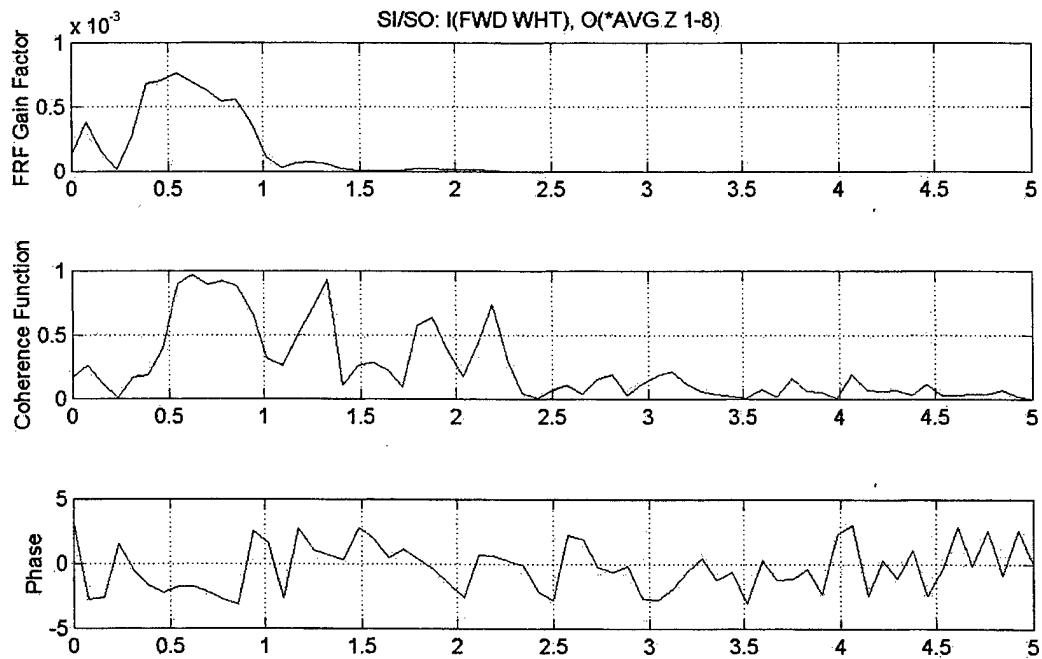
Figure D.3: SI/SO Input = FWD_WHT Output = Average Z

136
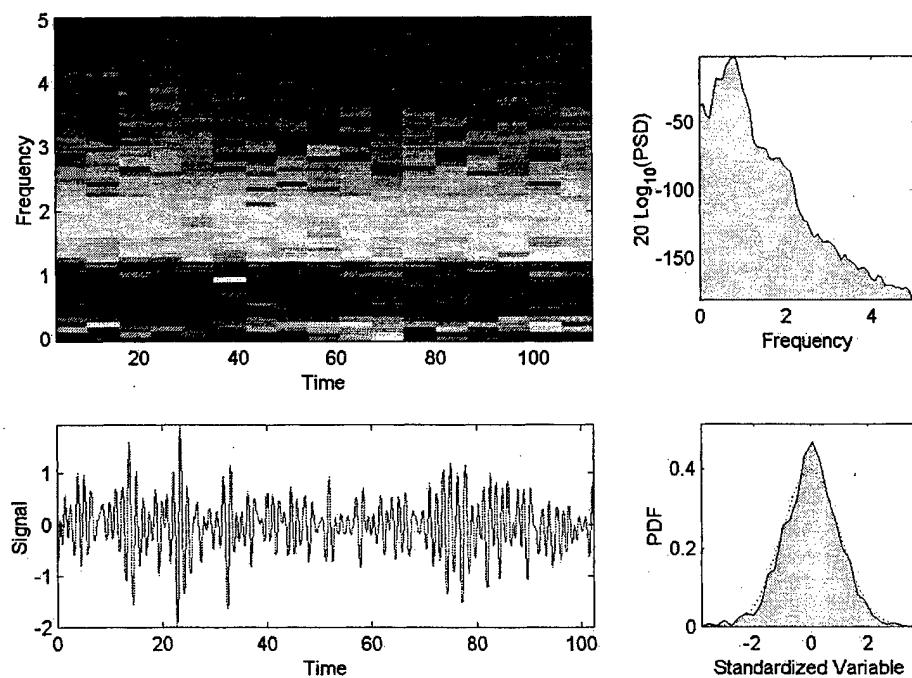
Figure D.4: Pitch Time History (Output Power)
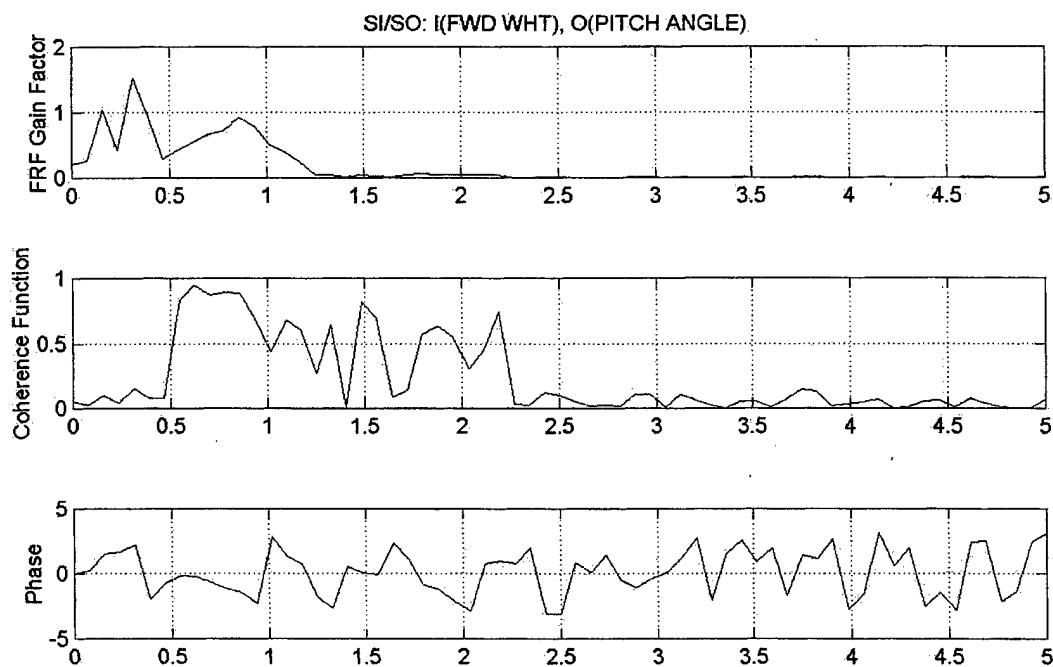
Figure D.5: SI/SO Input = FWD_WHT Output = Pitch

137

File: Ochi$_h$d Chan:Roll R [dt=0.1, N$_w$=128, df=0.078, N$_{av}$=9, Mean=0.03, Std=0.38]   03-Jul-2001 1:02 AM
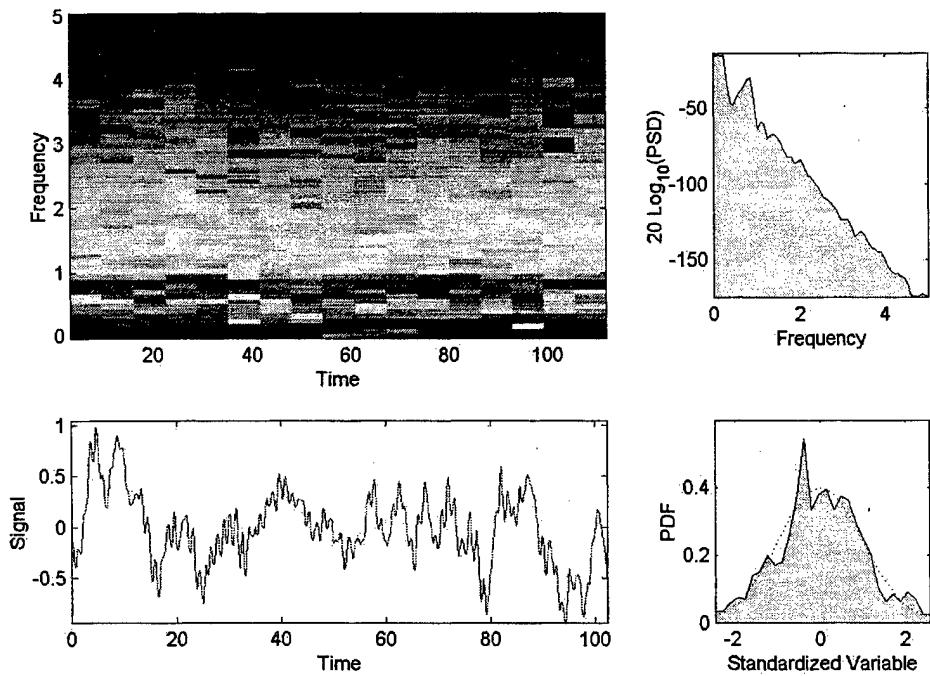
Figure D.6: Roll Time History (Output Power)

SI/SO: I(FWD WHT), O(ROLL ANGLE)
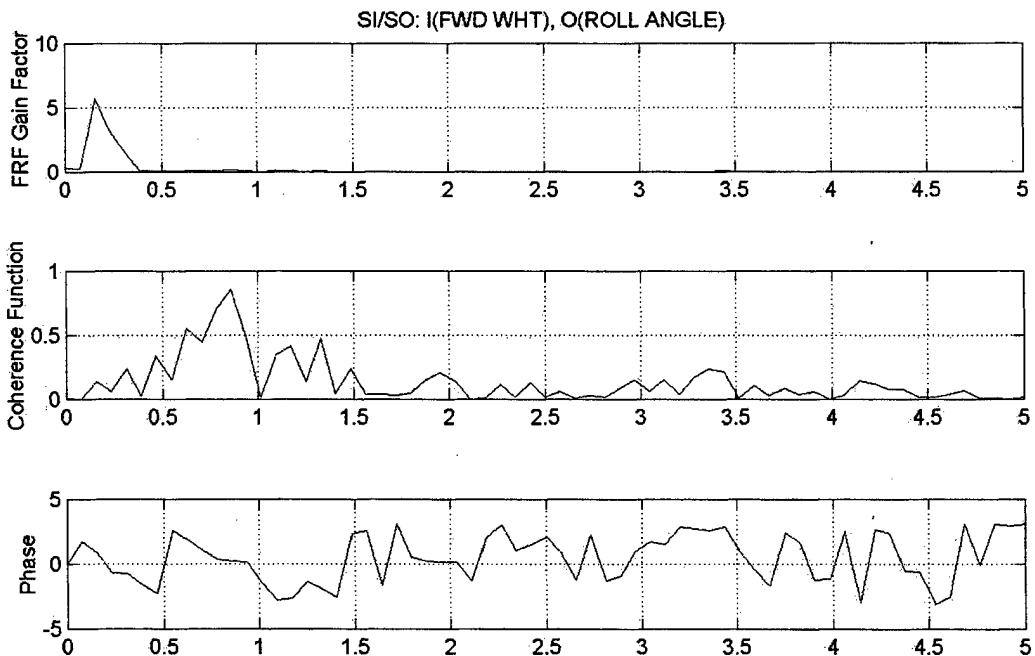
Figure D.7: SI/SO Input = FWD_WHT Output = Roll

138
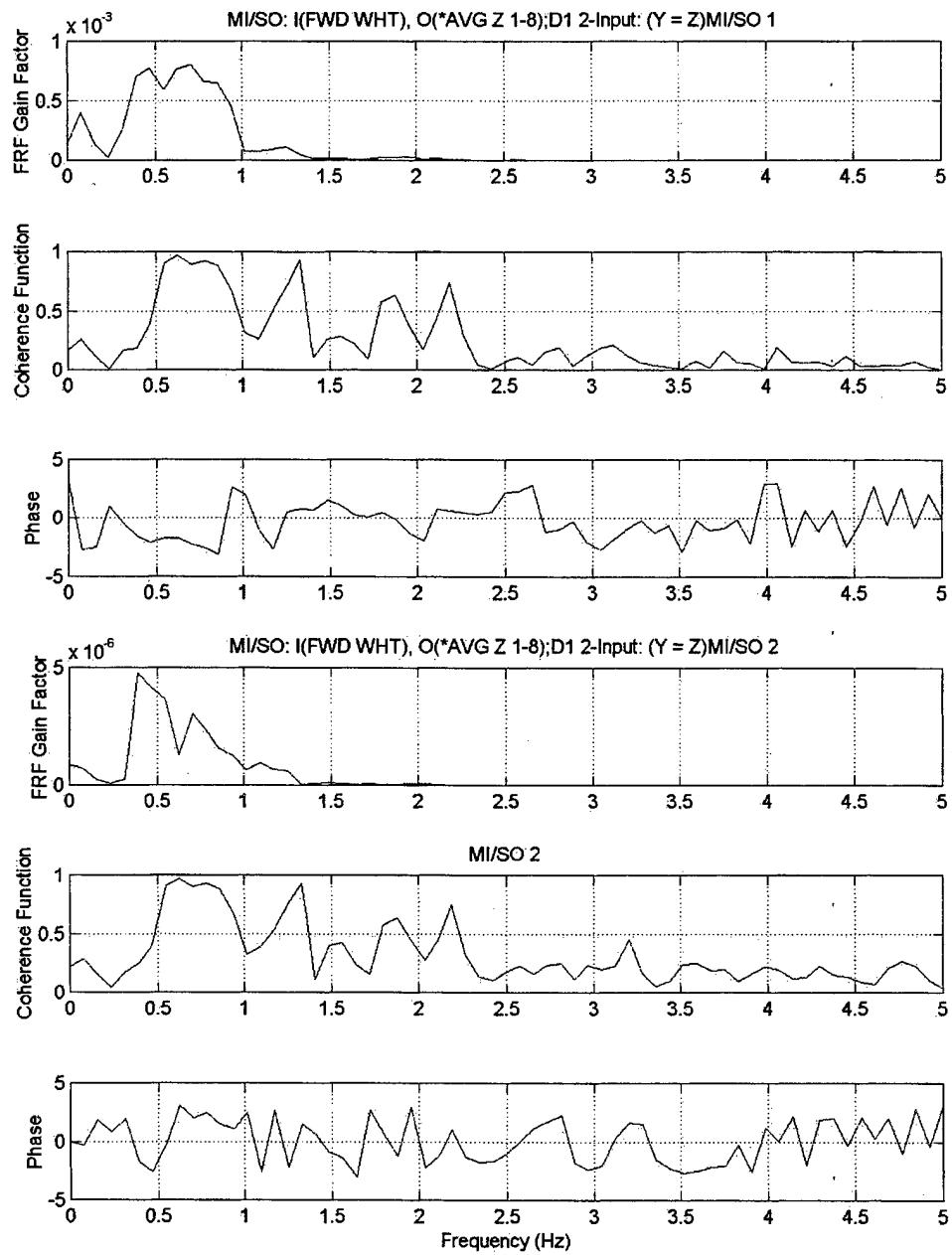
Figure D.8: Direct Two-Input MI/SO Model D1
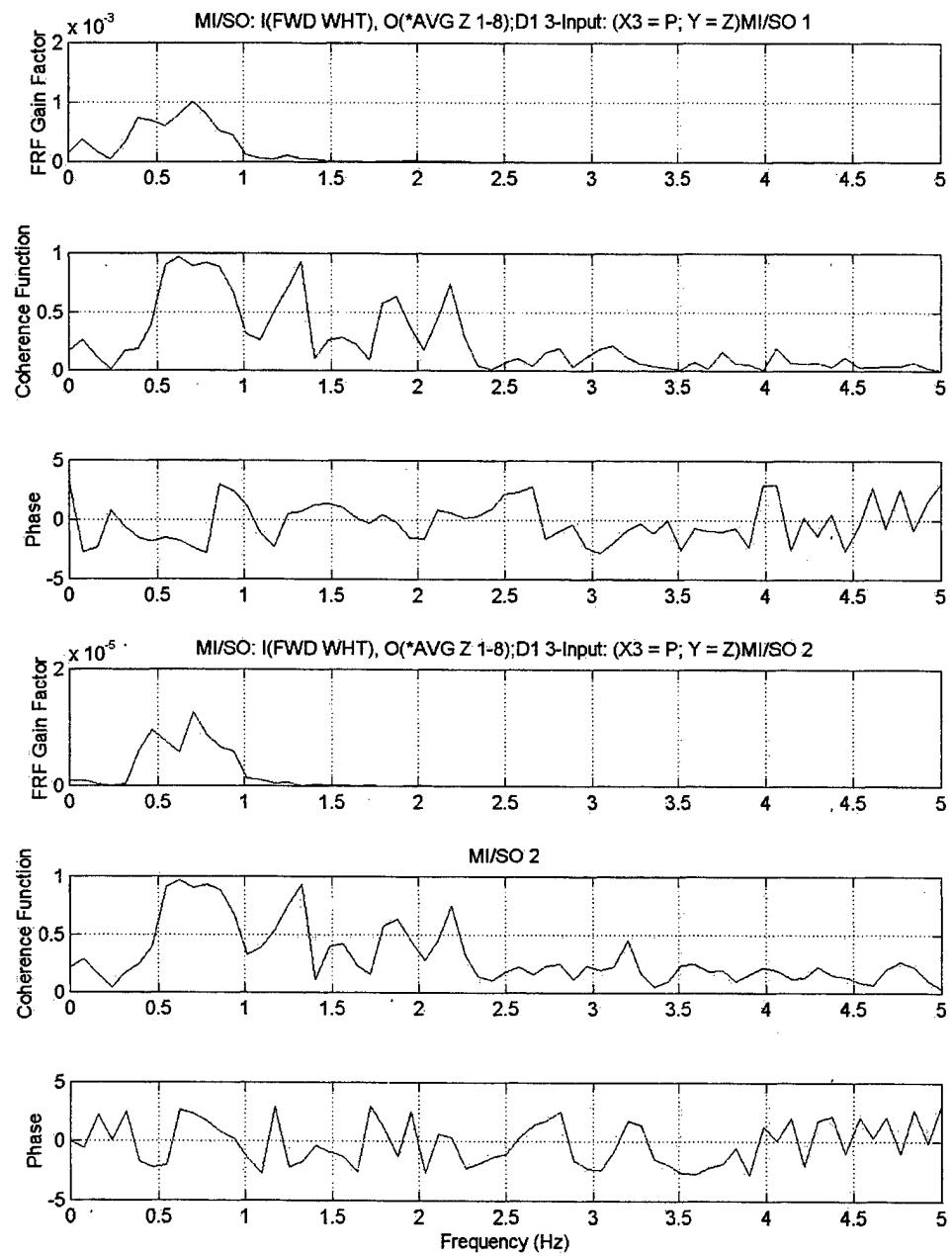
Figure D.9: Direct Three-Input MI/SO Model D1
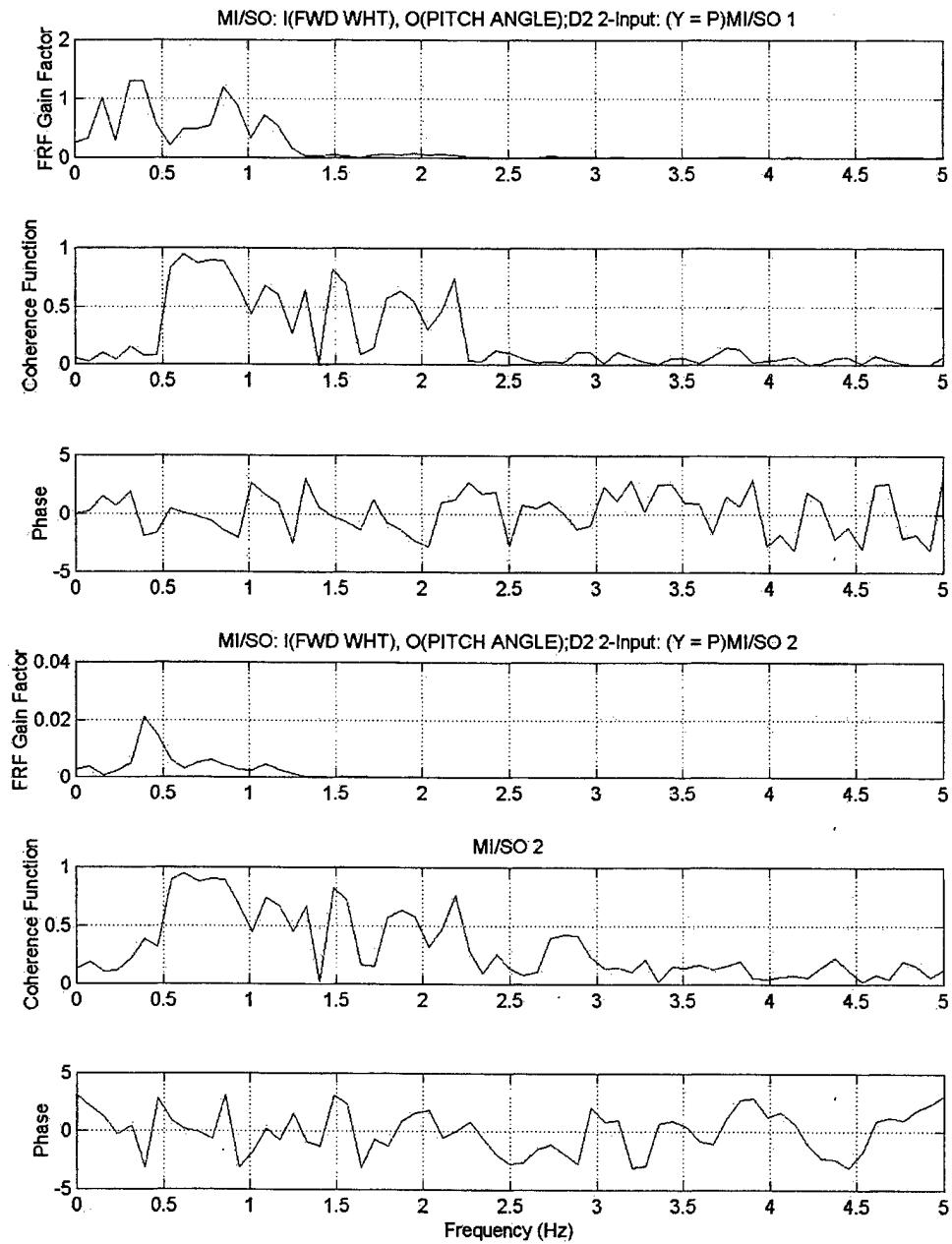
Figure D.10: Direct Two-Input MI/SO Model D2
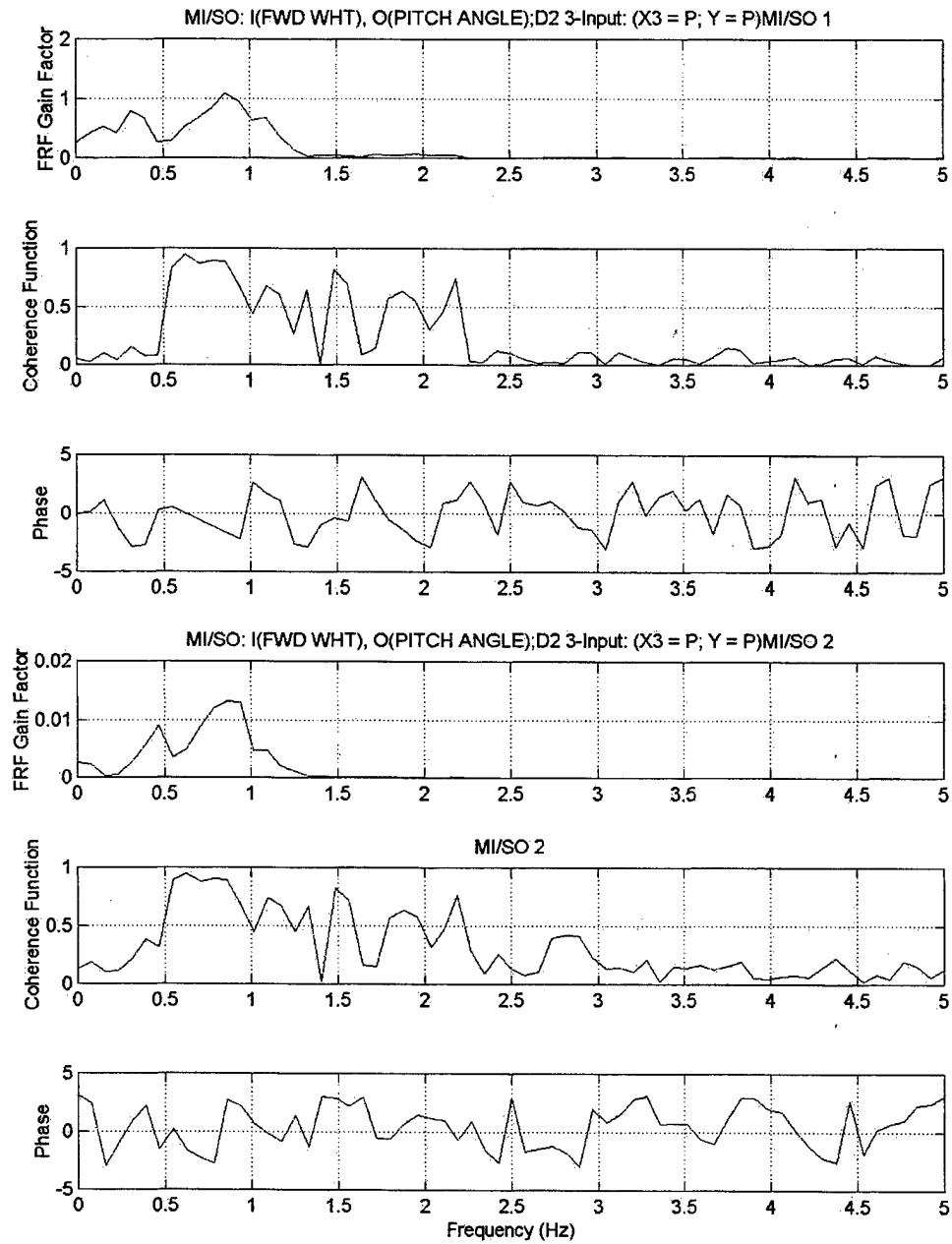
Figure D.11: Direct Three-Input MI/SO Model D2
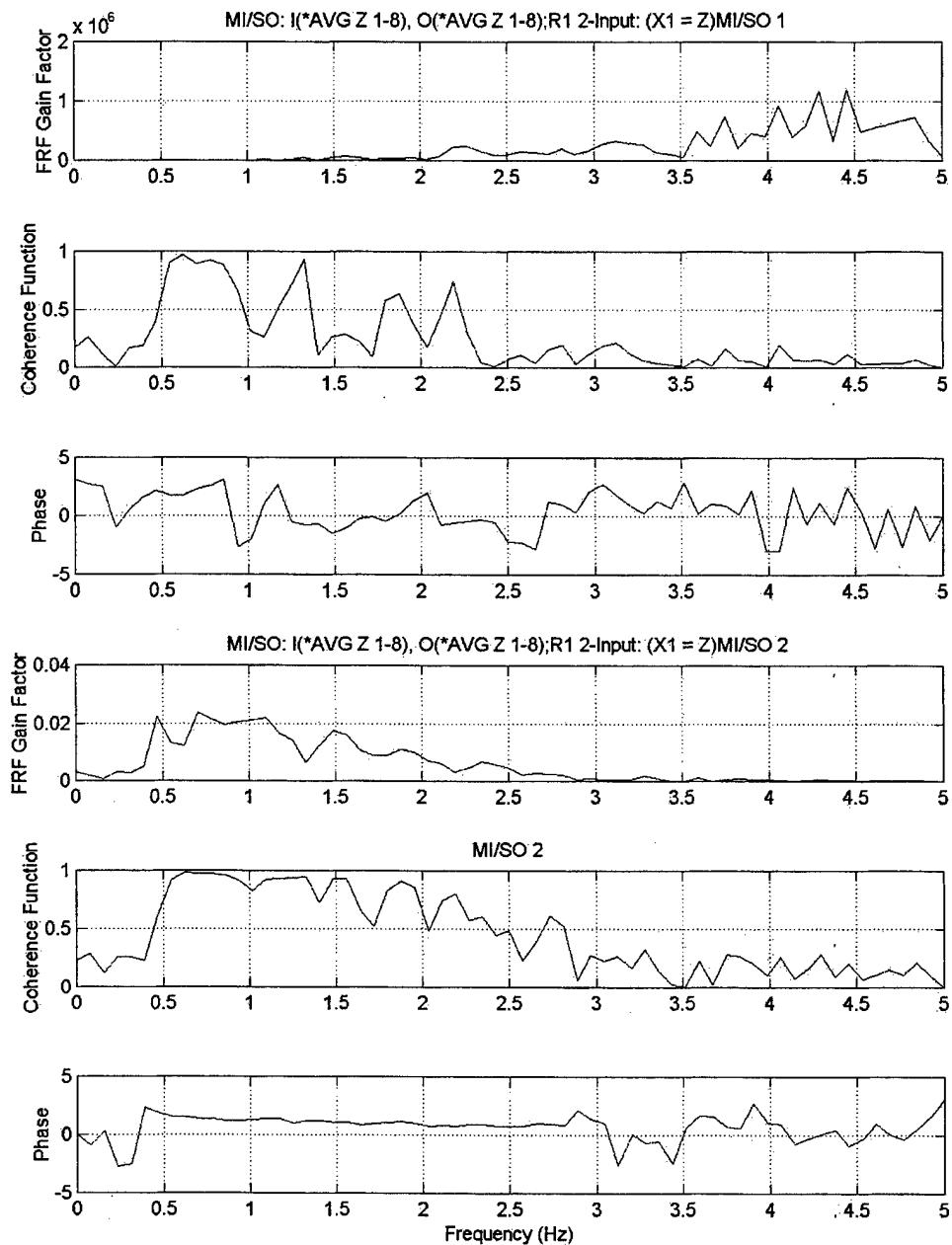
Figure D.12: Reverse Two-Input MI/SO Model R1

143
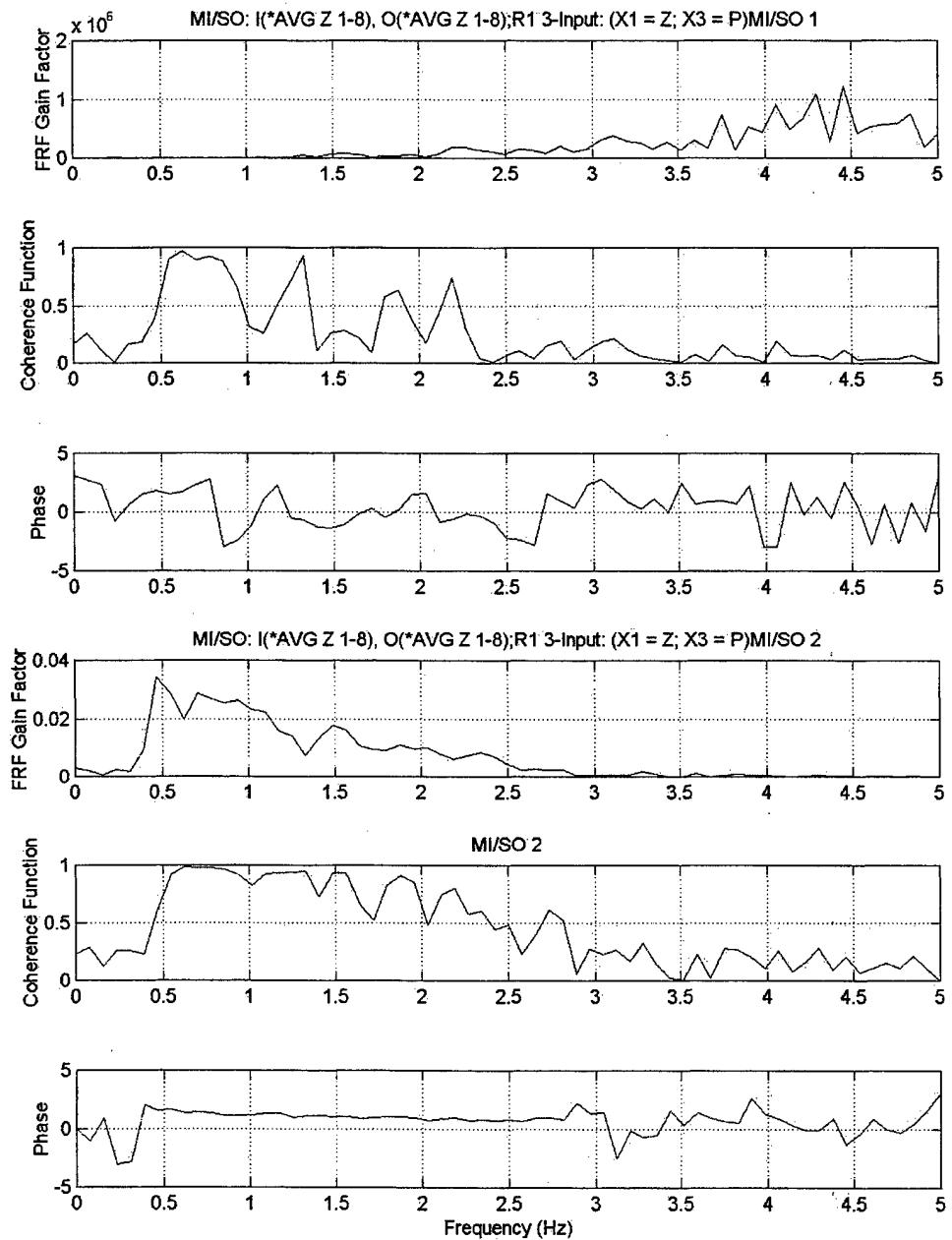
Figure D.13: Reverse Three-Input MI/SO Model R1

144
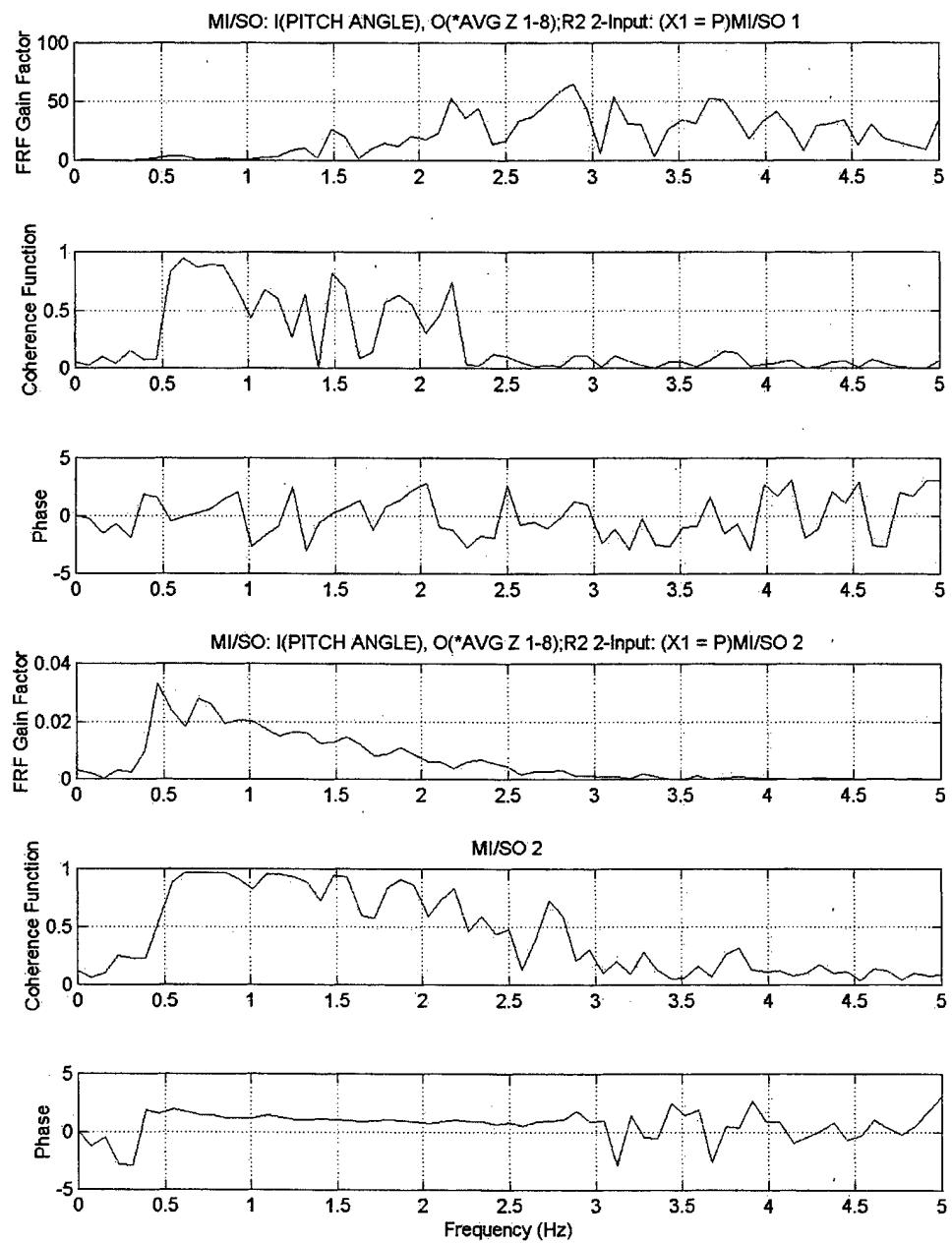
Figure D.14: Reverse Two-Input MI/SO Model R2
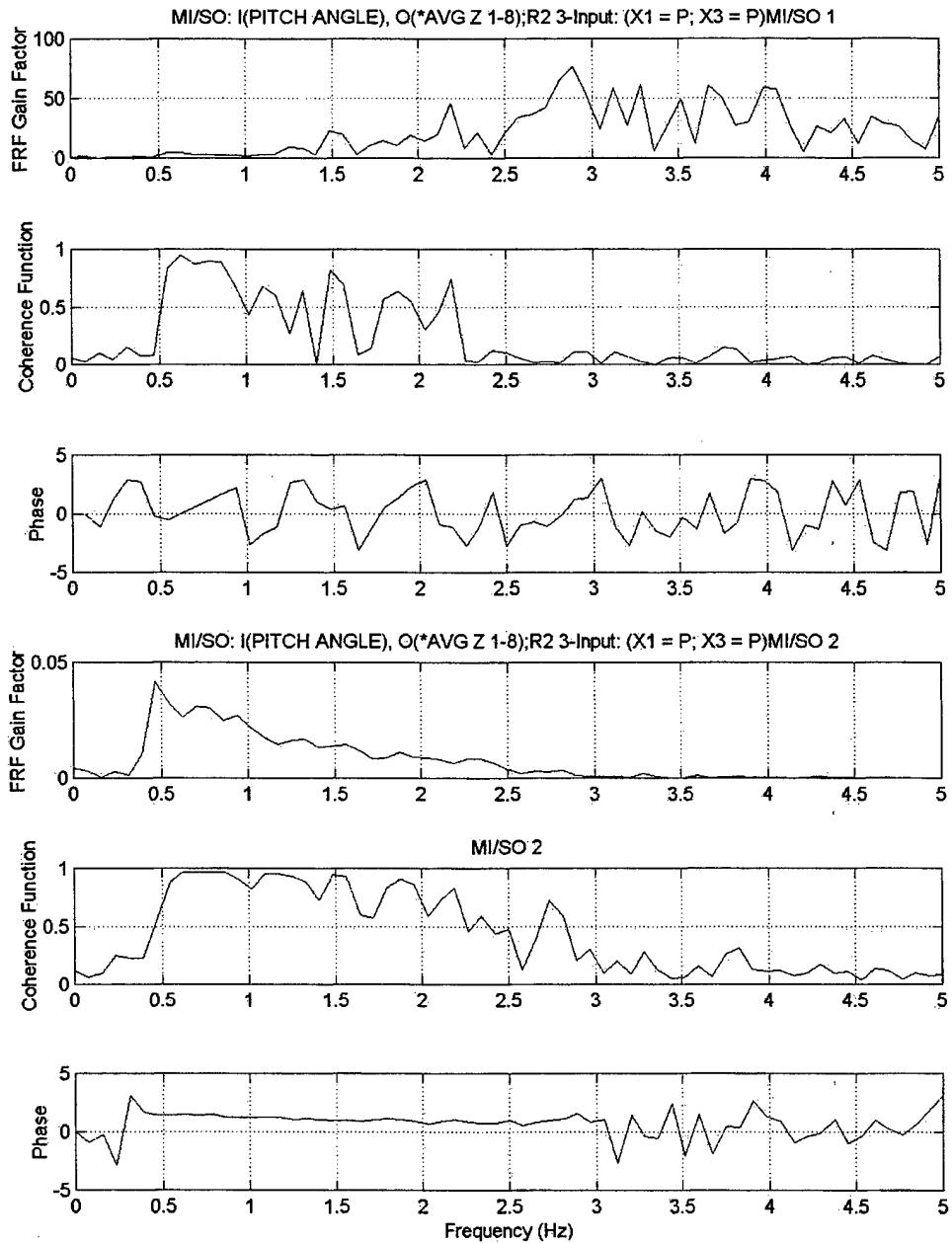
Figure D.15: Reverse Three-Input MI/SO Model R2

D.2 Bretschneider BOW66 (b) Quartering Sea 2_58per 1125RPM Data Set

File: FWD$_W$HT Chan:FWD$_W$HT [dt=0.1, N$_w$=128, df=0.078, N$_{av}$=13, Mean=-0.0044, Std=3] 11-Jul-2001 12:30PM
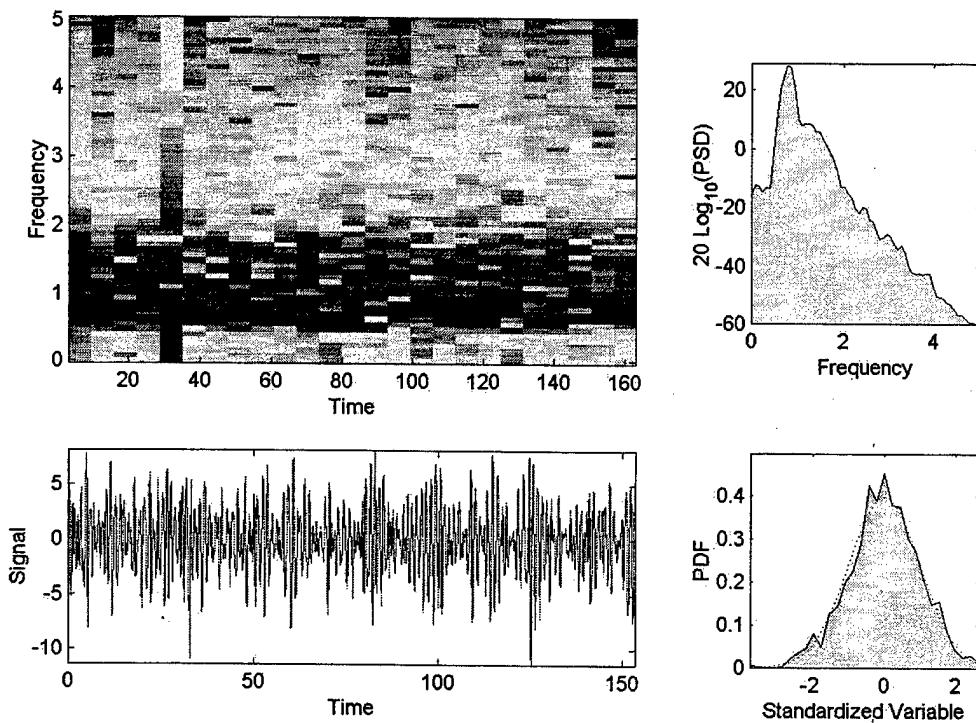
Figure D.16: FWD_WHT Time History (Input Power)
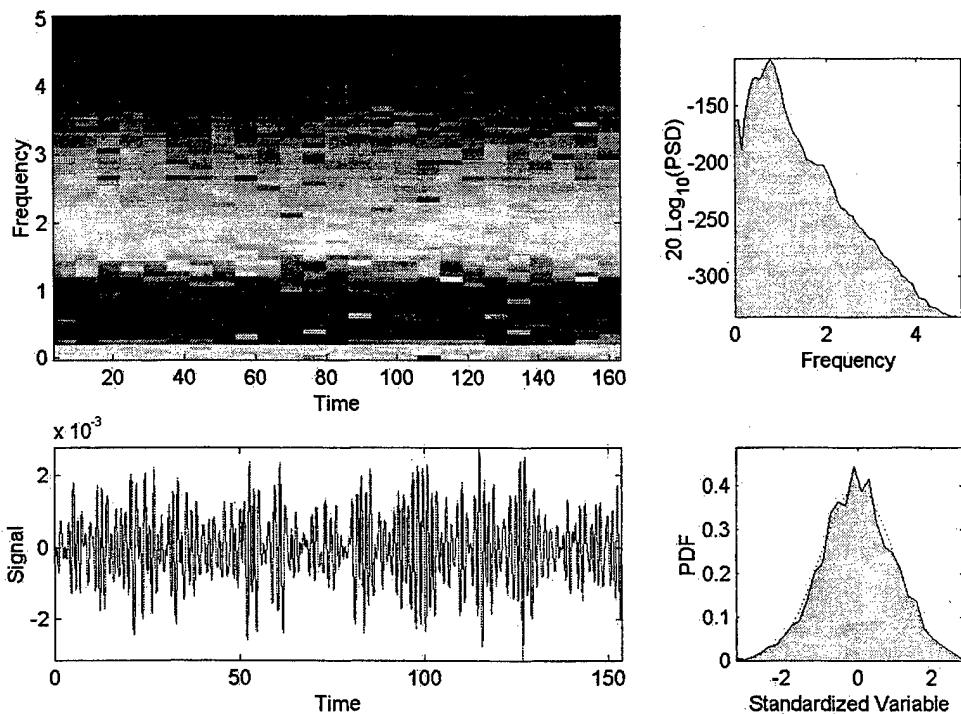
Figure D.17: Heave (Average Z) Time History (Output Power)
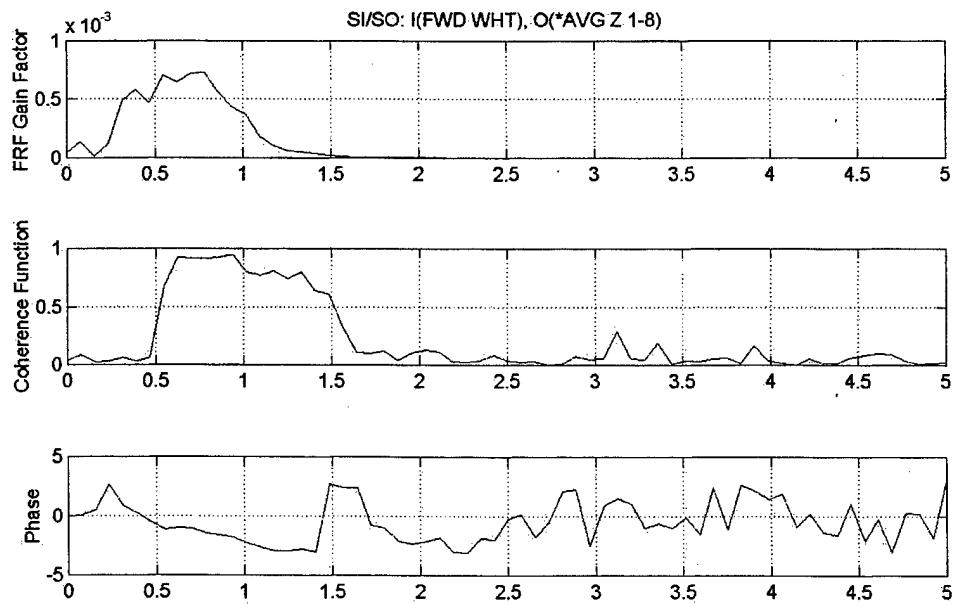
Figure D.18: SI/SO Input = FWD_WHT Output = Average Z
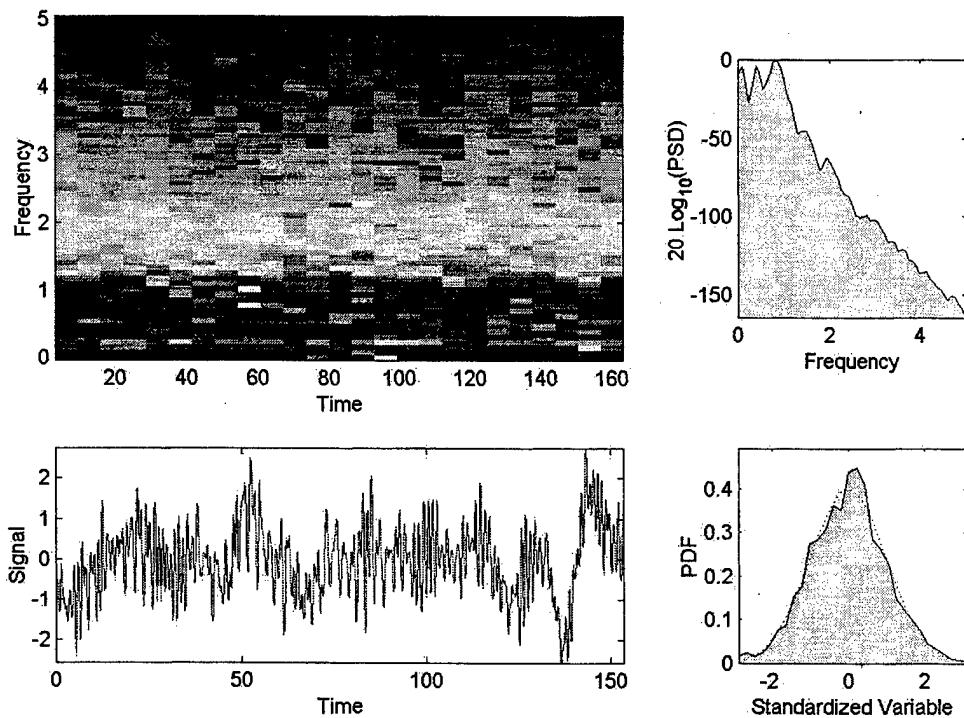
Figure D.19: Pitch Time History (Output Power)
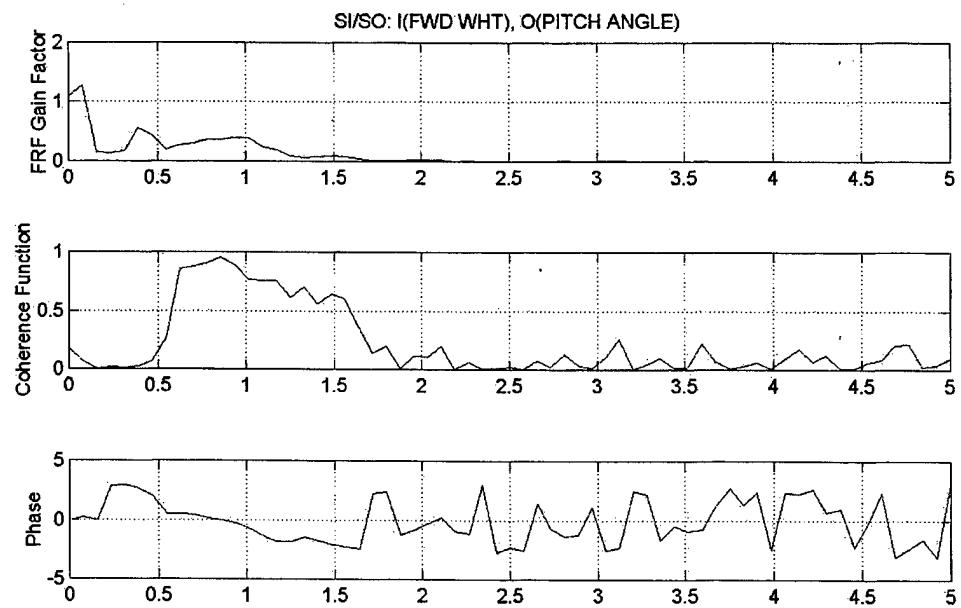
Figure D.20: SI/SO Input = FWD_WHT Output = Pitch

File: R Chan:R [dt=0.1, N$_w$=128, df=0.078, N$_{av}$=13, Mean=-0.023, Std=3.1]   11-Jul-2001 12:30PM
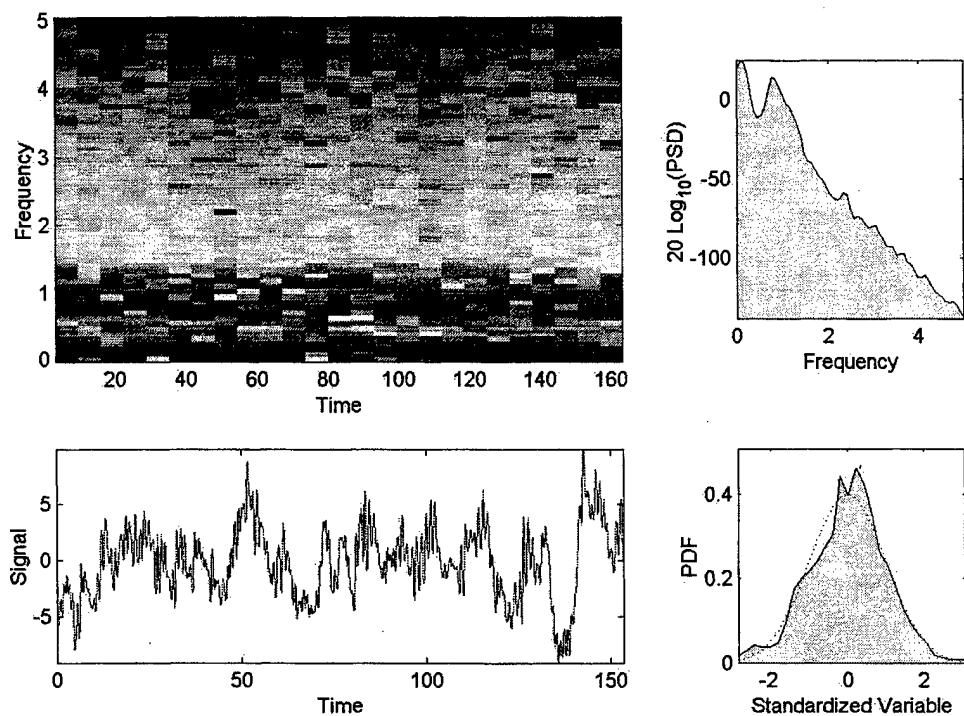
Figure D.21: Roll Time History (Output Power)

SI/SO: I(FWD WHT), O(ROLL ANGLE)
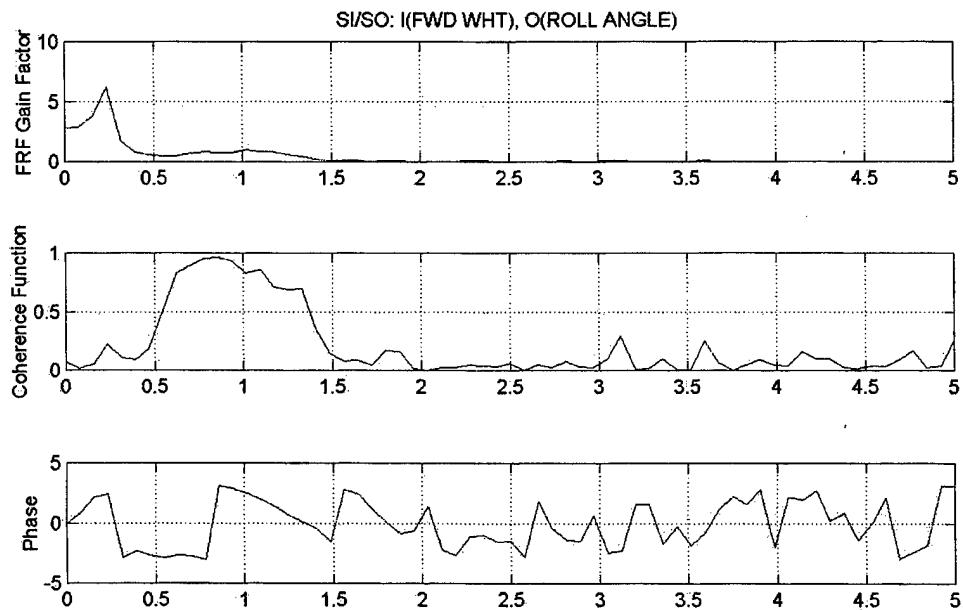
Figure D.22: SI/SO Input = FWD_WHT Output = Roll
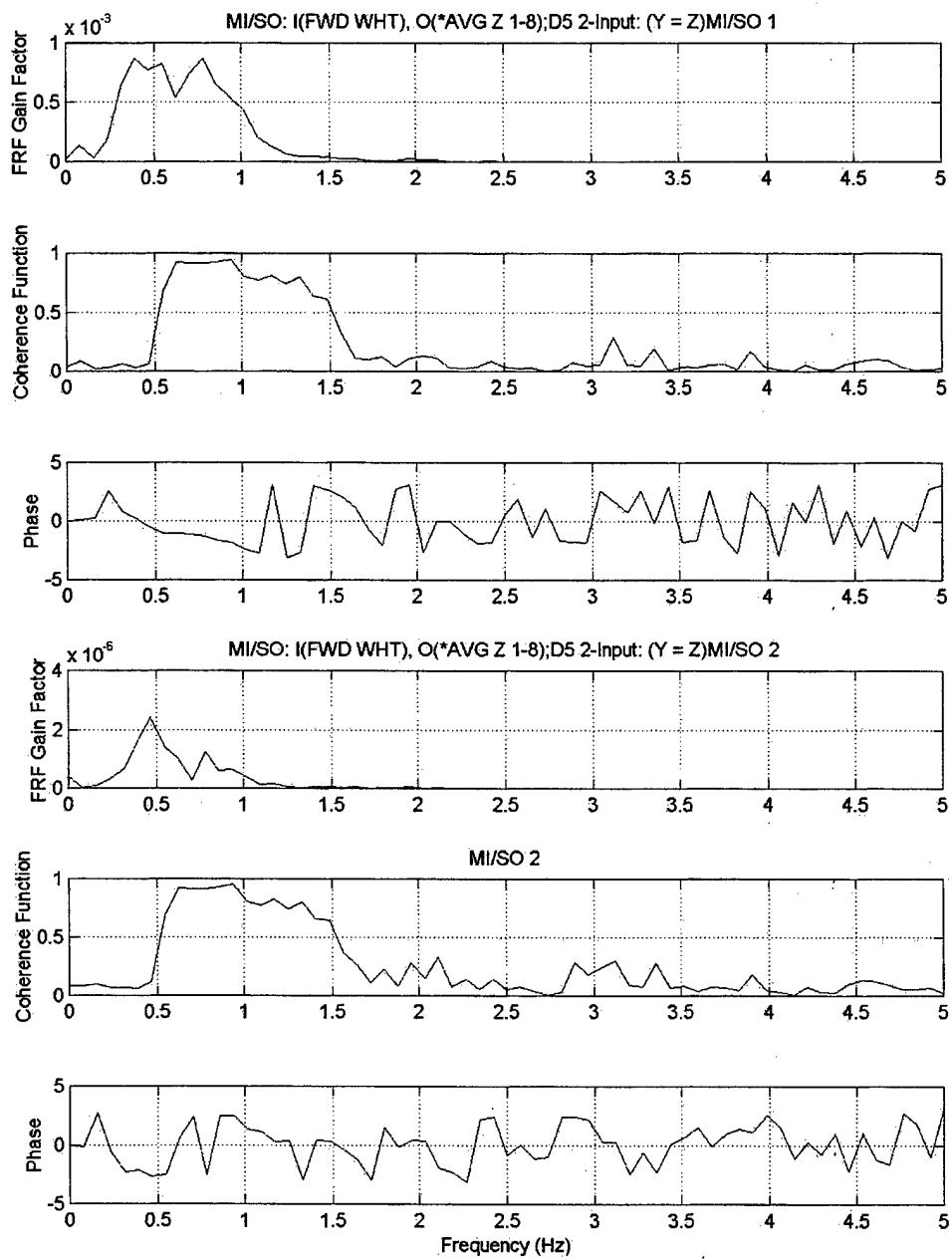
Figure D.23: Direct Two-Input Model D5
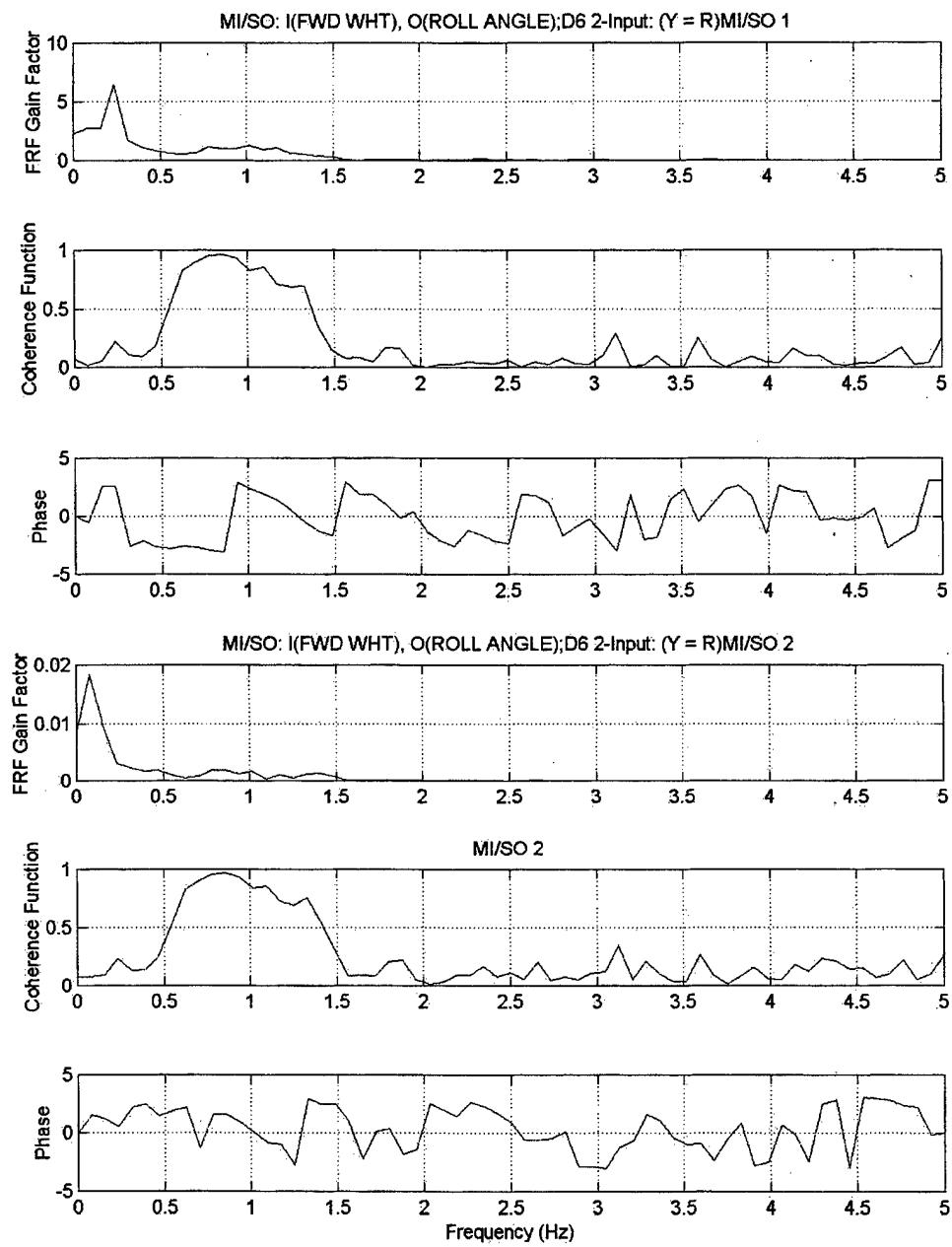
Figure D.24: Direct Two-Input Model D6

152
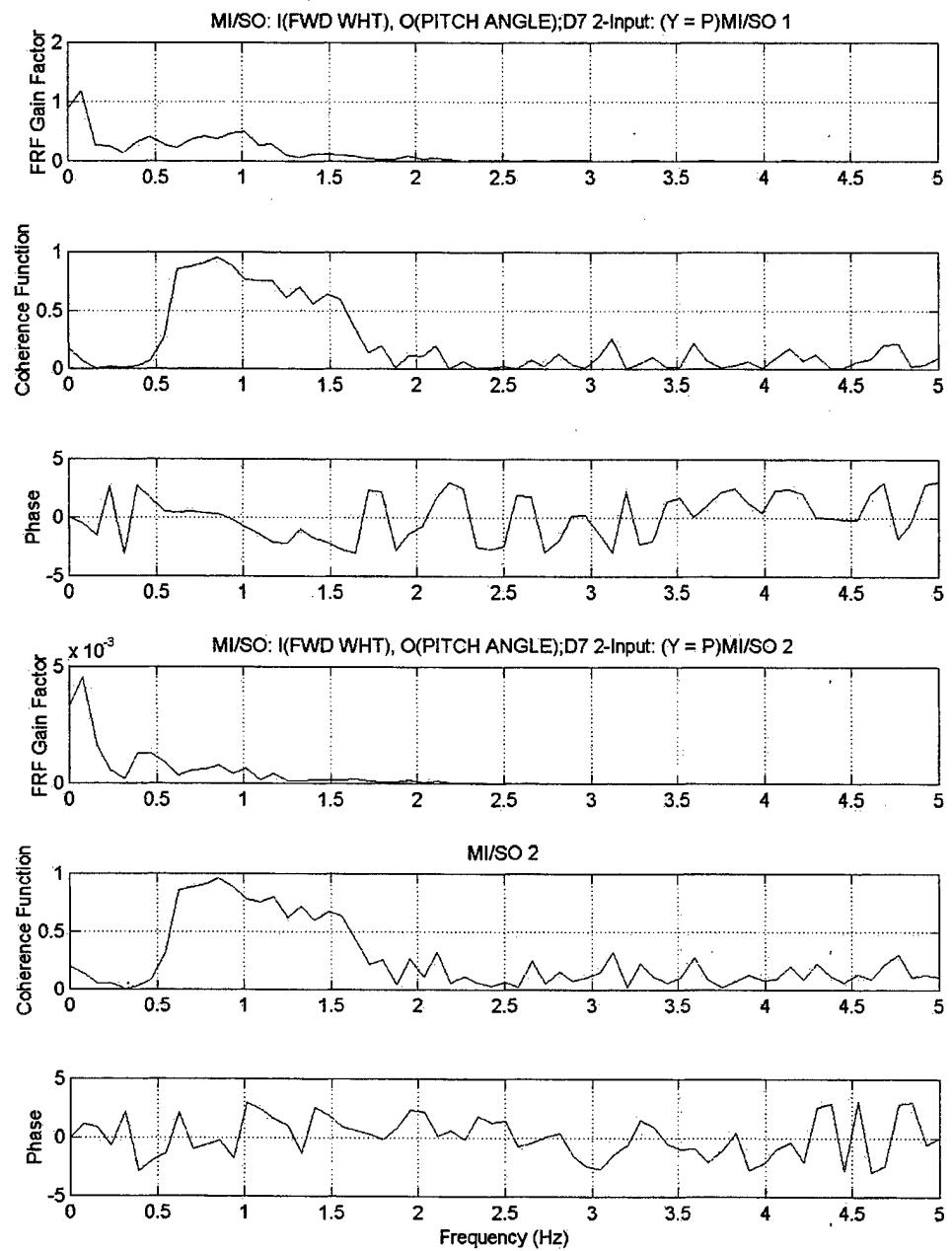
Figure D.25: Direct Two-Input Model D7
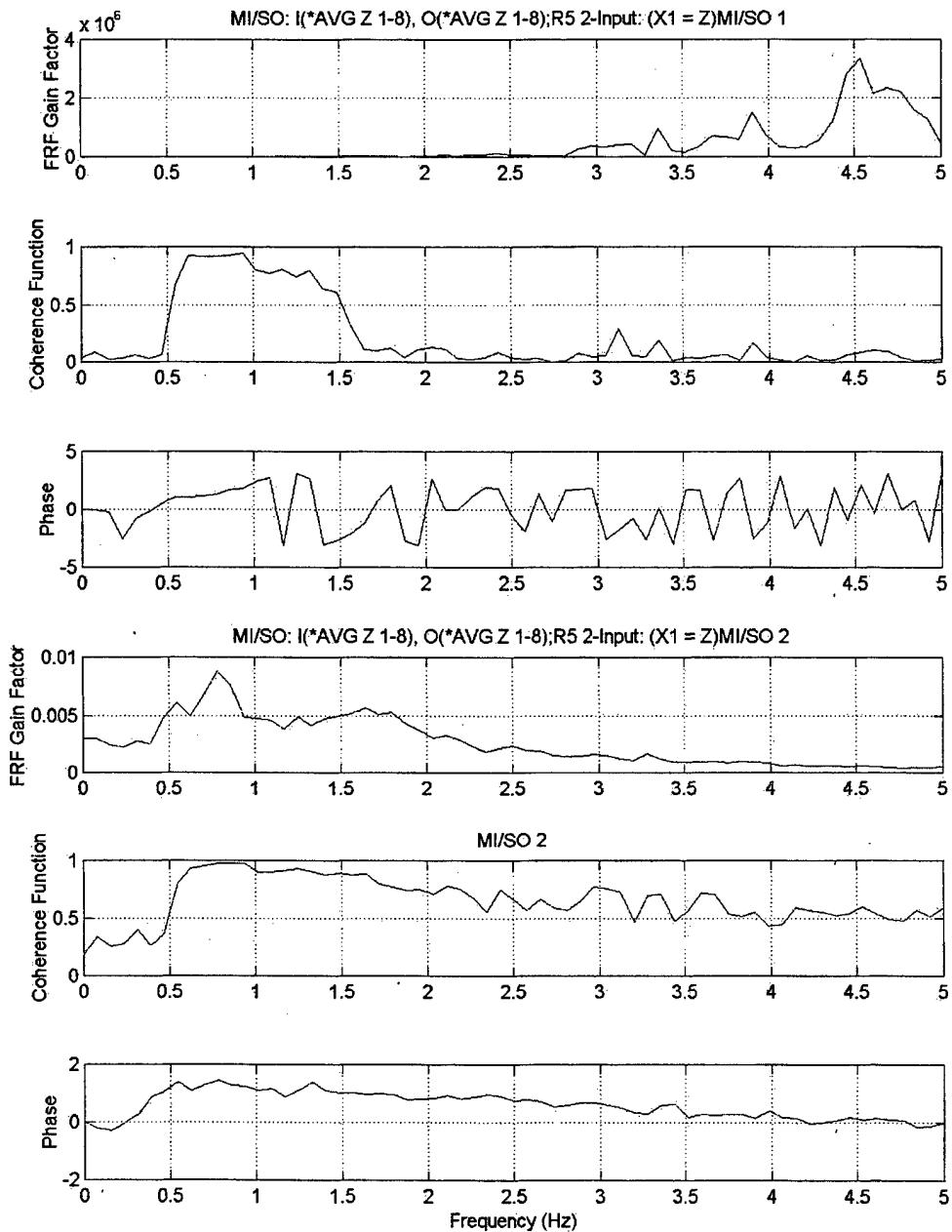
Figure D.26: Reverse Two-Input Model R5

154
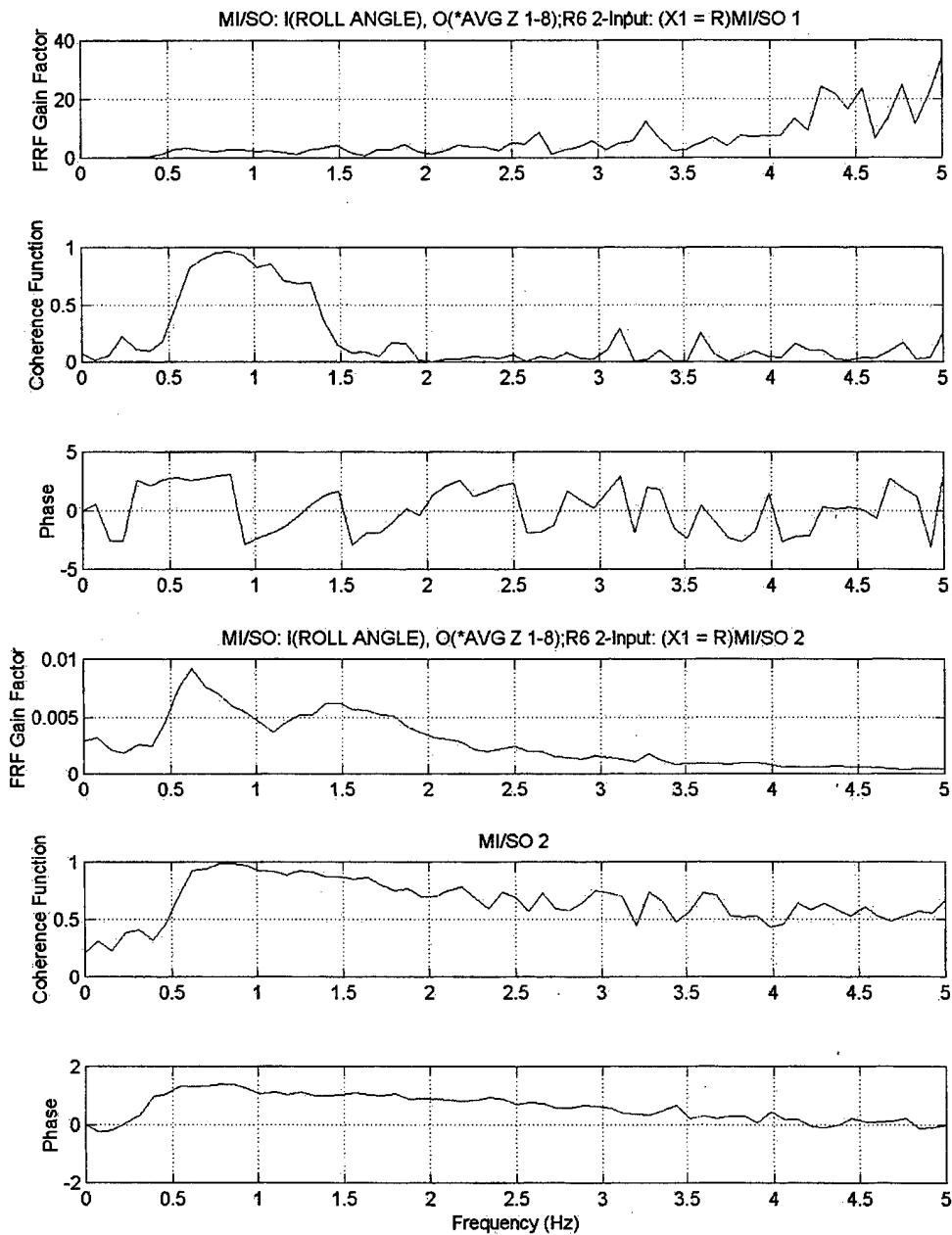
Figure D.27: Reverse Two-Input Model R6
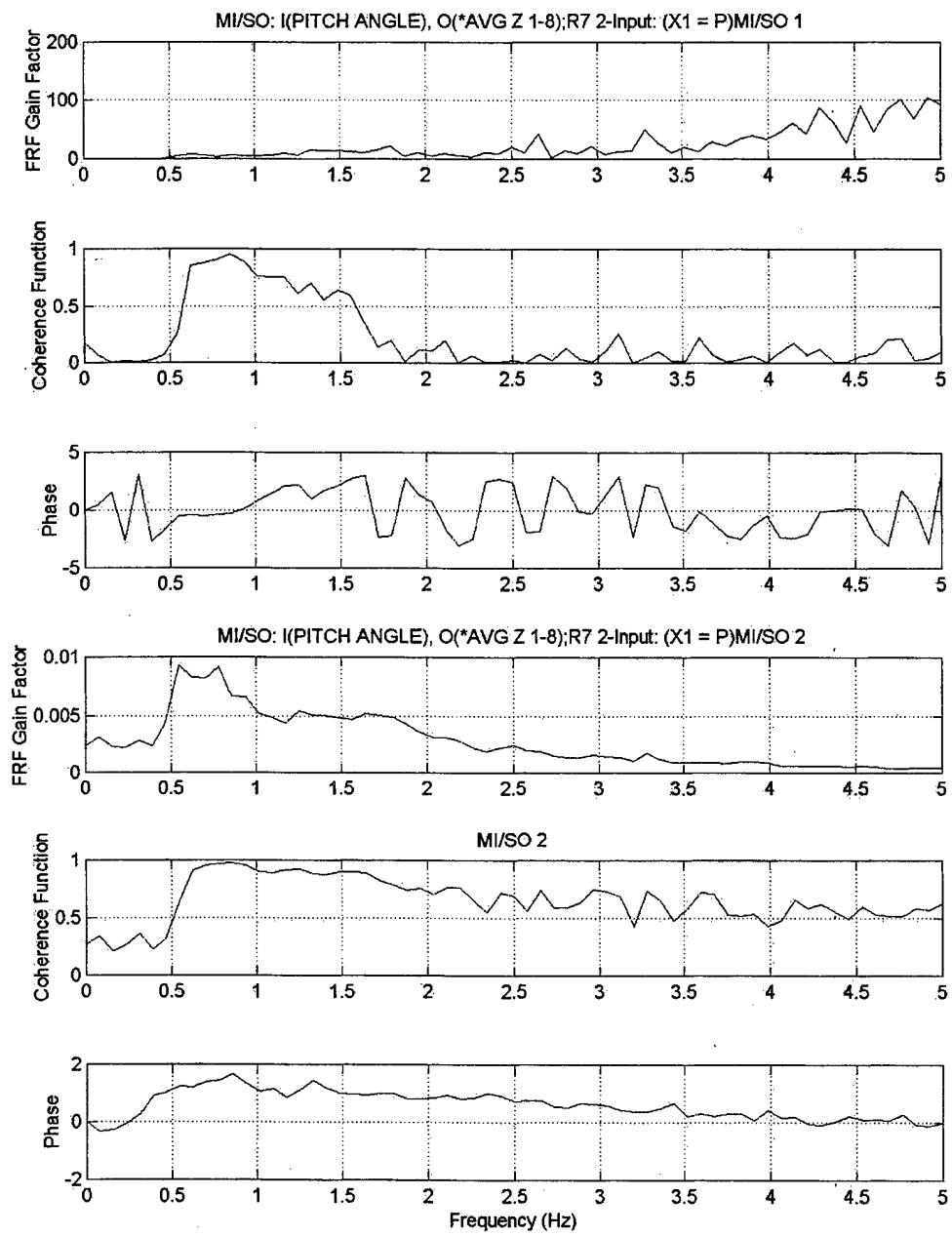
Figure D.28: Reverse Two-Input Model R7

Appendix E

Scaling Issue with the Four Module Acceleration Data

The acceleration (X,Y and Z) data for the four module data is spread across two data sets. They have different scaling factors with the acceleration data in the second data set being far higher in magnitude compared to that in the first data set. Since the primary concern of this thesis is with mode shape frequency and not amplitudes, the acceleration data is scaled in the frequency domain before performing the animation. Care has been taken to average the data and linearly scale data to avoid disrupting the mode shapes. However, a certainly uncertainty in the response of the connectors due to this scaling is present. Since there is only one set of connector sensor data in the data set, there is insufficient information available to compare and correct any discrepancy in the scaling.

The original spectrum from the two data sets is shown in Figure E.1. While the spectrums of one data set are prominently visible in the plot, the other set of spectrums is hardly visible. The average of the two spectrum sets are calculated (Figure E.2). Then the difference in scaling across the frequency is determined as the multiplication factor to reduce the magnitude of the second data set (Figure E.3). It can be noticed that the factor is not linear. After multiplying the second data set with the factor, the normalized spectrum of both data sets is obtained (Figure E.4).
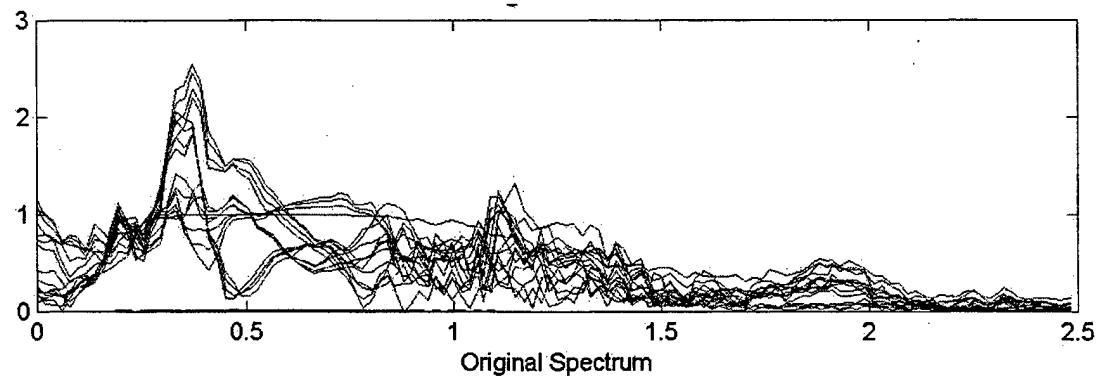
Figure E.1: Original Spectrum of the Acceleration Data
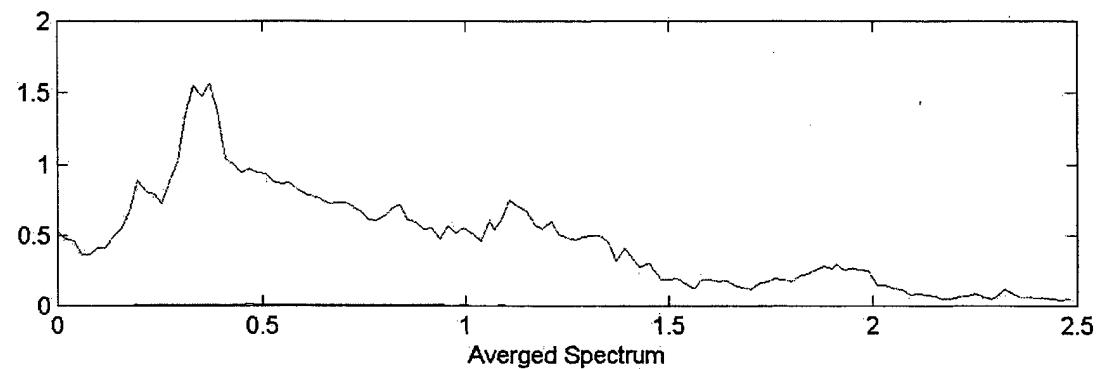

Figure E.2: Averaged Spectrum
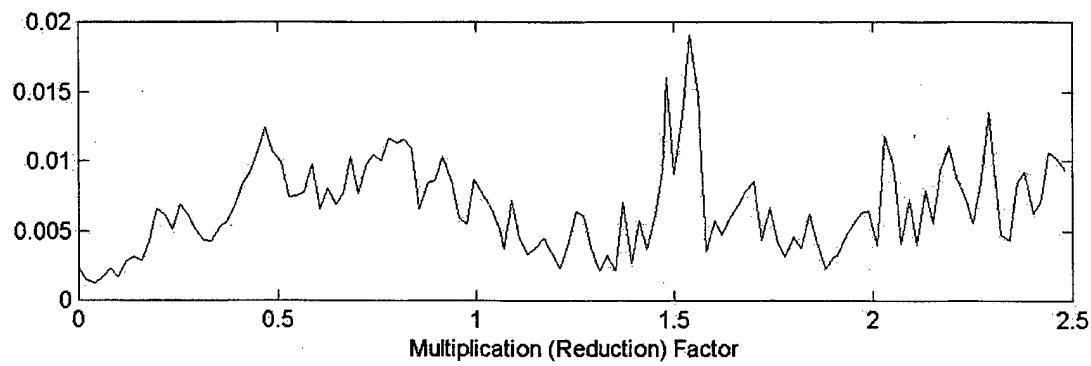
Figure E.3: Multiplication Factor to Reduce Magnitude of Second Data Set

158
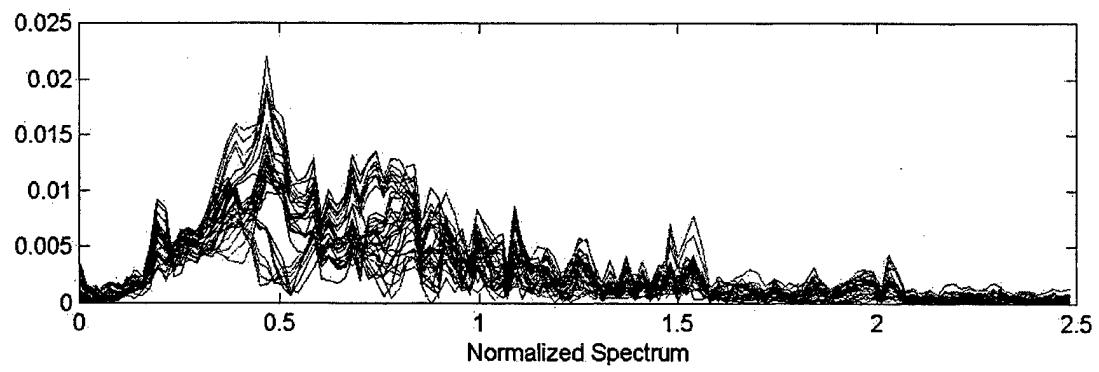
Figure E.4: Normalized Acceleration Response Spectrum

BIOGRAPHY OF THE AUTHOR

Vijay Venkataraman was born in Mumbai (formerly Bombay), India, on March 13, 1976. He attended Carmel Garden School from 1984-1994, and Bharatiar University, Coimbatore, India for two years in Mechanical Engineering. He then transferred to the University of Maine in 1996. While in college, he was a member of the Tau Beta Pi National Engineering Honor Society and the Phi Kappa Phi Honor Society and was awarded the George E. Clifford Memorial Scholarship twice. He graduated with a Bachelor's degree in Mechanical Engineering in December, 1998. Vijay is a candidate for the Master of Science degree in Mechanical Engineering from The University of Maine in August, 2001.

REPORT DOCUMENTATION PAGE

Public reporting burden for this collection of information is estimated to average 1 hour per response, including the time for reviewing instructions, searching data sources, gathering and maintaining the data needed, and completing and reviewing the collection of information. Send comments regarding this burden estimate or any other aspect of this collection of information, including suggestions for reducing this burden to Washington Headquarters Service, Directorate for Information Operations and Reports, 1215 Jefferson Davis Highway, Suite 1204, Arlington, VA 22202-4302, and to the Office of Management and Budget, Paperwork Reduction Project (0704-0188) Washington, DC 20503.

PLEASE DO NOT RETURN YOUR FORM TO THE ABOVE ADDRESS.

1. REPORT DATE (DD-MM-YYYY) 01-Dec-2001	2. REPORT TYPE Master's Thesis	3. DATES COVERED (From - To) 1-Sept-2000 to 30-Aug-2001

4. TITLE AND SUBTITLE

Dynamic Response of a Mobile Offshore Base Hydroelastic Test Model

5a. CONTRACT NUMBER

5b. GRANT NUMBER
N00014-97-1-0661

5c. PROGRAM ELEMENT NUMBER

6. AUTHOR(S)

Venkataraman, Vijay

5d. PROJECT NUMBER

5e. TASK NUMBER

5f. WORK UNIT NUMBER

7. PERFORMING ORGANIZATION NAME(S) AND ADDRESS(ES)
University of Maine
Office of Research and Sponsored Programs
5717 Corbett Hall
Orono, ME 04469-5717

8. PERFORMING ORGANIZATION REPORT NUMBER
C-9920-01

9. SPONSORING/MONITORING AGENCY NAME(S) AND ADDRESS(ES)

Office of Naval Research
Ballston Center Tower One
800 North Quincy St.
Arlington, VA 22217-5660

10. SPONSOR/MONITOR'S ACRONYM(S)
ONR

11. SPONSORING/MONITORING AGENCY REPORT NUMBER

12. DISTRIBUTION AVAILABILITY STATEMENT

Approved for Public Release, Distribution is Unlimited

13. SUPPLEMENTARY NOTES

14. ABSTRACT

The objective of the work presented in this thesis deals with the study of dynamic response of a Mobile Offshore Base (MOB) hydroelastic test model. The MOB is a very large floating structure consisting of multiple self-propelled, semi-submersible modules. Physical scale model testing of a notional MOB concept has been conducted and the experimental results have been provided for one, two and four module configurations. This thesis focuses on utilizing the experimental data to understand the dynamic response of the MOB hydroelastic scale module. The analysis of the data is conducted using popular linear and nonlinear data processing techniques. The objectives are to obtain the modal shapes of the dynamic response, investigate the effect of connector dynamics in multi-module scale models and determine the nonlinear characteristics of the response.

15. SUBJECT TERMS
Mobile Offshore Base; Inter-modular connectors; Connection dynamics; Modal response.

16. SECURITY CLASSIFICATION OF:			17. LIMITATION OF ABSTRACT	18. NUMBER OF PAGES	19a. NAME OF RESPONSIBLE PERSON Vincent Caccese
a. REPORT U	b. ABSTRACT U	c. THIS PAGE U	UU	160	19b. TELEPONE NUMBER (Include area code) (207) 581-2131